nature catalysis

SUPPLEMENTARY INFORMATION

https://doi.org/10.1038/s41929-019-0394-4

In the format provided by the authors and unedited.

Genetically engineered proteins with two active sites for enhanced biocatalysis and synergistic chemo- and biocatalysis

Sandra Alonso[1,10], Gerard Santiago[2,10], Isabel Cea-Rama[3,10], Laura Fernandez-Lopez[1], Cristina Coscolín[1], Jan Modregger[4], Anna K. Ressmann[4], Mónica Martínez-Martínez[1], Helena Marrero[1], Rafael Bargiela[5,6], Marcos Pita[1], Jose L. Gonzalez-Alfonso[1], Manon L. Briand[7], David Rojo[8], Coral Barbas[8], Francisco J. Plou[1], Peter N. Golyshin[5,6], Patrick Shahgaldian[7], Julia Sanz-Aparicio[3,11]*, Víctor Guallar[2,9,11]* and Manuel Ferrer[1,11]*

[1]Institute of Catalysis, Consejo Superior de Investigaciones Científicas (CSIC), Madrid, Spain. [2]Barcelona Supercomputing Center (BSC), Barcelona, Spain. [3]Department of Crystallography & Structural Biology, Institute of Physical Chemistry Rocasolano, CSIC, Madrid, Spain. [4]EUCODIS Bioscience, Vienna, Austria. [5]School of Natural Sciences, Bangor University, Bangor, UK. [6]Centre for Environmental Biotechnology, Bangor University, Bangor, UK. [7]Institute of Chemistry and Bioanalytics, School of Life Sciences, University of Applied Sciences and Arts Northwestern Switzerland, Muttenz, Switzerland. [8]Centro de Metabolómica y Bioanálisis (CEMBIO), Facultad de Farmacia, Universidad CEU San Pablo, Boadilla del Monte, Madrid, Spain. [9]Institució Catalana de Recerca i Estudis Avançats (ICREA), Barcelona, Spain. [10]These authors contributed equally: Sandra Alonso, Gerard Santiago, Isabel Cea-Rama. [11]These authors jointly supervised this work: Julia Sanz-Aparicio, Víctor Guallar, Manuel Ferrer.
*e-mail: xjulia@iqfr.csic.es; victor.guallar@bsc.es; mferrer@icp.csic.es

SUPPLEMENTARY INFORMATION

Genetically Engineered Proteins with Two Active Sites for Enhanced Biocatalysis and Synergistic Chemo- and Biocatalysis

Sandra Alonso[1,10], Gerard Santiago[2,10], Isabel Cea-Rama[3,10], Laura Fernandez-Lopez[1], Cristina Coscolín[1], Jan Modregger[4], Anna K. Ressmann[4], Mónica Martínez-Martínez[1], Helena Marrero[1], Rafael Bargiela[5,6], Marcos Pita[1], Jose L. Gonzalez-Alfonso[1], Manon Briand[7], David Rojo[8], Coral Barbas[8], Francisco J. Plou[1], Peter N. Golyshin[5,6], Patrick Shahgaldian[7], Julia Sanz-Aparicio[3,11,*], Víctor Guallar[2,9,11,*] and Manuel Ferrer[1,11,*]

[1]Institute of Catalysis, Consejo Superior de Investigaciones Científicas (CSIC), 28049 Madrid, Spain. [2]Barcelona Supercomputing Center (BSC), 08034 Barcelona, Spain. [3]Department of Crystallography & Structural Biology, Institute of Physical Chemistry "Rocasolano", CSIC, 28006 Madrid, Spain. [4]EUCODIS Bioscience GmbH, 1030 Vienna, Austria. [5]School of Natural Sciences, Bangor University, LL57 2UW Bangor, UK. [6]Centre for Environmental Biotechnology, Bangor University, LL57 2UW Bangor, UK. [7]University of Applied Sciences and Arts Northwestern Switzerland, School of Life Sciences, Institute of Chemistry and Bioanalytics, CH-4132 Muttenz, Switzerland. [8]Centro de Metabolómica y Bioanálisis (CEMBIO), Facultad de Farmacia, Universidad CEU San Pablo, 28668 Boadilla del Monte, Madrid, Spain. [9]Institució Catalana de Recerca i Estudis Avançats (ICREA), 08010 Barcelona, Spain. [10]These authors contributed equally: Sandra Alonso, Gerard Santiago, Isabel Cea-Rama. [11]These authors equally coordinated the work: Julia Sanz-Aparicio, Víctor Guallar and Manuel Ferrer. *e-mail: *(J.S.) Email: xjulia@iqfr.csic.es (J.S-A.); victor.guallar@bsc.es (V.G.) and mferrer@icp.csic.es (M.F.).

Supplementary Note 1

The original EH1 design with a native and a genetically engineered active site

In a recent study we rationally introduced in a natural serine Ester-Hydrolase ($EH1_A$) a second active site ($EH1_B$), by using protein engineering. Briefly, using the Protein Energy Landscape Exploration (PELE) software, we identified in the native scaffold a potential binding pocket and successfully turned it into a catalytic site by introducing a few mutations[1]. In details, the native active site of the target $EH1_A$ hydrolase (PDB code 5JD4) is formed by a catalytic triad (Ser161, Asp256 and His286) and an oxyanion hole (Gly88, Gly89 and Gly90), with Ser161 being the nucleophile. The artificial $EH1_B$ hydrolase variant was created by introducing Glu25Asp, Leu214His and Ser161Ala substitutions into the wild-type sequence ($EH1_A$), so that this variant would employ a new catalytic triad (Ser211, Asp25 and His214) with Ser211 as the nucleophile, and a new oxyanion hole (Gly207, Tyr208 and Phe209). The artificial $EH1_{AB}$ variant was created by incorporating the Glu25Asp and Leu214His substitutions into the wild-type sequence ($EH1_A$). This *plurizyme* would employ two active sites, one formed by the Ser161, Asp256 and His286 triad and the Gly88, Gly89 and Gly90 oxyanion hole, and a second one formed by Ser211, Asp25 and His214 triad and Gly207, Tyr208 and Phe209 oxyanion hole. The design and creation of the $EH1_B$ and $EH1_{AB}$ variants and confirmation that Ser161, Asp256, and His286 (conforming the native sites) and Ser211, Asp25, His214 (conforming the artificial site) are the functional groups supporting catalysis (ester-hydrolysis), which is constituted by a catalytic triad and not a diad or by a histidine or an aspartic residue, have been extensively described by Santiago et al. (2018)[1].

Supplementary Note 2

The remodeled EH1 design with a native and an optimized active site

Computational remodeling and characterization of remodeled sub-enzymes

Introducing the new artificial active site ($EH1_B$) in our target $EH1_A$ to produce an artificial *plurizyme* ($EH1_{AB}$) with two separate (and active) catalytic Ser-Asp-His triads along with their respective essential oxyanion holes, did not produce a catalytically efficient two active-sites biocatalyst[1]. This is most likely owing to the low catalytic performance of the artificial site ($k_{cat} \leq 0.03\ s^{-1}$) because of a sub-optimal configuration[1]. Thus, this artificial design cannot be used as starting point to design biomimetic chemo-biocatalytic systems, which was the foremost objective of this study.

For this reason, we herein considered a new round of rational engineering to design a more efficient *plurizyme* from our original $EH1_{AB}$ design. Before, we briefly summarize the computational protocol for a *plurizyme* design (more details can be found in Santiago et al. (2018)[1]). The protocol starts by mapping the surface diffusion of a probe ligand, a representative medium size ester for which we want to introduce activity. PELE can map the whole ligand diffusion and binding site search in only few hours when using its adaptive implementation. Most of times the active site appears as the best binding one, but we typically find 2-3 alternative binding sites in additional regions. Then, we perform a visual inspection of these sites and decide which one will be easier to transform into an active one, for example, sites that already poses one (or more) of the catalytic triad residues. Once the site(s) are selected, we engineer them aiming at finding a proper residue and catalytic triad alignment. For this, we select the local residues to be mutated and we try single and double combinations with a short PELE run (~ 1 hour, where we monitor the binding and catalytic distances, including the oxyanion wholes). Those that point to proper catalytic realignment are suggested for mutagenesis.

Due to the low activity in our initial site design, we run a new round of rational engineering, using the PELE software with $EH1_B$ as our initial model. We mapped glyceryl tripropionate dynamics, one of the preferred substrates of this site[1], in a longer PELE production run (~12 hours). The rationale was to investigate the cumulative effects of mutations in residues close to catalytic positions so that to improve the artificial site with a more appropriate catalytic configuration; PELE suggested the R23G mutation as best potential target for active site remodeling. This Arg amino acid seems to work to destabilize the artificial catalytic triad by partially sequestering Asp25, and substitution by Gly indicated a better stability of the His-Asp

interaction (Supplementary Figure 1). In addition, introducing the smaller side chain significantly increased the effective volume of the active site due to a higher cavity size, which increased from 58 to 66 Å^3; this parameter largely correlates with substrate broadening[2]. Such an increment allowed the new site to overcome the previously established threshold (62.5 Å^3) above which EH hydrolyze more than 24 substrates (from a set of 96 tested)[2].

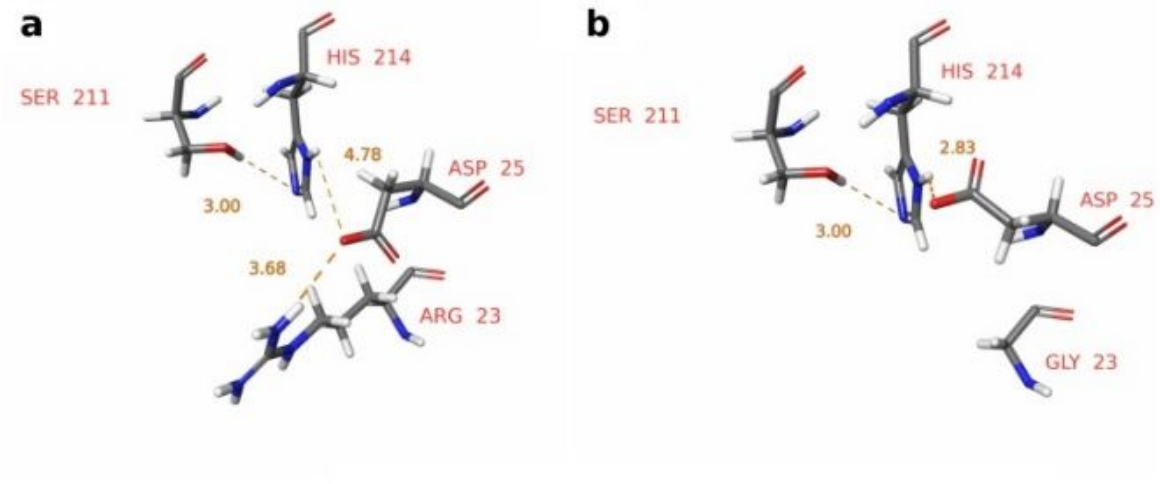

	EH1AB (A)	EH1AB1 (B)
SER211-HIS214 Distance (Å)	5,2 ± 1,8	3,4 ± 1,5
HIS214-ASP25 Distance (Å)	8.4 ± 1.6	5.5 ± 1.4

Supplementary Figure 1 Two representative snapshots of EH1$_B$ (a) and EH1$_{B1}$ (b) catalytic triads from the molecular dynamic simulations. The movement in Asp25 as a result of the R23G mutation is observed in the upper panels. The lower panel indicates the average distances between key catalytic amino acids obtained for both species along the molecular dynamics. The represented errors are the distances (obtained by molecular dynamics) standard deviation.

The EH1$_{A1}$, EH1$_{B1}$ and EH1$_{AB1}$ variants were created by adding R23G mutations to the EH1$_A$, EH1$_B$ and EH1$_{AB}$ variants previously described[1]. They were purified as described in Supplementary Methods and determination of K_m, k_{cat} and k_{cat}/K_m were evaluated using an indirect method based on a pH-indicator assay in which the hydrolysis of an ester is followed at 550 nm. The method and conditions have been extensively described elsewhere[1]. Mutations Ser161Ala, Asp256Gln, and His286Phe (conforming the native site) and Ser211Ala, Asp25Gln, His214Phe (conforming the artificial site) were herein performed in EH1$_{A1}$, EH1$_{B1}$ and EH1$_{AB1}$, and found that those mutations, individually and in combination, fully arrested the activity; this confirms the role of those residues in catalysis, as in the original designs.

No statistically significant differences were found in terms of k_{cat} values for all the 78 esters being converted by both EH1$_A$ and EH1$_{A1}$ (Supplementary Table 1; Supplementary Figure 1). Thus, R23G mutation *per se* did not cause any local negative side effect in the catalytic performance of the original enzyme. In summary, EH1$_{A1}$ (as the "mother" EH1$_A$ ester-hydrolase) converted 78 esters with a maximum k_{cat} of *ca*. 45.2±0.1 s^{-1}. It is also non enantio-specific by meaning of k_{cat} values for a set of 8 pairs of enantiomers when tested separately (Supplementary Table 1), and by meaning of e.e. values obtained for the kinetic resolution of a racemic mixture of methyl (2*R*/*S*)-2-phenylpropanoate (E-value ~1.2), as determined by GC analysis (see Supplementary Methods).

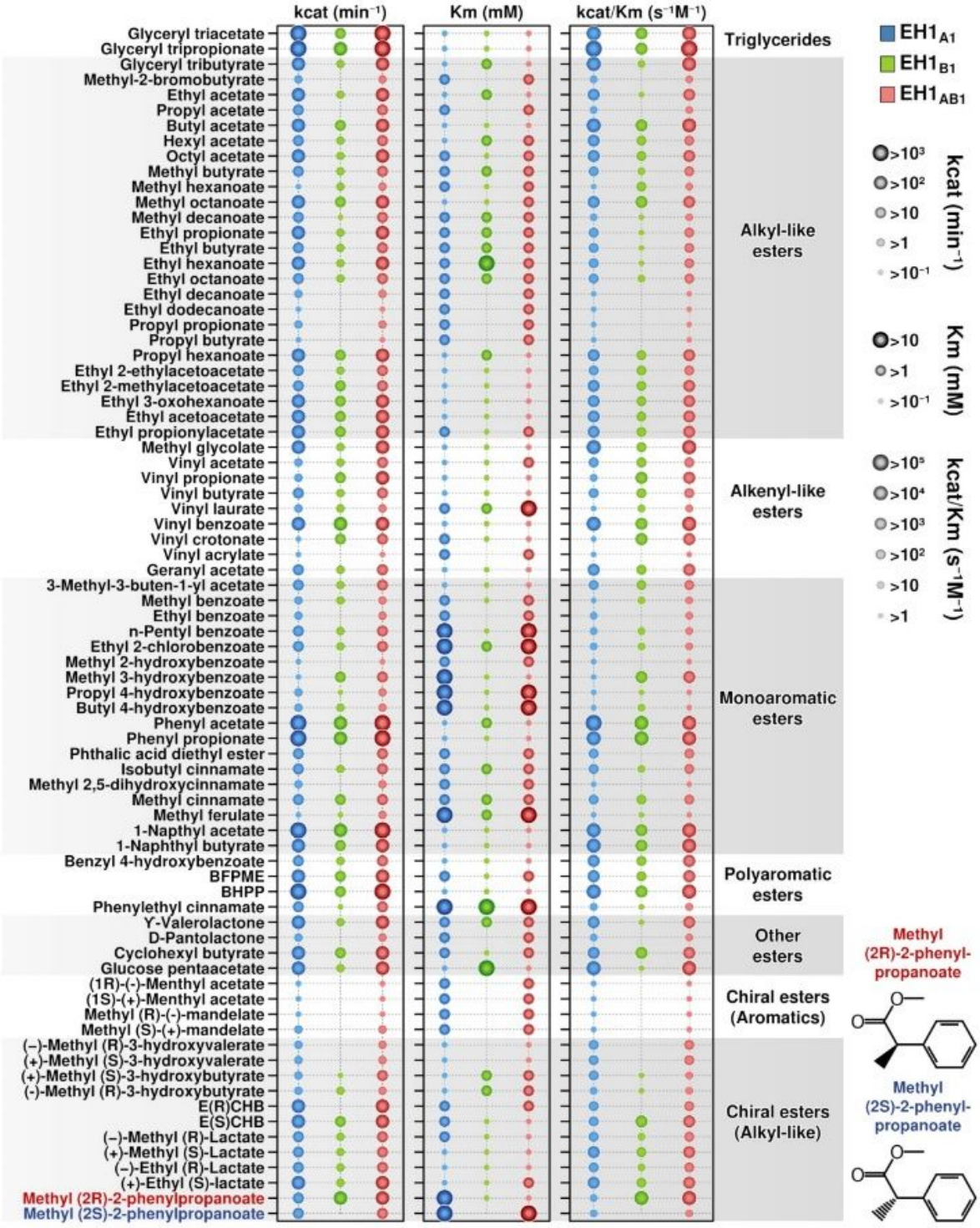

Supplementary Figure 2 The artificial remodeled site intensifies the bio-catalytic capability of the "mother" enzyme. Shown are the kinetic parameters, calculated on a continuous pH indicator assay[1], for a series of esters found to be hydrolyzed by any of the sub-enzymes. For K_m determination - [protein]: 4.5 μg/ml; [ester]: 0-100 mM; reaction volume: 44 μl; T: 30ºC; pH: 8.0. For k_{cat} determination - [protein]: 0-270 μg/ml; [ester]: 50 mM; reaction volume: 44 μl; T: 30ºC; pH: 8.0. The figure was created with the R language console using average values given in Supplementary Table 1 and Supplementary Table 2, where abbreviations can also be seen. The structures of the two chiral esters (color-coded) used to calculate enantio-selectivity are highlighted at the bottom right side.

Supplementary Table 1. Kinetic parameters. k_{cat} (min^{-1}) for $EH1_{A1}$, $EH1_{B1}$ and $EH1_{AB1}$ sub-enzymes against a set of structurally different esters. The assays, in triplicates for each concentration, were performed as in Supplementary Figure 2 legend. The standard deviation of the linear fit with Sigma Plot 13.0 is shown.

	k_{cat} (min^{-1})[1]					
Ester[1]	**$EH1_A$**	**$EH1_B$**	**$EH1_{AB}$**	**$EH1_{A1}$**	**$EH1_{B1}$**	**$EH1_{AB1}$**
Glyceryl triacetate	1116±13	0.051±0.014	5.12±0.9	1111±14	45.60±0.31	1195±7
Glyceryl tripropionate	2247±7.0	0.547±0.034	21.11±1.35	2205±18	221.9±3.6	2529±20
Glyceryl tributyrate	440.8±2.3	0.214±0.008	8.19±0.98	458.1±2.9	5.84±0.22	465.3±6.8
Methyl-2-bromobutyrate	9.14±1.79	0	0.12±0.05	9.23±0.16	0	9.39±6.97
Ethyl acetate	209.2±7.6	0	3.22±0.14	206.6±3.3	1.01±0.08	217.9±2.6
Propyl acetate	13.67±0.05	0	2.84±0.07	15.81±0.2	0	15.89±0.73
Butyl acetate	465.7±3.4	0.004±0.003	6.86±0.02	453.5±6.4	86.5±9.96	551.0±1.8
Hexyl acetate	34.11±0.45	0.007±0.003	6.88±0.06	33.47±0.49	9.39±0.04	48.14±0.49
Octyl acetate	147.0±9.5	0.005±0.001	3.31±0.06	152.9±1.2	6.53±0.22	147.2±0.8
Methyl butyrate	27.34±0.03	0	8.03±0.15	29.94±0.06	5.06±0.07	41.65±0.82
Methyl hexanoate	1.03±0.09	0.135±0.021	1.22±0.04	0.94±0.07	8.0±0.11	8.02±0.7
Methyl octanoate	107.2±4.2	0.01±0.002	4.02±0.14	109.6±2.2	14.84±0.09	123.0±1.2
Methyl decanoate	11.12±0.36	0	0.58±0.09	12.01±0.21	0.2±0.01	12.42±0.19
Ethyl propionate	207.9±4.5	0	3.9±0.35	201.9±3.2	1.65±0.08	207.6±2.2
Ethyl butyrate	82.13±3.48	0.007±0.002	13.78±0.28	83.52±0.13	2.69±0.09	86.24±1.7
Ethyl hexanoate	184.1±1.5	0.113±0.059	4.01±0.07	180.4±2.6	8.59±0.33	194.3±1.4
Ethyl octanoate	61.66±1.22	0.041±0.018	1.75±0.06	56.07±0.14	6.24±0.27	69.39±2.65
Ethyl decanoate	1.44±0.18	0	0.14±0.02	1.33±0.24	0	1.42±0.09
Ethyl dodecanoate	1.25±0.22	0	1.44±0.03	0.96±0.02	0	0.97±0.08
Propyl propionate	1.96±0.07	0	35.22±0.3	1.24±0.02	0	1.25±0.12
Propyl butyrate	0.48±0.03	0	115.5±0.7	0.44±0.08	0	0.47±0.14
Propyl hexanoate	154.7±4.6	0.075±0.03	5.27±0.13	156.4±2.0	10.23±0.66	176.2±1.3
Ethyl 2-ethylacetoacetate	13.20±1.24	0	0.52±0.02	13.46±0.27	9.76±0.13	31.73±0.7
Ethyl 2-methylacetoacetate	85.21±1.06	0	6.61±0.07	81.37±1.64	11.87±0.16	95.01±3.0
Ethyl 3-oxohexanoate	346.0±4.2	0	8.54±0.11	343.6±6.1	15.61±0.07	378.8±3.3
Ethyl acetoacetate	329.6±3.1	0	5.51±0.03	320.2±6.8	11.63±0.16	339.1±2.9
Ethyl propionylacetate	494.7±3.8	0	4.77±0.02	468.4±8.7	12.25±0.16	490.5±3.6
Methyl glycolate	470.8±2.0	0	2.02±0.04	470.3±7.4	5.29±0.25	519.6±4.5
Vinyl acetate	8.36±0.02	0.07±0.03	0.03±0.01	8.84±0.21	2.43±0.03	11.77±0.68
Vinyl propionate	3.36±0.22	0.786±0.03	2.59±0.38	3.14±0.62	91.34±2.21	100.8±1.5
Vinyl butyrate	11.12±0.16	0.342±0.089	2.96±0.16	11.83±0.24	5.21±0.19	23.91±0.45
Vinyl laurate	4.57±0.09	0	0.03±0.01	4.82±0.01	3.58±0.05	8.45±0.25
Vinyl benzoate	448.5±6.7	0.112±0.035	63.91±0.54	488.1±9.7	109.3±3.0	599.4±3.6
Vinyl crotonate	18.55±0.55	0.087±0.012	15.9±0.13	20.96±0.14	66.88±2.15	85.14±0.66
Vinyl acrylate	0.17±0.02	0	0.38±0.01	0.15±0.02	0	0.19±0.04
Geranyl acetate	55.38±2.74	0	3.53±0.09	59.43±1.40	6.57±0.88	67.42±1.18
3-Methyl-3-buten-1-yl acetate	28.91±0.1	0	10.18±0.29	29.02±0.66	9.55±0.07	41.7±1.11
Methyl benzoate	3.43±0.4	0	0.20±0.03	3.29±0.05	1.14±0.15	4.54±0.21
Ethyl benzoate	3.43±0.18	0	0.16±0.02	3.43±0.05	0	3.91±0.26
n-Pentyl benzoate	39.29±0.76	0	1.45±0.36	36.21±0.79	4.67±0.62	41.07±0.56
Ethyl 2-chlorobenzoate	15.1±0.2	0	1.84±0.10	15.24±0.28	2.47±0.03	21.33±0.81
Methyl 2-hydroxybenzoate	0.3±0.21	0	0.20±0.01	0.41±0.1	0	0.38±0.01

Methyl 3-hydroxybenzoate	0.66±0.04	0	0.09±0.01	0.83±0.02	58.25±0.26	61.26±0.47
Propyl 4-hydroxybenzoate	2.47±0.08	0	0.28±0.03	2.45±0.03	0.08±0.04	2.59±0.52
Butyl 4-hydroxybenzoate	3.65±0.1	0	0.51±0.03	3.14±0.15	1.49±0.01	4.90±0.89
Phenyl acetate	1310±19	0.331±0.087	81.09±1.57	1312±15	775.7±3.2	2153±12
Phenyl propionate	2797±18	1.490±0.151	267.0±1.6	2715±2	820.4±5.5	3468±13
Phthalic acid diethyl ester	13.25±0.15	0	0.36±0.59	14.35±0.22	0	14.11±0.38
Isobutyl cinnamate	51.07±1.27	0	1.79±0.19	51.5±1.19	5.71±0.08	61.26±0.57
Methyl 2,5-dihydroxycinnamate	1.92±0.02	0	0.07±0.03	1.66±0.03	0	1.66±0.12
Methyl cinnamate	61.01±0.25	0	3.48±0.01	64.12±1.22	10.59±0.14	74.84±1.91
Methyl ferulate	0.86±0.01	0	0.07±0.01	0.86±0.01	0.60±0.08	1.38±0.12
1-Napthyl acetate	1016±13	0.143±0.046	7.61±0.88	1045±13	181.7±8.0	1272±11
1-Naphthyl butyrate	234.9±6.4	0.069±0.005	3.38±0.21	216.4±3.9	60.81±2.4	283.3±1.7
Benzyl 4-hydroxybenzoate	76.69±1.29	0	2.13±0.04	79.29±1.61	4.27±0.12	83.77±1.61
BFPME[2]	316.5±3.4	0.02±0.012	2.70±0.02	313.9±6.7	11.6±0.71	328.1±3.2
BHPP[2]	1277±14	0.073±0.024	8.78±1.01	1250±15	95.63±5.1	1368±8
Phenylethyl cinnamate	13.56±0.04	0	0.27±0.09	12.97±0.32	0.32±0.04	14.82±0.23
ϒ-Valerolactone	343.8±2.9	0	0.50±0.04	380.4±5.9	3.45±0.81	398.5±2.8
D-Pantolactone	9.08±0.03	0	0.90±0.04	8.89±0.19	0	8.89±0.26
Cyclohexyl butyrate	416.6±1.2	0.084±0.001	50.82±0.86	415.0±4.6	41.12±0.33	460.9±1.6
Glucose pentaacetate	794.1±4.0	0	0.45±0.01	816.6±9.2	6.08±0.15	916.0±4.4
(1*R*)-(-)-Menthyl acetate	1.03±0.1	0	0.18±0.01	0.96±0.01	0	0.97±0.07
(1*S*)-(+)-Menthyl acetate	0.59±0.14	0	0.02±0.01	0.62±0.08	0	0.61±0.06
Methyl (*R*)-(-)-mandelate	0.51±0.03	0	0.02±0.01	0.49±0.06	0	0.39±0.1
Methyl (*S*)-(+)-mandelate	1.51±0.24	0	0.49±0.01	1.48±0.12	0	1.54±0.42
(−)-Methyl (*R*)-3-hydroxyvalerate	9.05±0.26	0	0.45±0.01	9.88±0.12	0	9.75±0.53
(+)-Methyl (*S*)-3-hydroxyvalerate	6.26±0.01	0	0.25±0.06	6.67±0.13	0	6.95±0.4
(+)-Methyl (*S*)-3-hydroxybutyrate	9.84±0.24	0	0.20±0.02	9.81±0.17	0.69±0.24	12.1±0.32
(-)-Methyl (*R*)-3-hydroxybutyrate	5.41±0.22	0	0.30±0.03	5.34±0.08	1.03±0.14	7.05±0.38
E(*R*)CHB[2]	105.95±0.03	0	2.31±0.06	104.9±1.8	0	105.9±4.7
E(*S*)CHB[2]	108.7±1.9	0	4.72±0.16	106.1±2.2	80.69±4.05	187.8±2.8
(−)-Methyl (*R*)-lactate	26.09±2.15	0	0.64±0.11	28.46±0.38	3.25±0.04	29.45±6.9
(+)-Methyl (*S*)-lactate	62.72±0.56	0	2.39±0.01	68.57±0.11	4.54±0.06	78.39±2.61
(−)-Ethyl (*R*)-lactate	24.38±0.58	0	0.7±0.01	27.32±0.48	2.45±0.08	36.12±2.75
(+)-Ethyl (*S*)-lactate	130.83±2.59	0	2.76±0.09	128.9±2.9	9.13±0.30	139.3±3.2
Methyl (2*R*)-2-phenylpropanoate	61.0±2.9	0	63.2±0.13	65.0±0.6	526.0±11.8	597.0±21.0
Methyl (2*S*)-2-phenylpropanoate	59.2±2.5	0	59.8±0.09	63.0±1.9	0	64.00±0.10

[1]Note: the number of esters found as potential substrates by Santiago et al. (2018) for $EH1_A$ was 72[1]. However, two of the esters found to not be hydrolyzed in the previous study were substituted by two new esters found to be converted, namely, methyl-2-bromobutyrate instead of triolein and methyl 2-phenyl propanoate instead of glyceryl tri-laurate. Additionally, ethyl acetate, ethyl benzoate and D-pantolactone, for which conversion was detected below the detection limit under the conditions used by Santiago et al. (2018)[1], were hydrolyzed in the substrate saturation conditions used in this study.

[2]Abbreviation as follows: Benzoic acid, 4-formyl-, phenylmethyl ester [BFPME]; Benzyl (*R*)-(+)-2-hydroxy-3-phenylpropionate [BHPP]; Ethyl (*R*)-(+)-4-chloro-3-hydroxybutyrate [E(R)CHB]; Ethyl (*S*)-(−)-4-chloro-3-hydroxybutyrate [E(S)CHB].

Supplementary Table 1 cont. Kinetic parameters. K_m (mM) for $EH1_{A1}$, $EH1_{B1}$ and $EH1_{AB1}$ sub-enzymes against a set of structurally different esters. The assays, in triplicates for each concentration, were performed as in Supplementary Figure 2 legend. The standard deviation of the simple hyperbolic fit with Sigma Plot 13.0 is shown.

	K_m (mM)[2]		
Ester[1]	**$EH1_{A1}$**	**$EH1_{B1}$**	**$EH1_{AB1}$**

Glyceryl triacetate	0.251±0.05	0.360±0.056	0.259±0.059
Glyceryl tripropionate	0.272±0.05	0.725±0.040	0.332±0.032
Glyceryl tributyrate	0.510±0.17	8.00±0.51	0.547±0.047
Methyl-2-bromobutyrate	5.53±0.03	-	5.20±0.082
Ethyl acetate	0.592±0.033	7.30±0.15	0.610±0.061
Propyl acetate	3.23±0.45	-	3.26±0.08
Butyl acetate	0.495±0.056	0.310±0.025	0.393±0.029
Hexyl acetate	0.405±0.069	1.41±0.04	1.82±0.08
Octyl acetate	1.05±0.10	0.620±0.075	1.30±0.03
Methyl butyrate	1.67±0.08	1.24±0.03	2.84±0.02
Methyl hexanoate	4.92±0.09	0.685±0.018	5.02±0.10
Methyl octanoate	0.930±0.110	0.225±0.037	1.05±0.10
Methyl decanoate	5.20±0.07	8.28±0.06	6.50±0.05
Ethyl propionate	7.03±0.08	5.55±0.06	6.76±0.07
Ethyl butyrate	8.86±0.22	9.28±0.09	9.70±0.07
Ethyl hexanoate	4.70±0.07	32.80±0.12	5.54±0.05
Ethyl octanoate	7.12±0.05	5.45±0.071	8.78±0.07
Ethyl decanoate	7.45±0.08	-	7.64±0.06
Ethyl dodecanoate	9.05±0.08	-	8.89±0.08
Propyl propionate	8.07±0.15	-	8.03±0.05
Propyl butyrate	5.52±0.05	-	5.19±0.12
Propyl hexanoate	0.512±0.057	1.16±0.04	0.747±0.045
Ethyl 2-ethylacetoacetate	0.420±0.031	0.493±0.150	0.850±0.058
Ethyl 2-methylacetoacetate	0.322±0.076	0.690±0.088	0.608±0.061
Ethyl 3-oxohexanoate	0.732±0.056	0.710±0.136	0.741±0.041
Ethyl acetoacetate	0.712±0.064	0.838±0.076	0.765±0.077
Ethyl propionylacetate	1.03±0.07	0.940±0.063	1.43±0.04
Methyl glycolate	0.602±0.145	0.740±0.075	0.658±0.046
Vinyl acetate	0.887±0.087	0.268±0.078	1.03±0.03
Vinyl propionate	0.927±0.098	0.475±0.082	0.725±0.073
Vinyl butyrate	0.835±0.192	0.215±0.045	0.948±0.048
Vinyl laurate	9.57±0.04	1.04±0.11	10.87±0.08
Vinyl benzoate	0.743±0.057	0.253±0.102	0.767±0.077
Vinyl crotonate	9.15±0.17	0.548±0.067	0.550±0.055
Vinyl acrylate	9.13±0.19	-	9.16±0.04
Geranyl acetate	0.592±0.056	0.290±0.040	0.480±0.048
3-Methyl-3-buten-1-yl acetate	0.582±0.065	0.490±0.092	0.953±0.050
Methyl benzoate	6.67±0.03	0.740±0.101	6.56±0.05
Ethyl benzoate	5.13±0.03	-	5.18±0.07
n-Pentyl benzoate	35.17±0.77	0.970±0.025	35.69±0.17
Ethyl 2-chlorobenzoate	16.00±0.04	1.38±0.05	16.72±0.07
Methyl 2-hydroxybenzoate	8.45±0.09	-	8.50±0.05
Methyl 3-hydroxybenzoate	12.33±0.56	0.180±0.020	0.19±0.01
Propyl 4-hydroxybenzoate	12.85±0.54	0.783±0.079	10.59±0.05
Butyl 4-hydroxybenzoate	15.85±0.04	0.958±0.080	16.55±0.05
Phenyl acetate	0.08±0.01	1.05±0.02	0.445±0.045
Phenyl propionate	0.965±0.03	0.703±0.122	0.998±0.100
Phthalic acid diethyl ester	1.12±0.08	-	1.06±0.06
Isobutyl cinnamate	2.52±0.05	1.04±0.10	2.70±0.071

Methyl 2.5-dihydroxycinnamate	4.50±0.062	-	4.53±0.06
Methyl cinnamate	3.241±0.03	1.41±0.06	4.23±0.02
Methyl ferulate	35.37±0.05	5.33±0.31	40.19±0.20
1-Napthyl acetate	0.422±0.050	0.775±0.053	0.530±0.013
1-Naphthyl butyrate	0.307±0.044	0.520±0.093	0.350±0.015
Benzyl 4-hydroxybenzoate	0.492±0.062	0.573±0.027	0.497±0.020
BFPME[1]	1.19±0.09	0.570±0.053	1.17±0.02
BHPP[1]	0.532±0.063	0.503±0.031	0.560±0.026
Phenylethyl cinnamate	17.32±0.42	38.30±3.93	20.21±0.02
ϒ-Valerolactone	1.02±0.04	8.00±0.245	1.15±0.01
D-Pantolactone	9.15±0.03	-	9.17±0.02
Cyclohexyl butyrate	1.21±0.03	0.497±0.096	1.20±0.02
Glucose pentaacetate	0.55±0.03	21.0±0.092	0.600±0.010
(1*R*)-(-)-Menthyl acetate	6.55±0.03	-	6.48±0.04
(1*S*)-(+)-Menthyl acetate	6.75±0.03	-	6.24±0.02
Methyl (*R*)-(-)-mandelate	5.22±0.07	-	5.19±0.01
Methyl (*S*)-(+)-mandelate	6.60±0.49	-	6.45±0.01
(−)-Methyl (*R*)-3-hydroxyvalerate	0.625±0.082	-	0.593±0.049
(+)-Methyl (*S*)-3-hydroxyvalerate	0.463±0.069	-	0.468±0.119
(+)-Methyl (*S*)-3-hydroxybutyrate	0.714±0.066	4.38±0.153	4.93±0.09
(-)-Methyl (*R*)-3-hydroxybutyrate	0.930±0.088	5.03±0.014	5.54±0.06
E(*R*)CHB[2]	4.71±0.063	-	4.69±0.05
E(*S*)CHB[2]	7.50±0.086	0.610±0.039	0.758±0.076
(−)-Methyl (*R*)-Lactate	2.25±0.089	0.620±0.075	0.637±0.064
(+)-Methyl (*S*)-Lactate	0.798±0.180	0.353±0.05	0.680±0.068
(−)-Ethyl (*R*)-Lactate	0.637±0.066	0.453±0.018	0.747±0.075
(+)-Ethyl (S)-lactate	0.690±0.049	0.473±0.037	1.62±0.16
Methyl (2*R*)-2-phenylpropanoate	21.10±1.80	0.33±0.02	0.44±0.03
Methyl (2*S*)-2-phenylpropanoate	22.40±3.20	-	22.10±2.20

[1]Abbreviation as follows: Benzoic acid, 4-formyl-, phenylmethyl ester [BFPME]; Benzyl (*R*)-(+)-2-hydroxy-3-phenylpropionate [BHPP]; Ethyl (*R*)-(+)-4-chloro-3-hydroxybutyrate [E(R)CHB]; Ethyl (*S*)-(−)-4-chloro-3-hydroxybutyrate [E(S)CHB].

[2]Michaelis-Menten fits for K_m determinations for each ester and sub-enzyme are provided in separate Supplementary files (file named K_M determinations fits). In the figures, created with the R language from average values or triplicates, the normalized μmol/minmL for each of the ester concentrations, is given.

Supplementary Table 2 Kinetic parameters of $EH1_{A1}$, $EH1_{B1}$ and $EH1_{AB1}$, for three model esters preferentially hydrolyzed by $EH1_{B1}$. The assays, in triplicates for each cocnetration, were performed as described in Supplementary Figure 2 legend. The standard deviation of the simple hyperbolic fit with Sigma Plot 13.0 is shown. The Michaelis-Menten fits for K_m determinations are provided below the table; the figures represent the average value of triplicates (calculated using Excel version 2019) of enzyme activity (μmol/min mL) of each sub-enzyme at different ester concentrations.

Substrates	Methyl 3-hydroxybenzoate	
	K_m (mM)	k_{cat} (min^{-1})
$EH1_{A1}$	12.33±0.56	0.83±0.02
$EH1_{B1}$	0.18±0.02	58.3±0.3
$EH1_{AB1}$	0.19±0.01	61.26±0.47
	Methyl (2*R*)-2-phenylpropanoate	

EH1$_{A1}$	21.1±1.8	65.0±0.6
EH1$_{B1}$	0.33±0.02	526.0±11.8
EH1$_{AB1}$	0.44±0.03	597.0±21.0
	Methyl (2*S*)-2-phenylpropanoate	
EH1$_{A1}$	22.4±3.2	63.0±1.9
EH1$_{B1}$	-	-
EH1$_{AB1}$	27.1±2.2	64.0±1.6

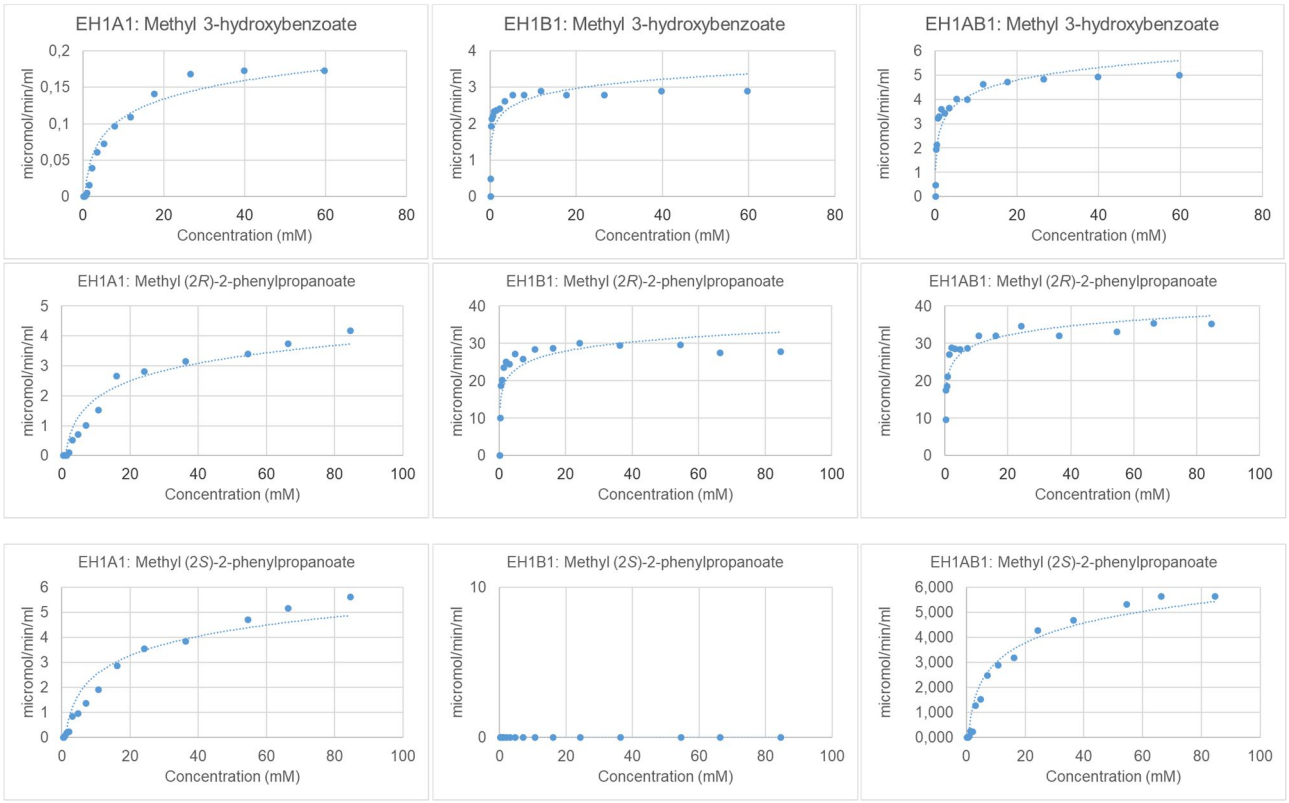

When examining EH1$_{B1}$ we found that the R23G mutation increased significantly the k_{cat} of the artificial site up to ca. 13.7±0.1 s^{-1}, and expanded the substrate spectrum to 58 chemically and structurally diverse esters (Supplementary Figure 2; Supplementary Table 1). Note that previous EH1$_B$ design was only capable of hydrolyzing 24 esters at a max. k_{cat} of 0.03 s^{-1}. This may be a direct consequence of disabling the Asp25-Arg23 interaction after R23G mutation such that Asp25, which is part of the artificial catalytic triad, can be better oriented towards the catalytic histidine (Supplementary Figure 1). Arg23 may also restrict substrate accessibility in the artificial site, and its mutation to Gly has a large effect in reducing these constraints such that the remodeled active site can accommodate larger substrates. The catalytic turnover of EH1$_{B1}$ is above those of the best artificial enzymes obtained to date, which achieved k_{cat} ca. 1 to 5 s^{-1} in best cases, and in the range of the "mother" enzyme (EH1$_{A1}$), capable of hydrolyzing 78 diverse esters with a max. k_{cat} of ca. 45.2±0.1 s^{-1}. We also found that EH1$_{B1}$ was stereo-specific by meaning of e.e. values obtained for the kinetic resolution of a racemic mixture of methyl (2*R*/*S*)-2-phenylpropanoate (E-value >1000; *R*-specificity), as determined by GC analysis (see Supplementary Methods). Therefore, compared to the original EH1$_B$ design, remodeling of the artificial site through a R23G mutation not only broadens its substrate spectra and increases prominently its hydrolytic rate, but also introduces stereo-preference (using as target reaction the kinetic resolution of a racemic mixture of methyl (2*R*/*S*)-2-phenylpropanoate), a feature that do not characterize neither the original EH1$_B$ design nor the native EH1$_{A1}$ site (see above).

Catalytic advantages of having two active sites in an ester-hydrolase

We further found that the incorporation of the remodeled additional site ($EH1_{B1}$) into the "mother" serine ester-hydrolase ($EH1_{A1}$) produced an artificial variant ($EH1_{AB1}$) with the ability to hydrolyze all 78 substrates that $EH1_{A1}$ and $EH1_{B1}$, combined, were able to convert (Supplementary Figure 2; Supplementary Table 1). The k_{cat} values of $EH1_{AB1}$ were close to the sum of the individual values from each site, with a maximum value of ca. 57.8±0.2 s^{-1} (Supplementary Table 1). Note that previous $EH1_{AB}$ design was only capable of hydrolyzing esters converted by the native and artificial sites at a max. k_{cat} of 1.35±0.03 s^{-1}. The significant higher k_{cat} for $EH1_{AB1}$ is a direct consequence of the increased catalytic performance of the remodeled extra site compared to the original design. The incorporation of $EH1_{B1}$ site was also found to intensify the k_{cat}/K_m of the "mother" $EH1_{A1}$ enzyme by up to ca. 5000-fold due to the differences in affinities and k_{cat} (Supplementary Figure 2; Supplementary Table 1; Supplementary Table 2), as some of the esters showed both a significantly higher affinity and turnover rate for the artificial remodeled site compared to the native site. $EH1_{AB1}$ was also stereo-specific by meaning of e.e. values obtained for the kinetic resolution of a racemic mixture of methyl (2*R*/*S*)-2-phenylpropanoate (E-value ~1380; *R*-specificity), as determined by GC analysis (see Supplementary Methods).

Finally, we should highlight that the analysis of the optimal temperature demonstrated that the artificial site when introduced to the "mother" $EH1_{A1}$ ester-hydrolase broadens the catalytic temperature window of the later (Fig. 2c main text, Supplementary Figure 3). Thus, using glyceryl tripropionate, one of the preferred substrates, we found that $EH1_{A1}$ is most activity at 35-45ºC, with the activity progressively reduced outside this range. $EH1_{B1}$ exhibited the reverse of this trend —it was strongly inactivated at temperatures above 35ºC, and more active at 8-35ºC. The enzyme with two reactive sites ($EH1_{AB1}$) exhibited a hybrid pattern, being most active at 8-45ºC. The two-active site enzyme thus retained the psychrophilic-like phenotype of the native site and the mesophilic-like phenotype introduced by the extra active site. As shown in Fig. 3, the addition of the extra site increased by *ca*. 20ºC the range of temperature at which the original enzyme retained more than 80% of its activity. It is plausible that the remodeled artificial site is less stable, probably because of the different configurations and positioning (larger exposure to the solvent) of the catalytic residues, which are differentially affected by thermal conditions. The higher activity at low temperatures may be associated with an easier diffusion of the substrates in the remodeled site, compared to the native site, due to its larger solvent exposure.

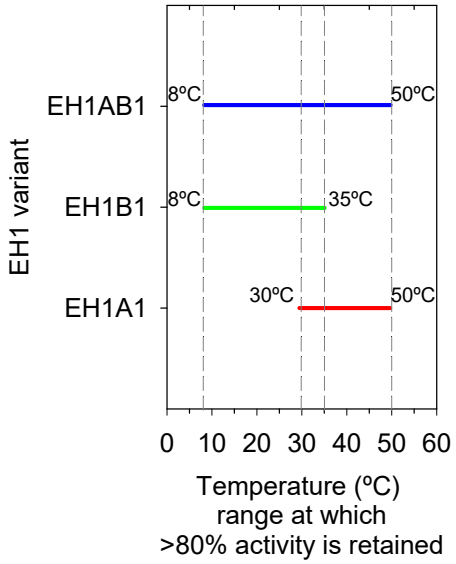

Supplementary Figure 3 Temperature range at which the $EH1_{A1}$, $EH1_{B1}$ and $EH1_{AB1}$ sub-enzymes retained more than 80% of the optimal activity. Data extracted from Fig. 2c in main text.

Together, through an in deep kinetic characterization of the substrate specificity, we demonstrated that a R23G mutation allowed remodeling a sub-optimal and low performance artificial site (k_{cat} of *ca*. 0.03 s^{-1}; capable of converting 24 esters but not any chiral esters among those tested) into a catalytically efficient one (k_{cat} up to *ca*. 14 s^{-1}; capable of converting 58 esters; >99.9% e.e.; T_{opt} *ca*. 30ºC). Its addition to the "mother" ester-hydrolase (k_{cat} ca. 45 s^{-1}; capable of converting 78 esters; e.e. *ca*. 50%; T_{opt} *ca*. 35-45ºC) was found to increase the catalytic performance of the later, as it boosted the conversion rates (up to *ca*. 57.8±0.2 s^{-1}) and the stereo-selectivity (>99.9% e.e.), and expanded the operational condition by 20ºC considering at least 80% of the activity at the optimal temperature (T_{opt} *ca*. 8-45ºC), because the additive effects of each of the sites. A catalytically efficient *plurizyme* with two enzymatic active sites capable of ester-hydrolysis was thus designed. We would like to highlight that in this study we added in our *plurizyme* design two enzymatic active sites with same chemistry catalyzed, namely ester hydrolysis.

Supplementary Note 3:

Crystallization and X-ray structure of the genetically engineered & remodeled *plurizyme*

Determination of EH1$_{AB1}$ structure and its complex with the suicide inhibitor methyl 4-nitrophenyl hexylphosphonate (M-4NHP)

Stereo views of the electron density map at the Ser161 and Ser211 catalytic sites in the free and complexed crystals with M-4NHP are provided in Supplementary Figures 4-5.

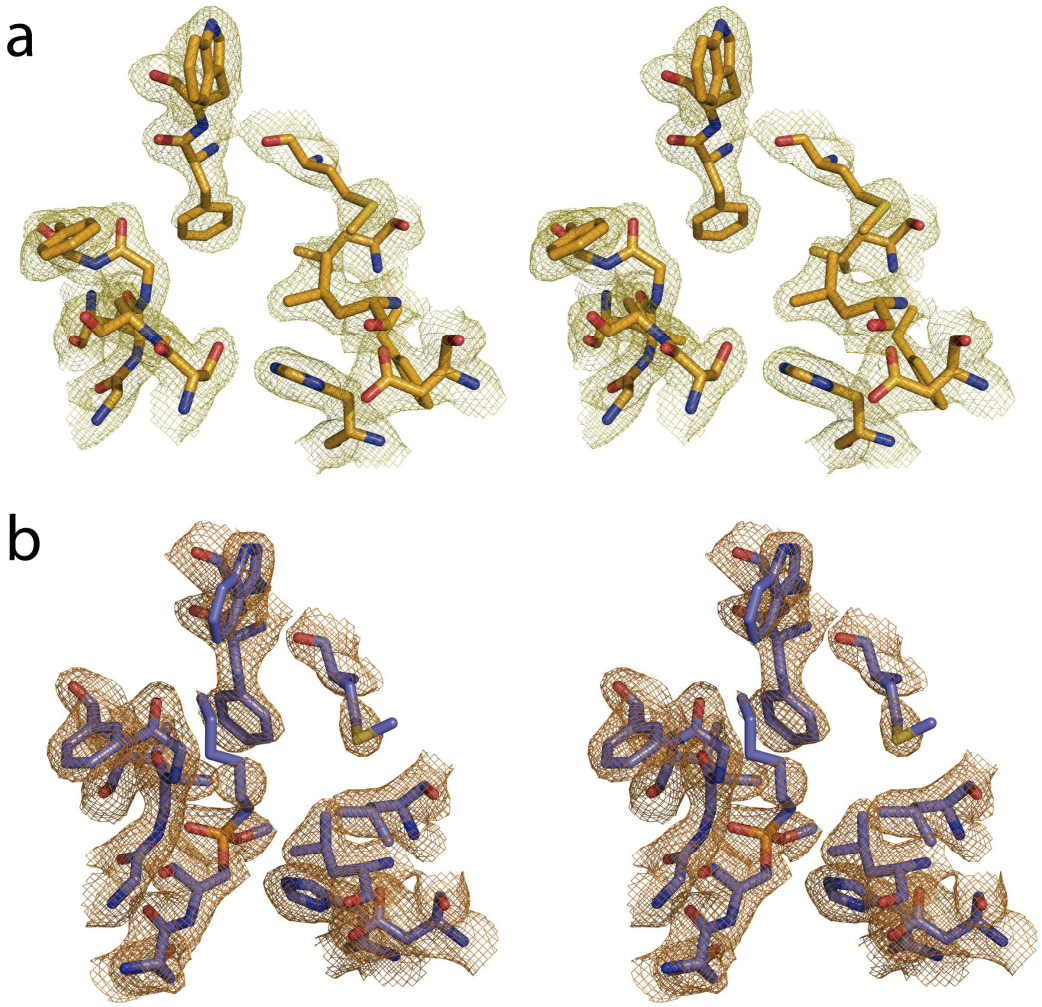

Supplementary Figure 4 Stereo view of the electron density map at the Ser161 catalytic site in the free (a) and complexed (b) crystals. The 2Fo-Fc map is contoured a 1.0 σ.

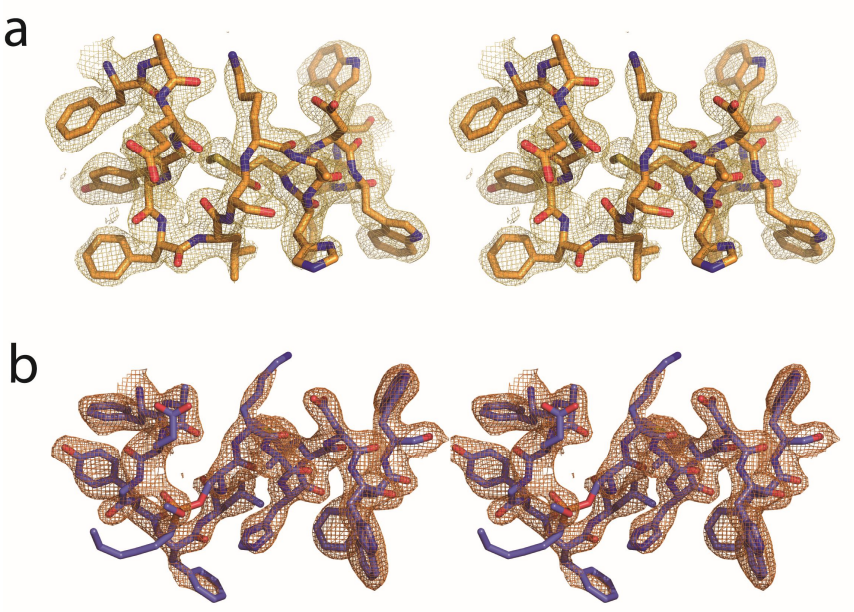

Supplementary Figure 5 Stereo view of the electron density map at helix Phe204-Trp219, containing the Ser 211/His214 motif, in the free (a) and complexed (b) crystals. The 2Fo-Fc map is contoured a 0.9 σ.

Crystal structure of $EH1_{AB1}$ / CuSI complex

The electron density map of the *$EH1_{AB1}$ / CuSI* complex obtained by cocrystallization, showing the Ser161 but not the Ser211 labelled with CuSI, is provided in Supplementary Figure 6.

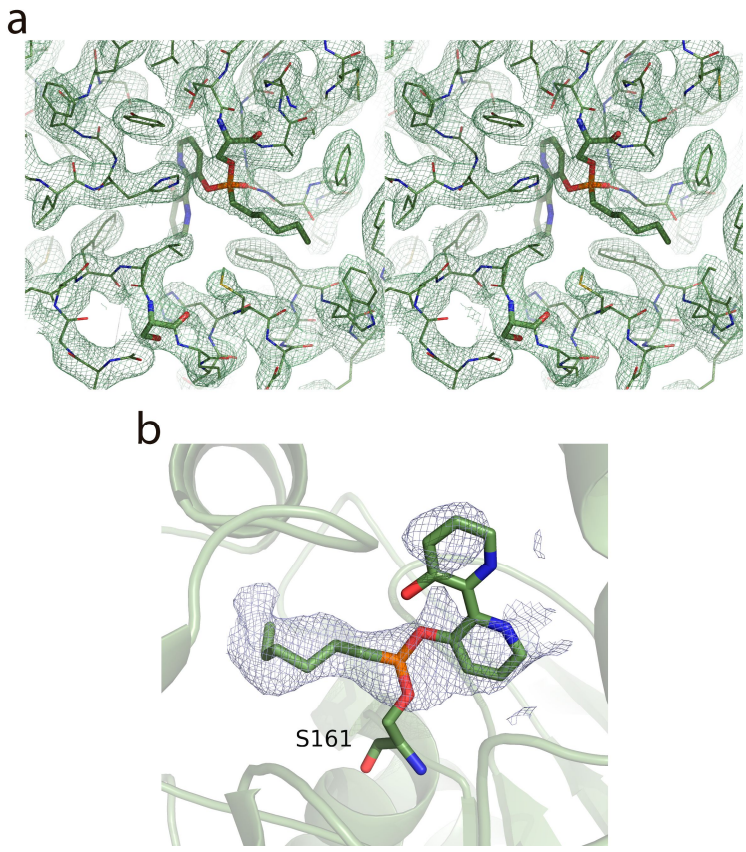

Supplementary Figure 6 (a) Stereo view of the electron density map of the complex, showing the Ser161 labelled with CuSI, and the free Ser211 highligthed as wider sticks. The final 2Fo-Fc

map is contoured a 1.0 σ cut-off. (b) Detail of the $EH1_{AB1}$ native active site showing the CuSI complex attached to Ser161 and the Polder omit map calculated at 3.0 s cut-off.

Supplementary Note 4:

Suicide inhibitors as substrates for $EH1_{AB1}$ *plurizyme* crystallization

As substrates for cocrystallization and for obtaining complexed crystals we used the so-called suicide inhibitors, namely, methyl, butyl and octyl 4-nitrophenyl hexylphosphonate (EUCODIS Bioscience GmbH, Vienna, Austria). The 4-nitrophenyl phosphonate inhibitors are susceptible to nucleophilic attack by the catalytic Ser of the active site of lipases and related enzymes. This leads to stable covalent modification of the serine residue in the active site and complete inactivation of the enzyme[3,4]. According to our inhibition experiments, treatment with M4-4NHP (also butyl-4NHP) resulted in inactivation of >99% for $EH1_{A1}$, $EH1_{B1}$ and $EH1_{AB1}$ when tested with glyceryl tripropionate (Supplementary Figure 7) in less than 20 sec. This substrate can thus be used for crystallographic structural analysis (co-crystallization) because of irreversible binding to the corresponding Ser161 and Ser211 catalytic nucleophiles.

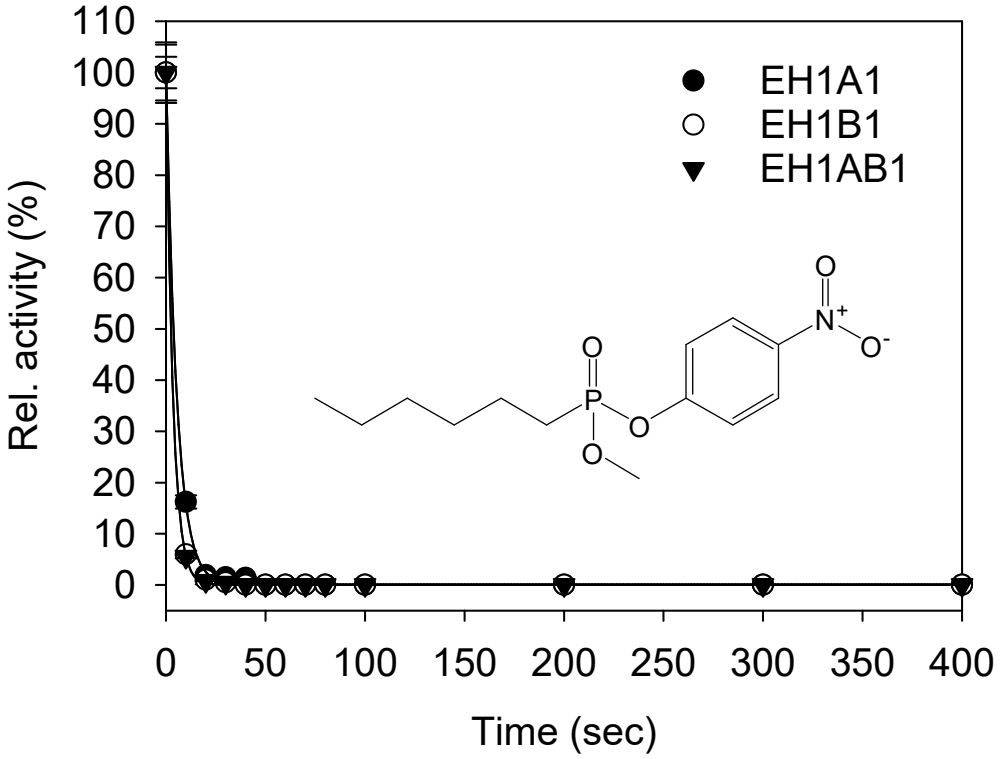

Supplementary Figure 7 Inhibition of $EH1_{A1}$, $EH1_{B1}$ and $EH1_{AB1}$ sub-enzymes by M4-4NHP. Experimental conditions as follow. For inhibition experiment - [sub-enzyme]: 7.5 mM; [inhibitor]: 30 mM; volume: 500 µl; T: 25ºC; pH: 7.5; incubation time: 0-400 sec. For activity test - [protein]: 1.7 mM; [glyceryl tripropionate]: 50 mM; reaction volume: 44 µl; T: 30ºC; pH: 8.0. Values are percentages of inhibition of the indicated sub-enzyme in comparison to enzyme activity without inhibitor. Reactions were performed in triplicates with average value and standard deviations (calculated using Excel version 2019) indicated. The structure of M4-4NHP is shown. Fits were performed using single exponential decay with Sigma Plot 13.0.

Supplementary Note 5:

Synthesis of 3'-hydroxy-[2,2'-bipyridin]-3-yl methyl hexylphosphonate

Supplementary Scheme 1 summarizes the synthesis the of 3'-hydroxy-[2,2'-bipyridin]-3-yl methyl hexylphosphonate (see details in Supplementary Methods). The product was obtained as brown oil and contained 5% of 2,2‘-bipyridine-3,3‘-diol.

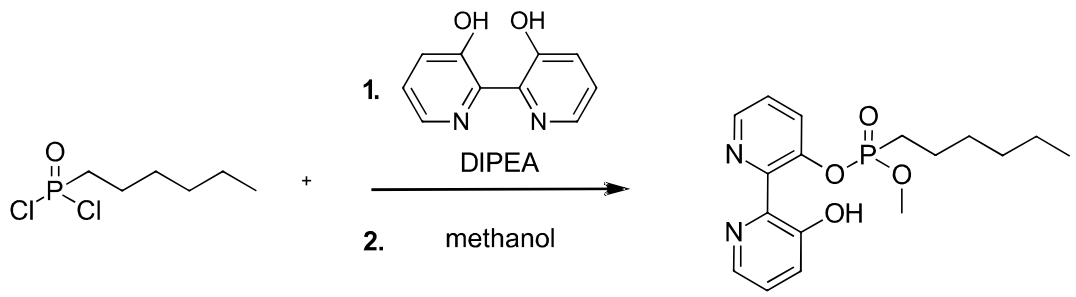

Supplementary Scheme 1 One pot reaction for the synthesis of 3'-hydroxy-[2,2'-bipyridin]-3-yl methyl hexylphosphonate.

The structure confirmation was performed by ^{1}H NMR, ^{13}C NMR, ^{31}P NMR and HR-MS as detailed in Supplementary Figures 8-10.

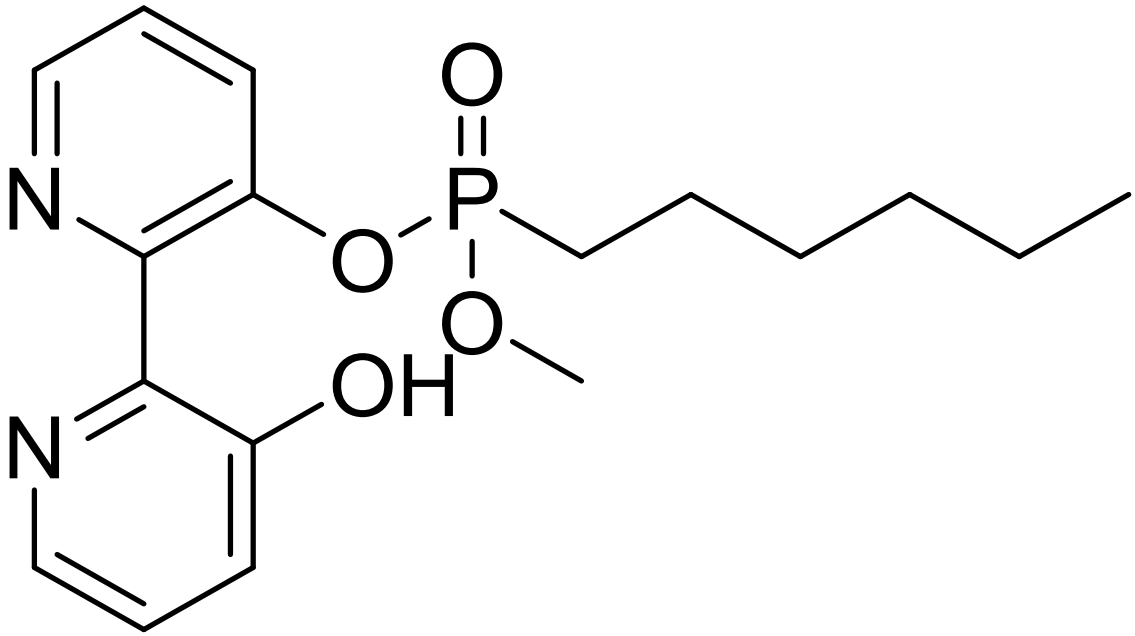

FW ($C_{17}H_{23}N_2O_4P$) = 350.35 g mol^{-1}

Yield: 80 mg brown oil (52% yield) containing 5% of starting material.

^{1}H NMR (600 MHz, Methanol-d_4) δ 8.49 (d, J = 4.6 Hz, 1H), 8.20 – 8.14 (m, 1H), 7.94 (dt, J = 8.4, 1.2 Hz, 1H), 7.55 (dd, J = 8.4, 4.8 Hz, 1H), 7.42 – 7.36 (m, 2H), 3.72 (d, J = 11.3 Hz, 3H), 2.02 – 1.69 (m, 2H), 1.48 – 1.35 (m, 2H), 1.34 – 1.16 (m, 6H), 0.89 (t, J = 7.2 Hz, 3H).

^{13}C NMR (150 MHz, MeOD) δ 154.99, 149.64 (d, J = 5.7 Hz), 147.28 (d, J = 8.9 Hz), 145.65, 142.46, 140.77, 131.35, 126.79, 126.00, 125.58, 53.78 (d, J = 7.2 Hz), 32.36, 31.10 (d, J = 17.7 Hz), 25.90 (d, J = 139.5 Hz), 23.42, 23.03 (d, J = 6.1 Hz), 14.34.

^{31}P NMR (MeOD) δ 31.92.

HR-MS m/z calcd. for $C_{17}H_{24}N_2O_4P$ $[M+H]^+$: 351.14682, found: 351.14681.

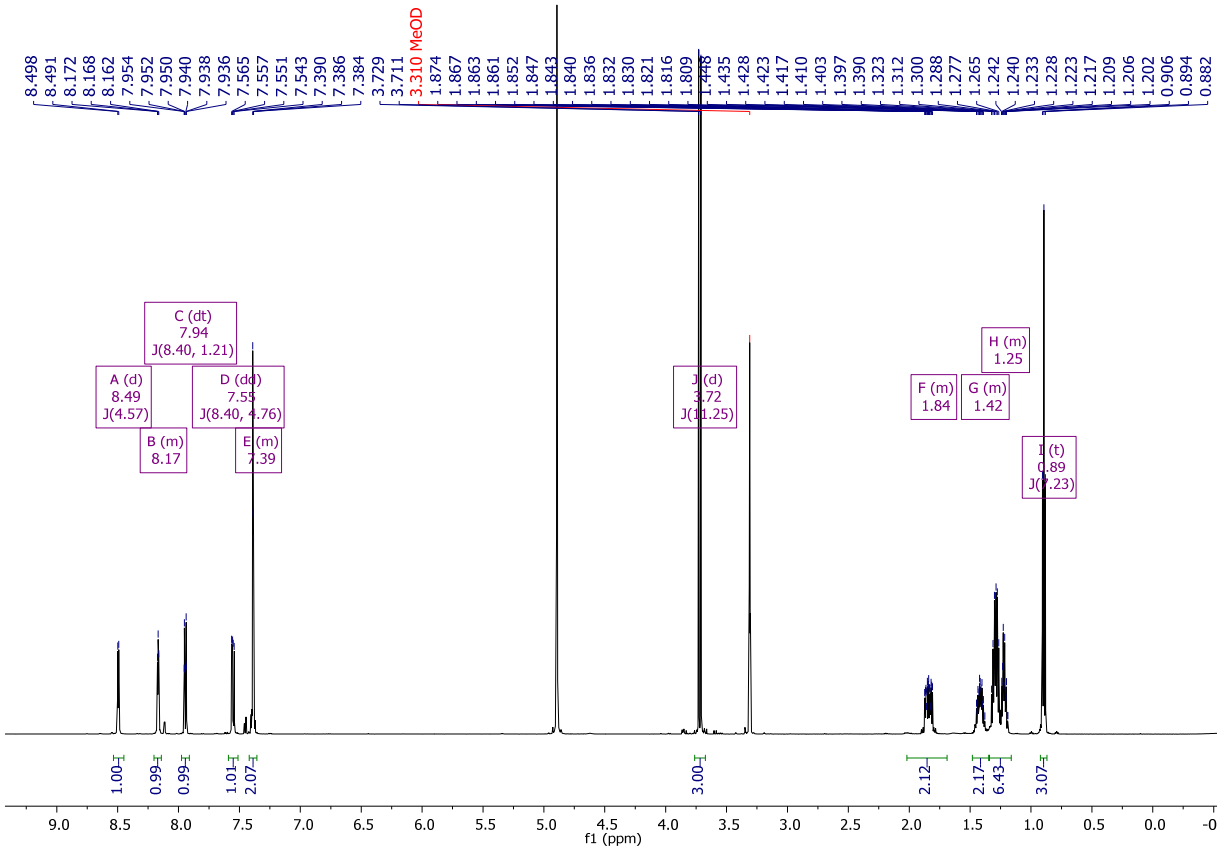

286

287 **Supplementary Figure 8** ^{1}H spectrum

288

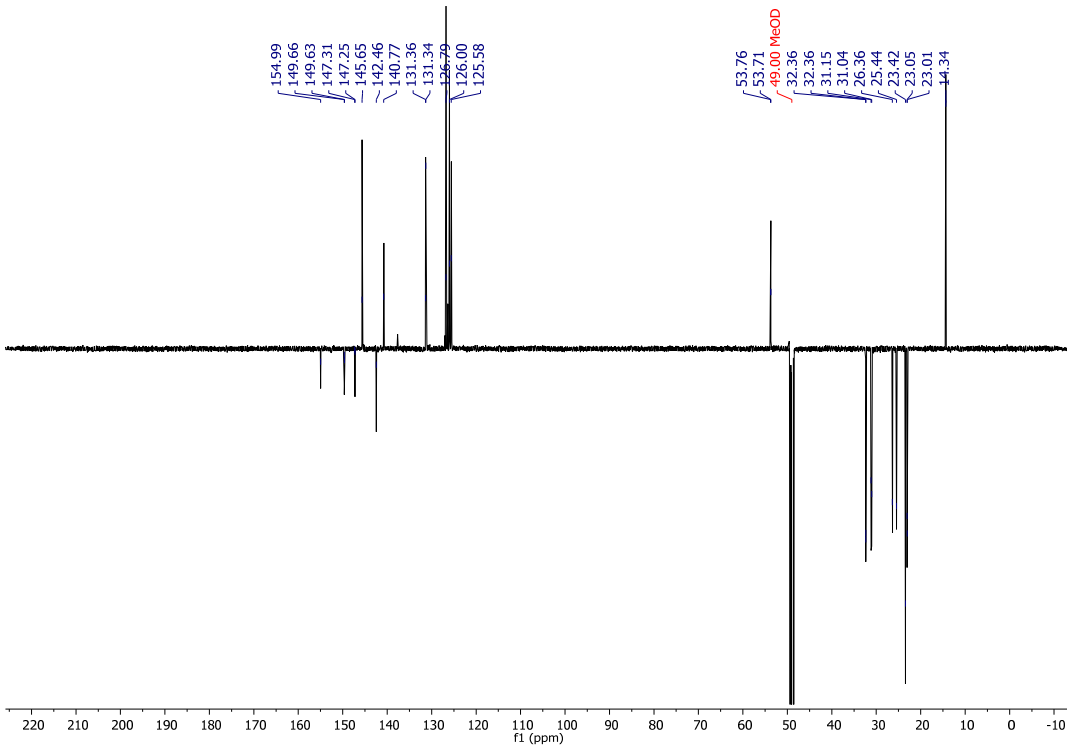

289

290 **Supplementary Figure 9** ^{13}C spectrum

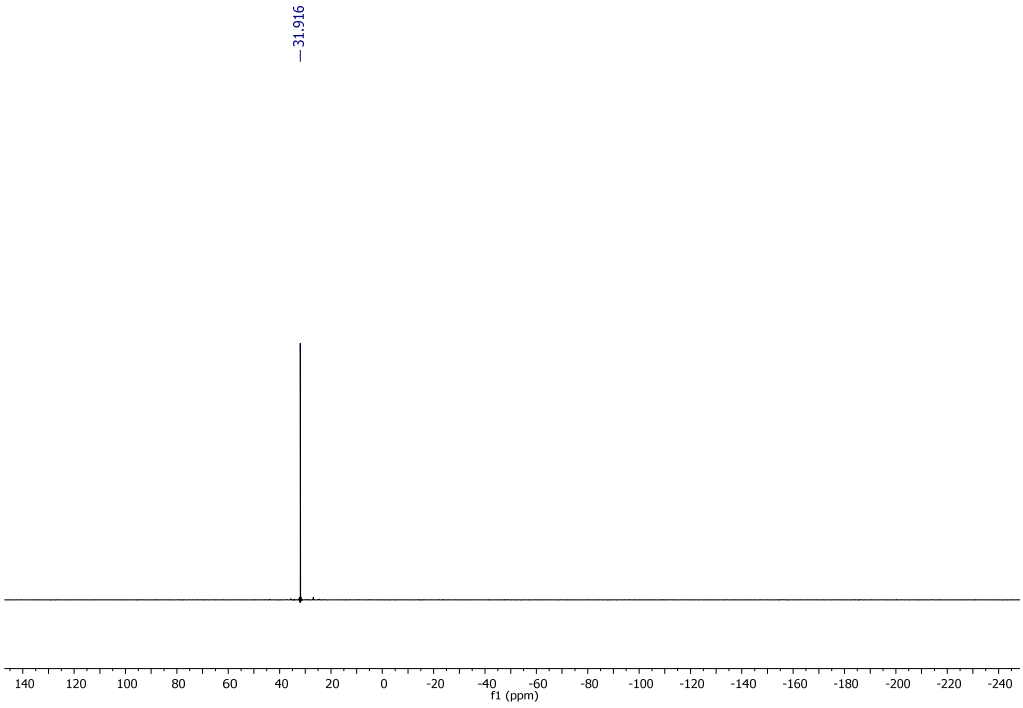

Supplementary Figure 10 ^{31}P spectrum

Supplementary Note 6:

Under excess conditions biochemical enzyme modification with 3'-hydroxy-[2,2'-bipyridin]-3-yl methyl hexylphosphonate occurs at both biological active sites

Inhibition tests under excess of inhibitor

According to our inhibition experiments (Supplementary Figure 11), treatment with an excess of 3'-hydroxy-[2,2'-bipyridin]-3-yl methyl hexylphosphonate resulted in inactivation of >99% for $EH1_{A1}$, $EH1_{B1}$ and $EH1_{AB1}$ when tested with glyceryl tripropionate. This substrate can thus be used for incorporating copper-bipyridine catalyst because of irreversible binding to the corresponding nucleophiles: Ser161 in $EH1_{A1}$, Ser211 in $EH1_{B1}$ and Ser161 and Ser211 in $EH1_{AB1}$.

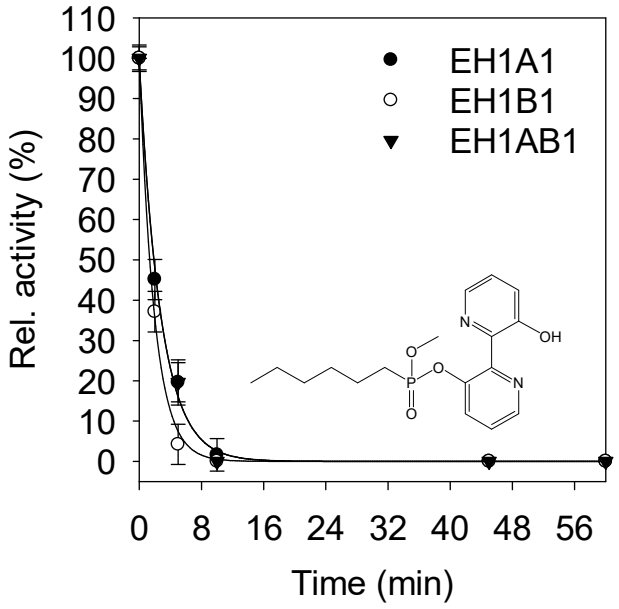

Supplementary Figure 11 Small-scale inhibition test of $EH1_{A1}$, $EH1_{B1}$ and $EH1_{AB1}$ sub-enzymes by 3'-hydroxy-[2,2'-bipyridin]-3-yl methyl hexylphosphonate (SI). Experimental

conditions as follow. For inhibition experiment - [sub-enzyme]: 15 µM; [inhibitor]: 120 µM; volume: 250 µl; T: 25ºC; pH: 6.5; incubation time: 0-60 min. For activity test - [protein]: 3.4 µM; [glyceryl tripropionate]: 50 mM; reaction volume: 44 µl; T: 30ºC; pH: 8.0. Values are percentages of inhibition (in triplicates with standard deviation calculated using Excel version 2019) of the indicated sub-enzyme in comparison to enzyme activity without inhibitor. The structure of the SI inhibitor is shown. Fits were performed using single exponential decay with Sigma Plot 13.0.

Electrochemical characterization of sub-enzymes modified with SICu under excess conditions

The incorporation of the Cu^{2+}-organic complex was evaluated by recording its redox properties. For that, we analysed the electrochemical response on differently modified gold electrodes for the following entities: (*i*) sub-enzymes $EH1_{A1}$, $EH1_{B1}$ and $EH1_{AB1}$ into which SICu was incorporated or not as described above, and (*ii*) SICu prior to its incorporation in the sub-enzymes. The modification of gold electrodes was performed by the formation of self-assembled monolayers (SAMs) of different thiols: 4-aminothiophenol (AmTP), 6-mercapto-1-hexanol (MH), 6,8-dihydrolipoic acid (TOA), mercaptoundecanoic acid (MUA) and 3-mercaptopropanoic acid (MPA). A schematic representation of an electrode surface modified by self-assembled monolayers and modified sub-enzymes is shown in Supplementary Figure 12.

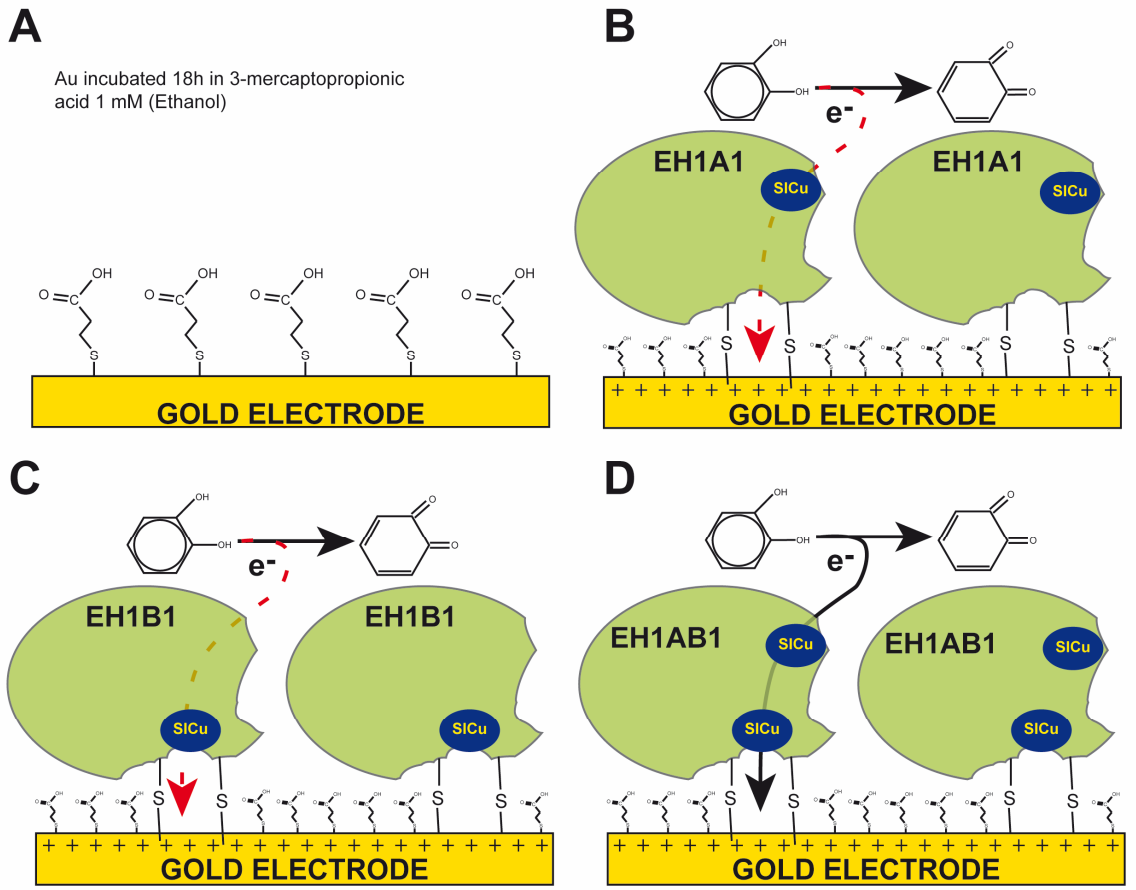

Supplementary Figure 12 Schematic representation of the immobilized SICu-modified sub-enzymes in the gold electrode. The image shows a schematic representation, which may not represent the exact positioning of each of the active sites within the protein and towards the electrodes.

The first measurement is a control of the signal provided by the Cu^{2+}-modified SI inhibitor, SICu, compared to the separate substrate inhibitor (SI) and copper nitrate. Different behaviour between the free Cu^{2+}-organic complex and the SICu complex was observed (Supplementary Figure 13).

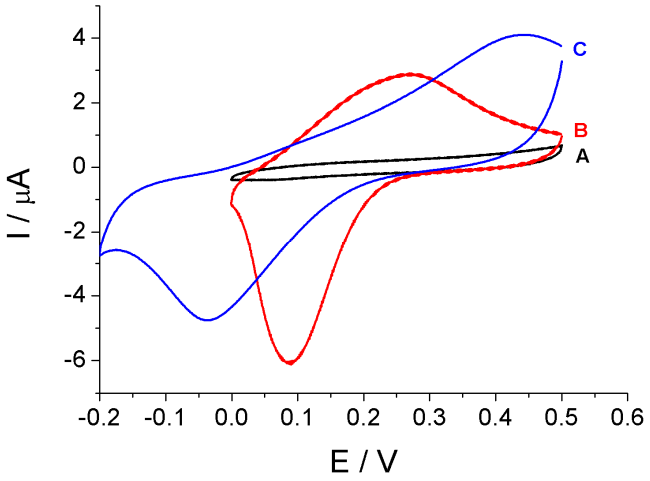

Supplementary Figure 13 Cyclic voltammetry measurements of (A) the substrate inhibitor (SI), (B) copper nitrate and (C) SI after complexing with Cu^{2+}. All cyclic voltammograms were recorded using a 20 $mV \cdot s^{-1}$ scan rate and 50 mM phosphate buffer pH 6.5 electrolyte. The working electrode was a gold disk with a 0.2 cm^2 diameter modified with an MPA SAM. The reference electrode was 3 M Ag/AgCl, and the counter electrode was Pt wire. Reproducibility as in Fig. 5 legend.

The results with other self-assembled monolayers are shown in Supplementary Figures 14-15. In Supplementary Figure 14 we compare SICu response measured with either an amino-terminated thiol, 4-aminothiophenol (ATP) and hydroxyl-terminated thiol, 6-mercapto-1-hexanol (MH) or MPA. In Supplementary Figure 15 we compare $EH1_{A1}$ SICu signal *vs* different thioacids and different chain length: 11-mercaptoundecanoic acid (MUA), thioctic acid (TOA) and MPA. The electrode surface modified with MPA resulted in the best SAM agent tested to favour the enzyme electrostatic absorption. This result is attributed to two facts: the carboxylate moieties facing the solution and the short length of the chain, which produces the SAMs, are not very tightly assembled and allow substitution with other thiols. In the case of the EH1 enzyme, it is known that there are two methionine residues very close to the entrance channel in which the two active sites are located (Met13 and Met39). Therefore, it is expected that CuSI, after being socketed in the sub-enzyme active sites, may be observed electrochemically.

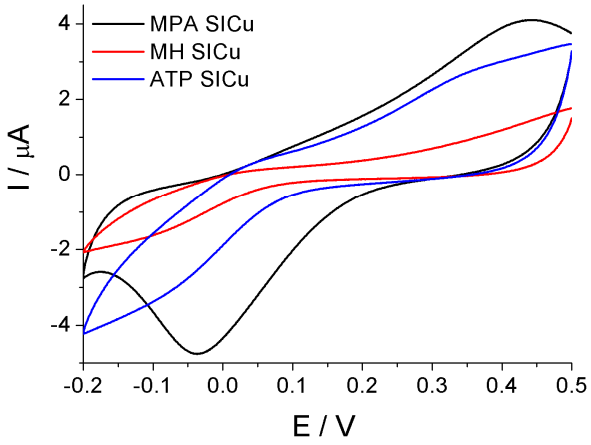

Supplementary Figure 14 Electrochemical characterization of SICu against differently charged self-assembled monolayers. Cyclic voltammetries of the copper-linked Substrate Inhibitor (SICu) *ca*. 0.43 mM measured with gold electrodes modified with either MPA, MH or ATP thiol monolayers. All the cyclic voltammograms were recorded using 100 $mV \cdot s^{-1}$ scan rate

and 50 mM phosphate buffer pH 6.5 electrolyte, the working electrode was a gold disk of 0.2 cm^2 diameter, the reference electrode was Ag/AgCl 3M, counter electrode was Pt wire. Reproducibility as in Fig. 5 legend.

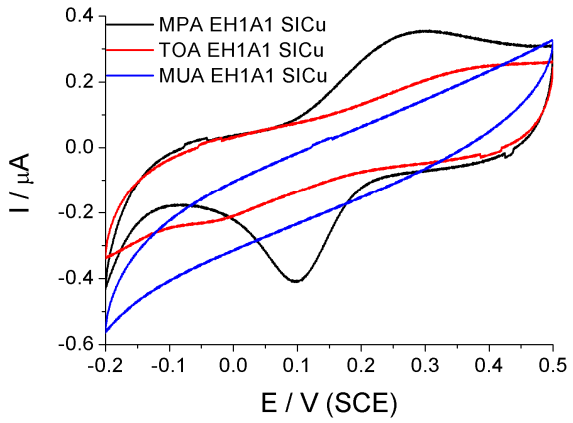

Supplementary Figure 15 Electrochemical characterization of $EH1_{A1}$ SICu on gold electrodes. Cyclic voltammetries of $EH1_{A1}$ SICu immobilized on gold electrodes modified with either MUA, TOA or MPA self-assembled monolayers. All the cyclic voltammograms were recorded using 100 $mV \cdot s^{-1}$ scan rate and 50 mM phosphate buffer pH 6.5 electrolyte, the working electrode was a gold disk of 0.2 cm^2 diameter modified with a MPA SAM, the reference electrode was Ag/AgCl 3M, counter electrode was Pt wire. Reproducibility as in Fig. 5 legend.

The activity of modified gold electrodes for catechol oxidation is shown in Supplementary Figures 16-17. The experimental results in Supplementary Figure 16 show that there is an interaction between catechol and the SICu deposited on the electrode. The signal obtained measuring catechol directly (Supplementary Figure 17a) is more irreversible and less intense than the one obtained in presence of SICu (Supplementary Figure 17b).

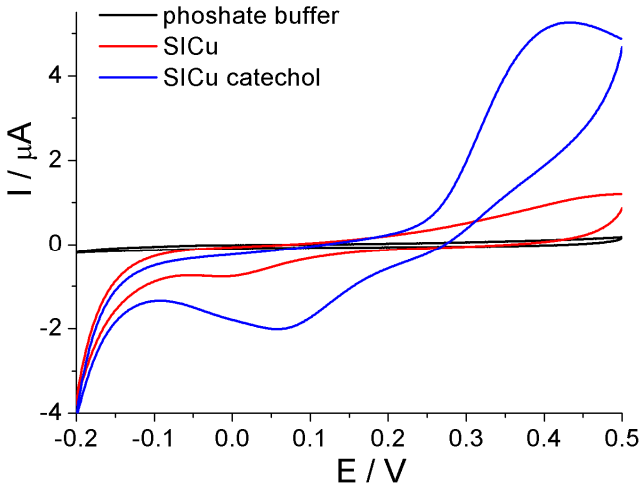

Supplementary Figure 16 Cyclic voltammetries of a gold electrode modified with MPA measured in 50 mM phosphate buffer pH6.5 50 mM, in the same buffer containing SICu 1 mM, and in phosphate buffer containing both SICu and catechol 1 mM. All the cyclic voltammograms were recorded using 20 $mV \cdot s^{-1}$ scan rate and phosphate buffer 50 mM pH 6.5 electrolyte, the working electrode was a gold disk of 0.2 cm^2 diameter modified with a MPA SAM, the reference electrode was Ag/AgCl 3M, counter electrode was Pt wire. Reproducibility as in Fig. 5 legend.

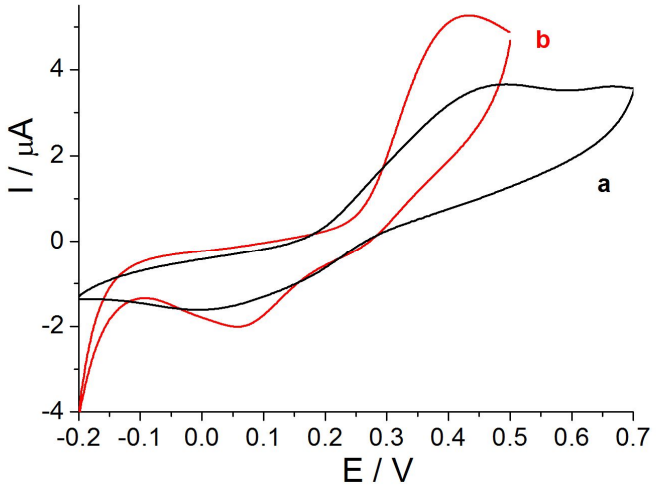

Supplementary Figure 17 Cyclic voltammetries of catechol 1 mM measured with a MPA-gold electrode (a) and a MPA-SICu gold electrode (b). All the cyclic voltammograms were recorded using 20 $mV \cdot s^{-1}$ scan rate and 50 mM phosphate buffer pH 6.2 electrolyte, the working electrode was a gold disk of 0.2 cm^2 diameter modified with a MPA SAM, the reference electrode was Ag/AgCl 3M, counter electrode was Pt wire. Reproducibility as in Fig. 5 legend.

EIS experiments were also performed with the conventional redox probe ferro/ferricyanide (Supplementary Figure 18), which showed a different behavior. $[Fe(CN)_6]^{3-/4-}$ is repelled from the surface of the $EH1_{AB1}$-modified electrode mainly to the proteic surface, as the isoelectric point of the enzyme is 5.06 and the pH at which the measurements were recorded was 7. The EIS measurements in presence of $[Fe(CN)_6]^{3-/4-}$ indicate no interaction with the active site, whereas the measurements in presence of catechol, which lacks any net charge, might indicate some interaction. This is why catechol was selected as target for electrochemical analyses.

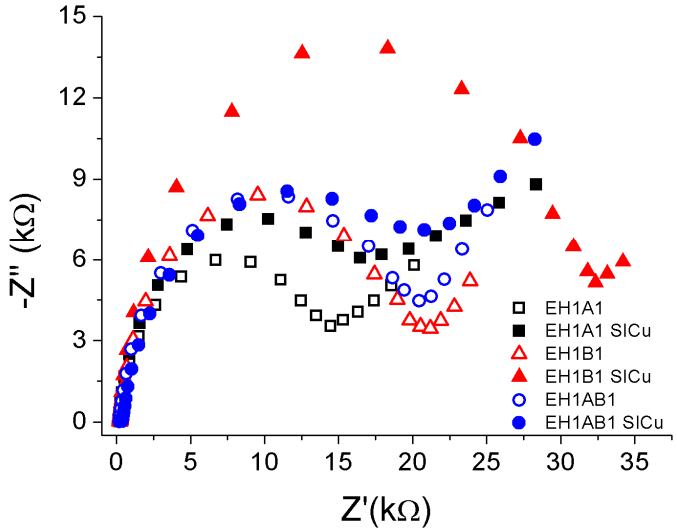

Supplementary Figure 18 Impedance spectroscopy showing that $EH1_{AB1}$-CuSI presents a much lower electron transfer resistance that any other combination of sub-enzymes with or without CuSI. The measurements were performed using ferro/ferricyanide 1 mM, a bias potential of 0.23 V *vs* Ag/AgCl. The experimental setup was the same 3-electrode configuration used for cyclic voltammetry. Reproducibility as in Fig. 5 legend.

Enzymatic electron transfer has been a matter of research for many metalloenzymes[5]. For instance, multicopper oxidases' electron transfer on different gold-carbon nanostructured electrodes, with different distances between the electrode surface and the enzyme active site, has also been studied[6], finding out a very sensitive dependence on the closeness between the active site and the electrode. It would be very interesting such study with the present enzyme, although it is out of the scope of the present work, which unveils a biotechnological strategy to produce enzymes with multiple active sites, and would be a whole work in itself. Electrochemical measurements of the present work were performed for characterization purposes.

Conformation by ESI-MS of SI binding under excess of inhibitor

By using ESI-MS we confirmed that, using under excess of SI, conjugation occurs in the native site of $EH1_{A1}$ and the artificial site of $EH1_{B1}$, as well as in the native and artificial sites of $EH1_{AB1}$ (Supplementary Figure 19). Indeed, a Cu^{2+}-organic molecule (MW of *ca*. 335) was found to bind to $EH1_{A1}$ and $EH1_{B1}$ and two Cu^{2+}-organic molecules were bio-conjugated to $EH1_{AB1}$.

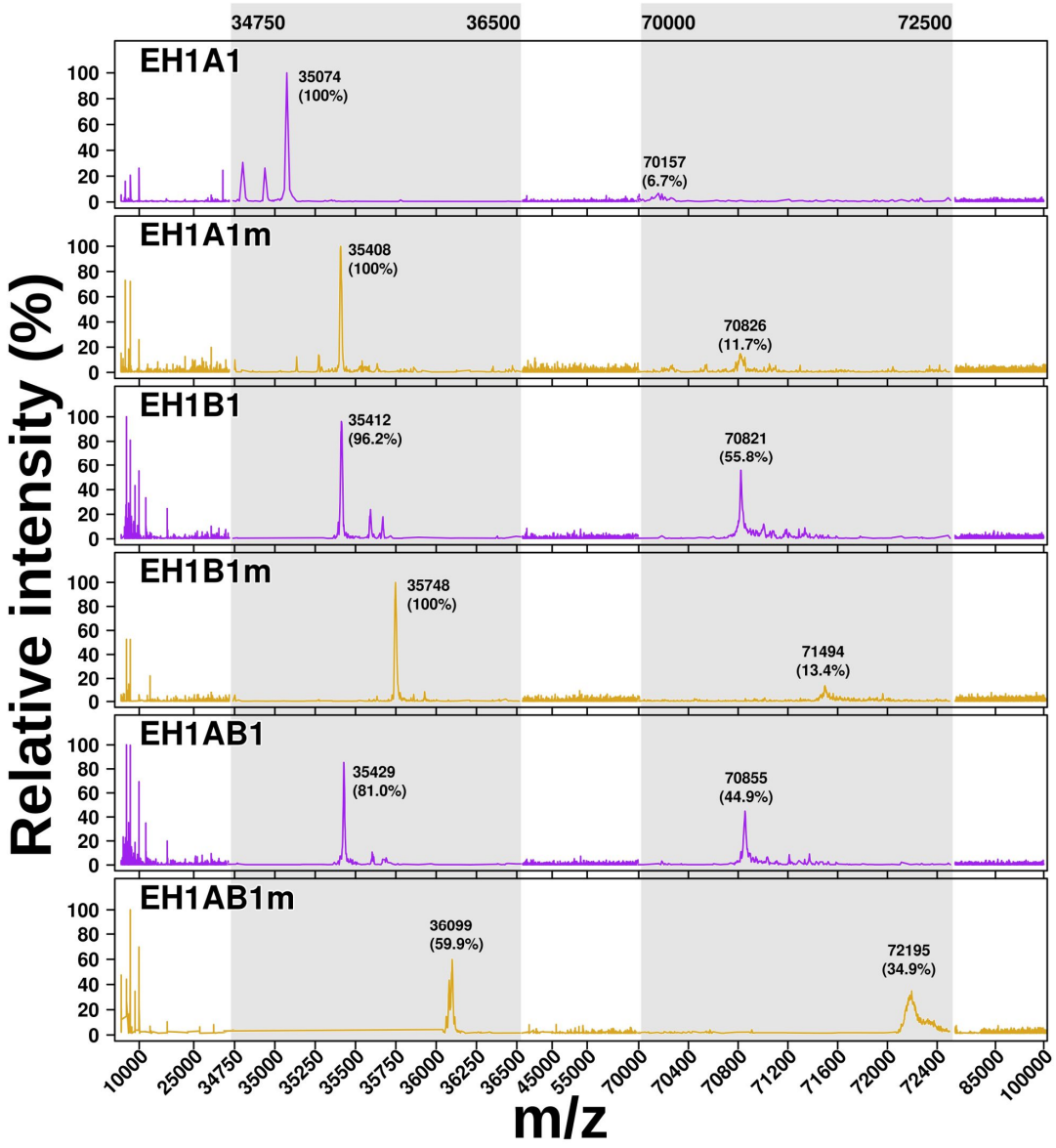

Fig. 19 ESI analysis of modified (m) and unmodified $EH1_{A1}$, $EH1_{B1}$ and $EH1_{AB1}$ sub-enzymes produced under excess of SI. Modified sub-enzymes were prepared in the presence

of an excess of inhibitor - [sub-enzyme]: 15 µM; [inhibitor]: 120 µM; volume: 1000 µl; T: 25ºC; pH: 6.5. After inhibition, the samples were extensively dialyzed with 50 mM K_2HPO_4 buffer pH 6.5, before ESI-MS analysis.

Supplementary Note 7:

Site-selective biochemical enzyme modification with 3'-hydroxy-[2,2'-bipyridin]-3-yl methyl hexylphosphonate

Dose-dependent and site-selective bio-conjugation: specificity of the labeling

The above results confirm that in the presence of an excess of the SI, both the native and the artificial nucleophiles are capable of bio-conjugation because a complete inactivation of the sub-enzymes. The affinity of SI for both the native and the remodeled artificial site was further evaluated by quantifying the activity of $EH1_{A1}$ (V_{max} of *ca*. 65.7 units/mg using glyceryl tripropionate), $EH1_{B1}$ (V_{max} of *ca*. 11.6 units/mg) and $EH1_{AB1}$ (V_{max} of *ca*. 77.2 units/mg) sub-enzymes at a fixed concentration (85 µM or approx. 3 mg/ml), when incubated 10 min with SI at different concentrations. Results shown in Supplementary Figure 20a revealed a significantly higher affinity of SI by the native site compared to the remodeled artificial site. Thus, below *ca*. 35 µM inhibitor the activity of $EH1_{B1}$ was not affected (no appreciable activity loss), whereas the loss of activity of $EH1_{A1}$ and $EH1_{AB1}$ sub-enzymes was evident even at very low doses. This suggests that both the native and the artificial sites may show very different steric constraints within their active site, and as a consequence, very different inhibitor affinity, as observed for many other substrates (see Supplementary Note 2). Noteworthy, above 35 µM both active sites are inhibited, and consequently the loss of activity of $EH1_{AB1}$ sub-enzyme increased because the additive effect of inhibition at both Ser161 and Ser211 sites.

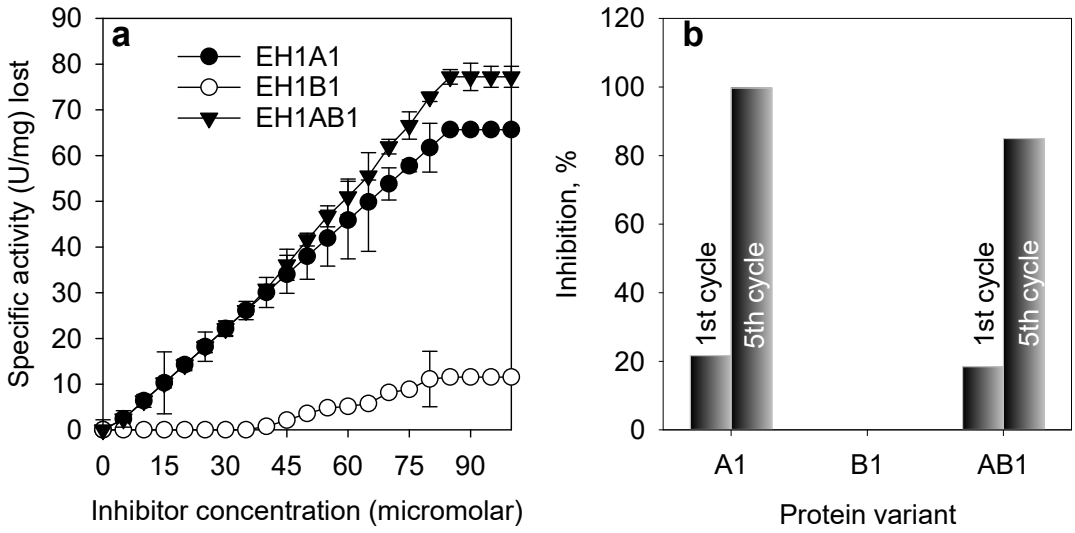

Supplementary Figure 20 Dose-dependent inhibition of $EH1_{A1}$, $EH1_{B1}$ and $EH1_{AB1}$ sub-enzymes by 3'-hydroxy-[2,2'-bipyridin]-3-yl methyl hexylphosphonate (SI). a, Concentration-dependent inhibition. Experimental conditions as follow. For inhibition experiment - [sub-enzyme]: 85 µM; [inhibitor]: 0-100 µM; volume: 1000 µl; T: 25ºC; pH: 50 mM K_2HPO_4 buffer pH 6.5; incubation time: 10 min. For activity test - [protein]: 18 µM; [glyceryl tripropionate]: 50 mM; reaction volume: 44 µl; T: 30ºC; pH: 8.0. Values are the loss of activity (units/mg), from 0 when no inhibition occurs to *ca*. 65.7 units/mg (for $EH1_{A1}$), *ca*. 11.6 units/mg (for $EH1_{B1}$), and *ca*. 77.23 units/mg (for $EH1_{AB1}$) in case of 100% inhibition; these values corresponds to the V_{max} of each sub-enzyme. Reactions were performed in triplicates with average value and standard deviations (calculated using Excel version 2019) indicated. The data are not fitted to any model. **b**, Scale-up dose-dependent inhibition. Experimental conditions as follow. For scale-up inhibition experiment - [sub-enzyme]: 80 µM; [inhibitor x 5 cycles x 10 min each]: 20 µM; volume: 1000 µl; T: 25ºC; pH: 6.5. For activity test

- [protein]: 18 µM; [glyceryl tripropionate]: 50 mM; reaction volume: 44 µl; T: 30ºC; pH: 8.0. Values are average percentages (calculated using Excel version 2019) of triplicates inhibition tests of the indicated sub-enzyme in comparison to enzyme activity without inhibitor after the first and last inhibition cycle. Both panels were created using Sigma Plot 13.0.

Based on the results of the affinity tests, by controlling the dose of inhibitor added it is possible to specifically modify Ser161 (original nucleophile) but not to Ser 211(artificial nucleophile). Thanks to this strategy (detailed in Supplementary Methods and Supplementary Figure 21) we prepared 3 mg of pure catalysts by incubating during 10 min a solution of 80 µM (per monomer) of $EH1_{AB1}$ with a dose of inhibitor below the affinity level for the artificial site; in the scale up process we used 20 µM inhibitor. Under these conditions and because a higher affinity for the native site, the inhibitor bio-conjugates at this site. This incubation step produced a *ca*. 18.4% activity inhibition. After 10 min incubation the inhibition was repeated for a total of 4 cycles (accumulated concentration of inhibitor being 100 µM at the end of the 5 cycles), after which a final loss of activity of *ca.* 85% was achieved (Supplementary Figure 20b). Note that the artificial site in $EH1_{AB1}$ was not inhibited at concentration below 20 µM and this is why the modified sub-enzyme retains its full "artificial" activity, that is, 15% of the total activity - V_{max} of the native and artificial sites are 65.7 and 11.6 units/mg for glyceryl tripropionate, respectively, and 77.2 units/mg when both together in $EH1_{AB1}$. When this protocol was repeated with $EH1_{A1}$ protein, 100% inhibition was achieved, whereas in the case of $EH1_{B1}$ inhibition below detection level was achieved.

To insert the copper cations, the modified sub-enzymes obtained by using the dose-dependent inhibition reaction, were incubated for 24 h with an excess of $Cu(NO_3)_2$, after which the samples were extensively dialyzed (see Supplementary Methods).

Supplementary Figure 21 summarizes the dose-dependent strategy and protocol to specifically bio-conjugate the Cu^{2+}-organic complex to Ser161.

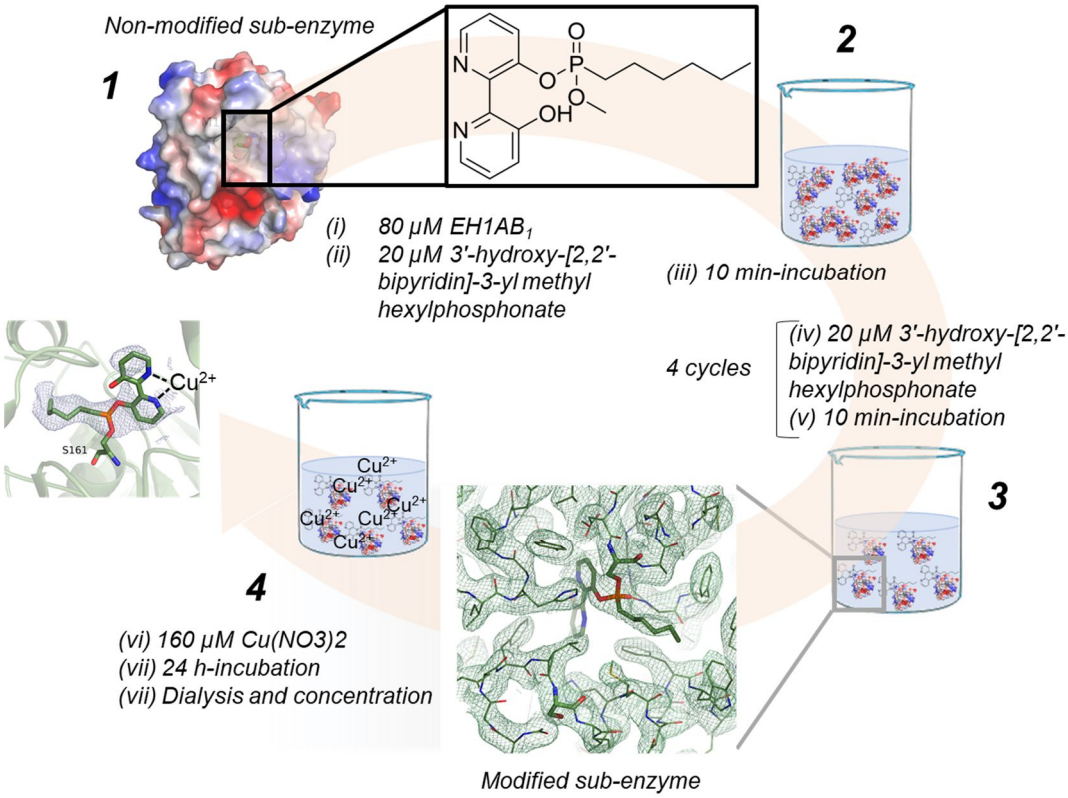

Supplementary Figure 21 Schematic representation of the dose-dependent protocol used for the specific coupling of Cu^{2+}-organic molecule into Ser 161.

By using ESI-MS (Supplementary Figure 22) we confirmed that, using the dose-dependent inhibition strategy, the coupling efficiency in the native site of $EH1_{A1}$ and $EH1_{AB1}$ was quantitative (>98%); indeed, the abundance of non-conjugated sub-enzyme was negligible or below detection limit. Opposite, no conjugation was observed for $EH1_{B1}$ sub-enzymes. Thus, purity of higher than 98% coupled proteins was thus obtained thank to the dose-depending coupling strategy. In addition to that, the mass increase (*ca*. 335; Supplementary Figure 23) agrees with the binding of a single inhibitor molecule to both $EH1_{A1}$ and $EH1_{AB1}$ after hydrolysis of the methyl ester and with the 3'-hydroxy-[2,2'-bipyridin]-3-yl moiety remaining. The UV-Vis analysis also confirmed the incorporation of a Cu^{2+}-organic molecule to $EH1_{A1}$ and $EH1_{AB1}$ but not $EH1_{B1}$ (Supplementary Figure 24).

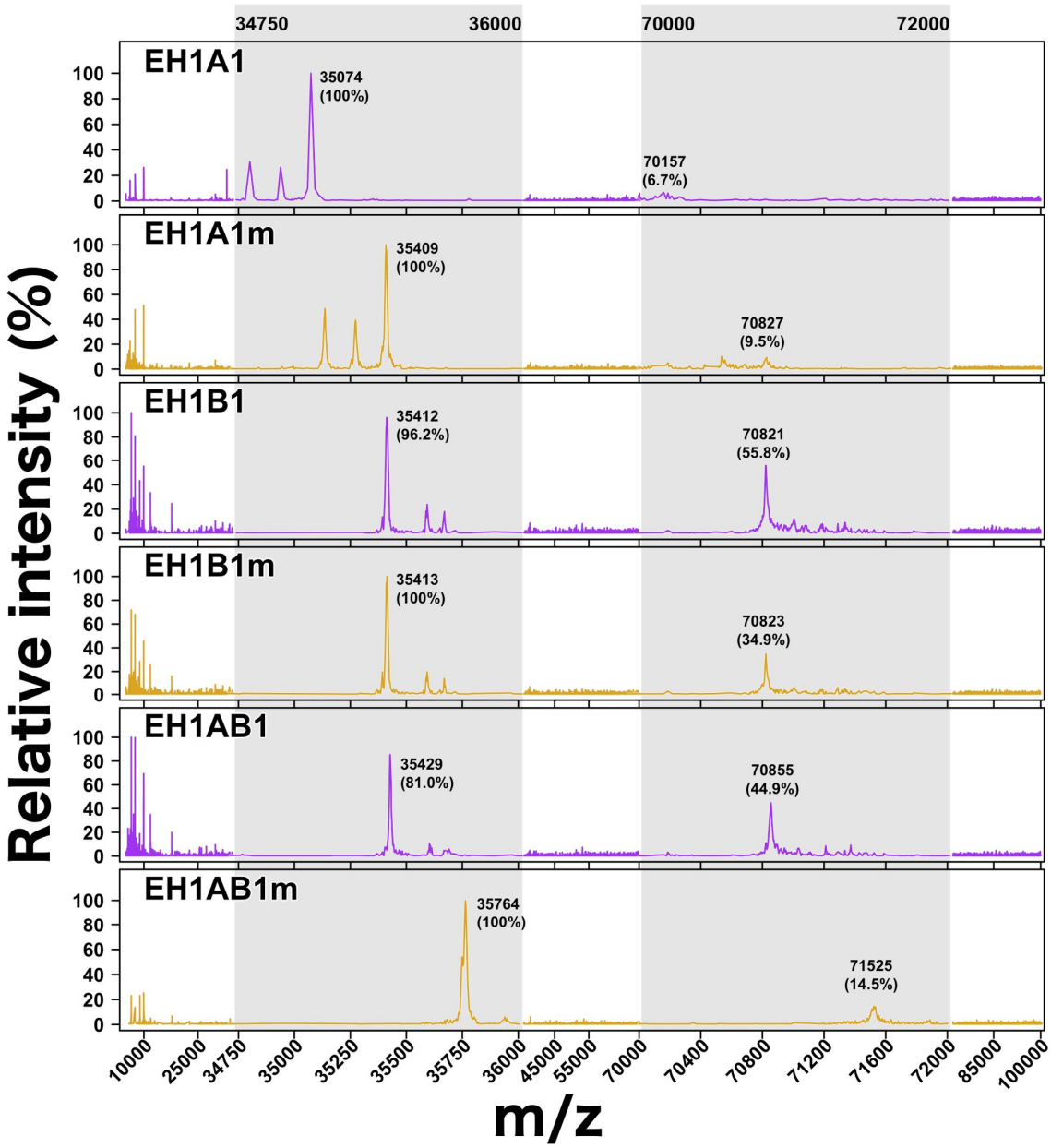

Supplementary Figure 22 ESI analysis of modified (m) and unmodified $EH1_{A1}$, $EH1_{B1}$ and $EH1_{AB1}$ sub-enzymes. Modified sub-enzymes were prepared by using the dose-dependent strategy described in Supplementary Methods and in the legend of Supplementary Figure 13b and Supplementary Figure 14 - [sub-enzyme]: 80 µM; [inhibitor x 5 cycles x 10 min each]: 20 µM; volume: 1000 µl; T: 25ºC; pH: 6.5. After inhibition, the samples were extensively dialyzed

with 50 mM K_2HPO_4 pH 6.5, before ESI analysis. Note: (1) The peaks eluting before the main peak in $EH1_{A1}$ (also in $EH1_{A1m}$) corresponds to associations with sodium trifluoroacetate (difference in mass within peaks of *ca*. 136), and not to contaminations; these associations (with one being preferred) were found reproducible and only for this sub-enzyme, possibly because different configurations compared to $EH1_{B1}$ and EH_{AB1} sub-enzymes. (2) the MW of non-modified $EH1_{A1}$ was slightly lower than that of non-modified $EH1_{B1}$ and EH_{AB1} sub-enzymes; this difference which could not be explained by the differences in mutations introduced, was associated to partial hydrolysis of this sub-enzyme (because slight differences in configuration) during ESI analysis; this difference was however not observed by MALDI-TOF/TOF (see Supplementary Figure 33 and Supplementary Figure 34) where the nature and purity of the protein was also confirmed.

a) Molecular mass of SI

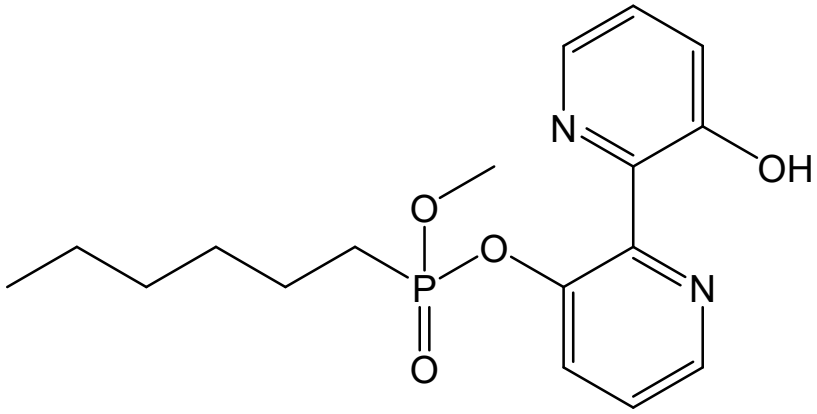

Molecular formula: $C_{17}H_{23}N_2O_4P$
Exact mass: 350.349

b) After coupling to the protein:

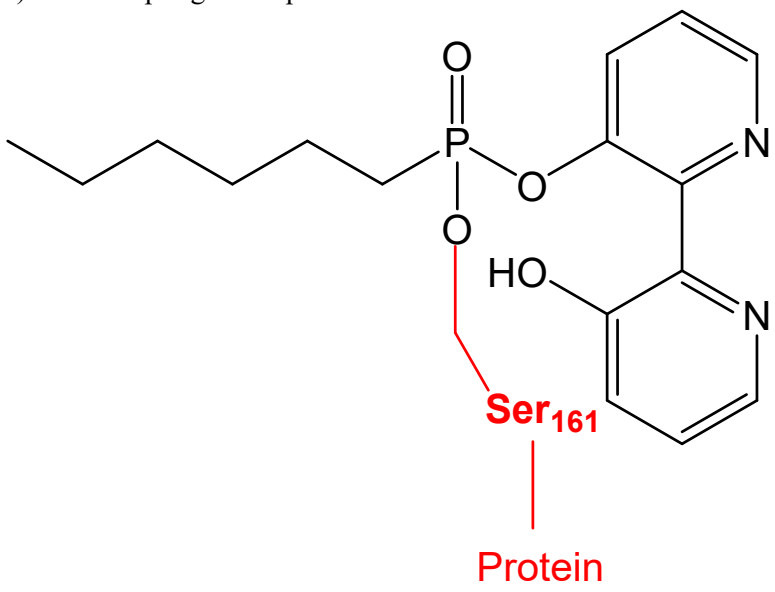

Exact increase: 335.314

Supplementary Figure 23 Expected molecular mass increase of the protein after treatment with bipyridine-like suicide inhibitor. a, Structure and molecular mass of the inhibitor. **b**, Structure of the molecule coupled to the catalytic serine with expected molecular mass increase shown.

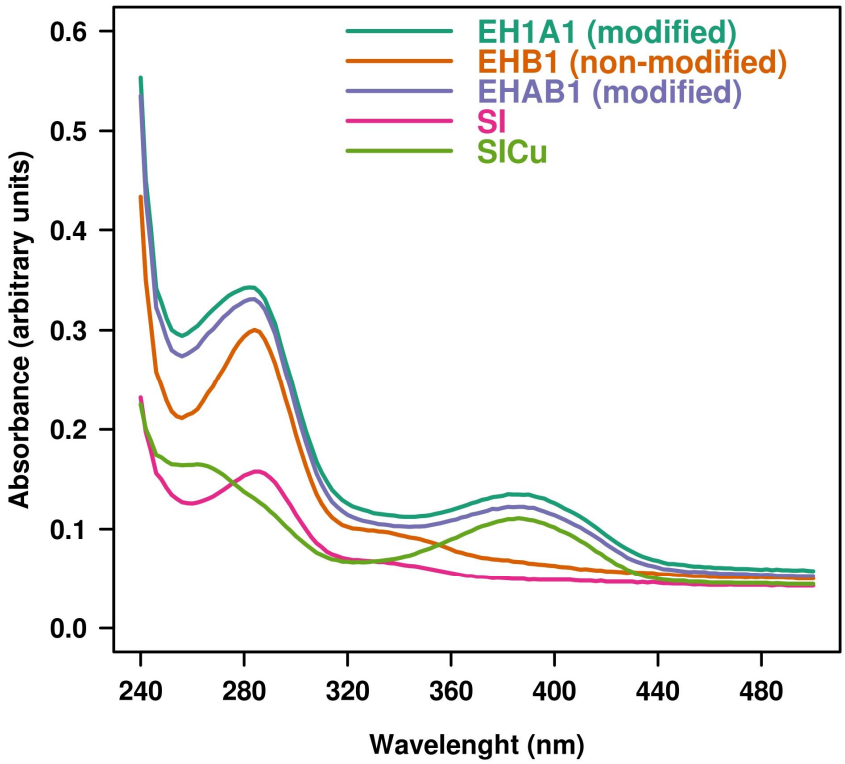

Supplementary Figure 24 Absorption spectra of modified $EH1_{A1}$ and $EH1_{AB1}$ and non-modified $EH1_{B1}$ sub-enzymes obtained after the dose-dependent inhibition reaction. a, Incorporation of Cu^{2+}-SI (SICu) as detected by UV-Vis. Spectra were recorded in 96-well plates using 7.5 µM Cu^{2+}-modified $EH1_{A1}$ and $EH1_{AB1}$ and non-modified $EH1_{B1}$ sub-enzymes prepared using a dose-dependent inhibition strategy (see Supplementary Methods), in a total volume of 200 µl. Shown are average values (calculated using Excel version 2019) of triplicates measurements.

Taken together, UV-Vis and electrochemical characterization demonstrated that under excess of the SI suicide inhibitor both the native and the artificial sites in EH1 scaffold are capable of bio-conjugation. However, by differences in affinities and a dose-dependent strategy a selective bio-conjugation was achieved with a coupling efficiency and purity of modified protein higher than 98%; this was demonstrated by UV-Vis, ESI characterization and co-crystallization.

Remarks to the bio-conjugation strategy

While introducing in an esterase scaffold a second active site with the same reactivity as the first (native) site for chemo-catalyst conjugation may create selectivity problems that do not exist for other bio-conjugation approaches (see Introduction and Conclusion sections), it is also true that both sites in our *plurizyme* design have different affinities by which one can control the coupling specificity (as demonstrated here), because differences in active sites architecture. It is also plausible that both active sites in our *plurizyme* may have different specificity for other metal-complexes, because different active site configuration, allowing specific bio-conjugation, yet to be investigated. Or, that in other *plurizymes* to be developed such selectivity problems may not occur because different active site configurations. Having said that, it is to note that aside this, the *plurizyme* design and dose-dependent strategy herein designed allow introducing two different catalytic entities in a single protein scaffold (one chemical and one biological), and this was shown to introduce benefits compared to a multi-catalysts system (see Supplementary Note 8, below).

In this study we used as 3'-hydroxy-[2,2'-bipyridin]-3-yl methyl hexylphosphonate as inhibitor for Cu^{2+}-bio-conjugation. This inhibitor contains a 3'-hydroxy-[2,2'-bipyridin]-3-yl moiety and a methyl moiety linked to the phosphonate. All tests performed demonstrate that the leaving group preferred by EH1 is the methyl, so that the 3'-hydroxy-[2,2'-bipyridin]-3-yl moiety will remain after the suicide inhibition reaction, allowing Cu^{2+} coupling. Note that about 25 esters containing a methyl group were converted by EH1 sub-enzymes (see Supplementary Note 2), indicating its preference for this leaving group. Having said that, we cannot guarantee that the methoxy group is preferred by other ester-hydrolases, given that hydroxypyridine moiety is commonly a good leaving group, like p-nitro phenyl. Therefore, the suicide inhibitor herein synthesized can only be employed for plurizymes with ester hydrolase activity capable of converting the methoxy but not the 3'-hydroxy-[2,2'-bipyridin]-3-yl moiety of the phosphonate group. Having said that, the synthesis of similar suicide inhibitors where the chelating organic complex could not be displaced in any case (e.g. by its incorporation through a P-C bond and not through a phosphonate bond), would solve this issue; actually, this possibility in under investigation.

Supplementary Note 8:

A reproducibility test: a second genetically engineered *plurizyme*

Design of a second plurizyme and characterization of sub-enzymes

To test reproducibility of adding a second site, we chose a serine ester-hydrolase, referred to as $EH102_A$ (5JD3), isolated from the same habitat as $EH1_A$[7]. Its exposed native active site hydrolyzes only 16 substrates out 96 tested[2], with the V_{max} from 1038.3 ± 0.2 to 145.1 ± 22.1 U g^{-1} (Supplementary Figure 25a; Supplementary Table 3).

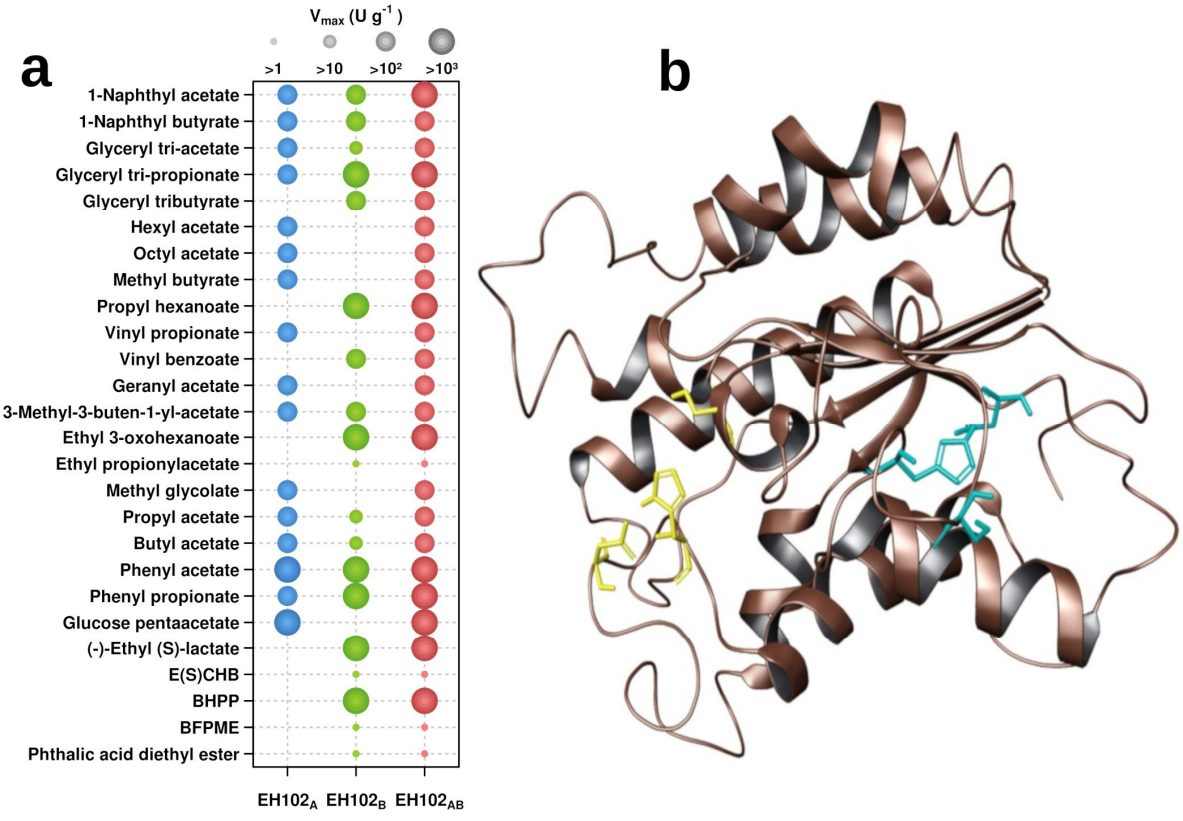

Supplementary Figure 25 The artificial remodeled site intensifies the bio-catalytic capability of the "mother" enzyme. a, V_{max} values for model esters. Values were calculated on a continuous pH indicator assay[1], for a series of esters found to be hydrolyzed by any of the sub-enzymes. Conditions are as follows - [protein]: 4.5 µg/ml; [ester]: 50 mM; reaction volume: 44 µl; T: 30ºC; pH: 8.0. The figure was created with the R language console using average values

given in Supplementary Table 3, where abbreviations can also be seen. (+)-Ethyl (R)-lactate and ethyl (S)-(−)-4-chloro-3-hydroxybutyrate are not shown as no appreciable activity was detected under our assay conditions for any of the tested hydrolase variants. **b**, Relative positions in EH102 of the original ($EH102_A$; in yellow) / artificial ($EH102_B$; in blue) catalytic triad (Ser15, Asp192 and His195 / Ser30, His34 and Asp57) and oxyanion hole (Gly64 / Asn43).

Supplementary Table 3 Substrate spectra of EH102 sub-enzymes. The chemically and structurally distinct esters out 96 tested[2], for which activity was detected, are listed on the left side of the table. V_{max} calculations, in triplicates for each concentration, were performed as described in Supplementary Figure 25. The standard deviation of the simple hyperbolic fit with Sigma Plot 13.0 is shown.

	V_{max} (U g^{-1})		
Substrates[1]	**$EH102_A$**	**$EH102_B$**	**$EH102_{AB}$**
1-Naphthyl acetate	952.8±11.9	917.4±13.0	1832.3±45.3
1-Naphthyl butyrate	688.3±6.6	132.8±5.0	846.9±7.5
Glyceryl tri-acetate	784.7±3.3	92.0±3.7	884.6±10.5
Glyceryl tripropionate	896.2±13.0	2120.5±9.2	3089.4±59
Glyceryl tributyrate	0	346.1±9.4	350.3±2.5
Hexyl acetate	225.2±5.1	0	224.7±12.0
Octyl acetate	145.1±22.1	0	141.6±5.3
Methyl butyrate	193.7±1.2	0	200.0±1.9
Propyl hexanoate	0	1878.9±7.8	1885.1±1.5
Vinyl propionate	783.7±2.5	0	794.9±4.3
Vinyl benzoate	0	859.1±9.4	855.1±4.3
Geranyl acetate	168.0±1.6	0	167.2±2.8
3-Methyl-3-buten-1-yl-acetate	256.4±7.0	417.2±11.7	661.6±3.7
Ethyl 3-oxohexanoate	0	1430.8±12.6	1470.4±2.7
Ethyl propionylacetate	0	7.68±1.11	7.58±0.55
Methyl glycolate	565.6±3.0	0	560.0±9.1
Propyl acetate	621.5±6.2	69.0±2.5	707.8±4.9
Butyl acetate	656.9±3.9	11.4±1.8	672.4±8.5
Phenyl acetate	1001.5±8.4	4147.3±21.2	5171.8±1.5
Phenyl propionate	544.0±2.7	5726.5±71.2	6282.8±5.8
Glucose pentaacetate	1038.3±11.2	0	1073.6±2.9
(−)-Ethyl (*S*)-lactate	0	1227.7±10.8	1236.7±0.6
Ethyl (*S*)-(−)-4-chloro-3-hydroxybutyrate [E(S)CHB]	0	6.64±1.49	6.41±0.12
Benzyl (*R*)-(+)-2-hydroxy-3-phenylpropionate [BHPP]	0	2147.8±5.7	2193.3±6.4
Benzoic acid, 4-formyl-, phenylmethyl ester [BFPME]	0	6.58±0.38	6.54±0.84
Phthalic acid diethyl ester	0	1.44±0.70	1.52±0.05

[1]Note: the number of esters found as potential substrates by Martínez-Martínez et al. (2018) for $EH102_A$ was 11[2]. Additionally, hexyl acetate, octyl acetate, vinyl propionate, 3-methyl-3-buten-1-yl-acetate, methyl glycolate, for which conversion was detected below the detection limit of the conditions used by Martínez-Martínez et al. (2018)[2], were hydrolyzed in the conditions used in this study, which correspond to conditions at which substrate saturation exists. No activity was detected for (+)-ethyl (*R*)-lactate and ethyl (*R*)-(+)-4-chloro-3-hydroxybutyrate for any of the hydrolase variants, and for this reason these esters are not shown in the table.

To design a second catalytic triad we applied the same protocol using the PELE software to locate potential pockets where target substrates can be accommodated[1]. Glyceryl tripropionate was used as a target compound, as it was found as an ester commonly hydrolyzed by most ester hydrolases[1], including $EH102_A$ (Supplementary Table 3). PELE simulations revealed a second binding site located ~23 Å from the native catalytic position at Ser15 (Supplementary Figure 26a) that already contains a histidine residue (His34). Thus, we computationally designed

additional mutations, adding Asp and Ser residues to build a proper catalytic triad, taking special care concerning catalytic distances, and the resulting effective volume. We found that the Leu57Asp and Leu30Ser double mutant revealed good enzyme-substrate interaction energies (Supplementary Figure 26b) and a suitable catalytic position for the glyceryl tripropionate substrate (Supplementary Figure 26c). In addition, our results showed that residue Asn43 acts as a potential oxyanion hole, a key element in ester hydrolase catalysis (Supplementary Figure 26c). Moreover, extensive MD simulations indicate proper stabilization of the double mutant.

By using site-directed mutagenesis, we created two variants, referred to as $EH102_B$ and $EH102_{AB}$, following the nomenclature of EH1. $EH102_B$ introduced Leu57Asp, Leu30Ser and Ser15Ala substitutions, so that this variant would employ only the new catalytic triad; the second variant, $EH102_{AB}$, carried both the native and the artificial sites (Supplementary Figure 25b).

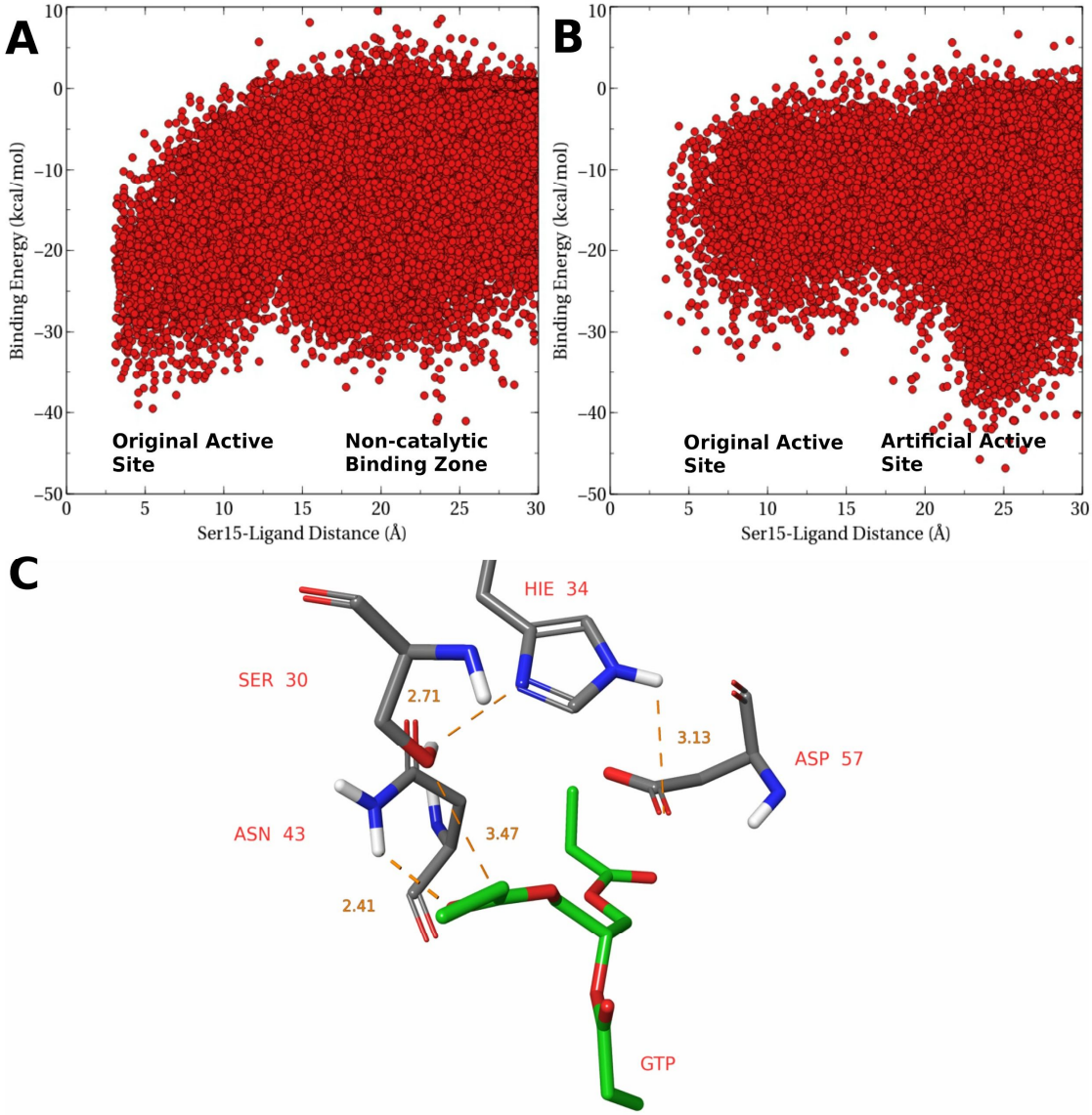

Supplementary Figure 26 PELE exploration of EH102. a, PELE exploration for glyceryl tripropionate diffusion in $EH102_A$. **b**, New catalytic triad interaction energies profile for $EH102_{AB}$. **c**, Glyceryl tripropionate binding mode as obtained with PELE in the artificial site.

As shown in Supplementary Figure 25a and Supplementary Table 3, $EH102_B$ hydrolyzed 19 esters with V_{max} values ranging from 5726.5 ± 71.2 to 1.44 ± 0.70 U g^{-1}, values which are in the

range of those of the native site. Interestingly, $EH102_B$ does show stringent stereo-chemistry for (+)-ethyl (*R*)-lactate (1227.7 ± 10.8 U g^{-1}) and ethyl (*S*)-(−)-4-chloro-3-hydroxybutyrate (6.64 ± 1.49 U g^{-1}), substrates for which $EH102_A$ shows activity below detection limit (Supplementary Table 3). $EH102_{AB}$, with two active sites, was able to convert 26 substrates that $EH102_A$ and $EH102_B$ combined converted, with V_{max} values (from 6282.3 ± 5.8 to 1.52 ± 0.05 U g^{-1}) which were close to the sum of the individual values from variants containing each of the separate sites (Supplementary Figure 25a and Supplementary Table 3), thus demonstrating that additivity exists between the native and the artificial sites, as it was observed in $EH1_{AB1}$. This variant also retained the capacity to efficiently hydrolyze esters initially not converted by the native enzyme but converted by the newly introduce active site, thus demonstrating that the extra active site expands the substrate spectrum of the original ester-hydrolase. By kinetic resolution of enantiomers in a racemic mixture and GC analysis (see Supplementary Methods) we found that the addition of the artificial site (E-value >1000 for (+)-ethyl (*R*)-lactate and ethyl (*S*)-(−)-4-chloro-3-hydroxybutyrate) increases the E-value of the "mother" enzyme from no conversion (in $EH1102_A$) to >1000 (for $EH102_{AB}$) in both cases.

Using glyceryl tripropionate, we further found that $EH102_A$ was strongly active (>70% rel. act.) at temperatures in the range 4-40ºC, with the activity progressively reduced at higher temperatures (Supplementary Figure 27). The T_{opt} was ~12ºC. $EH102_B$, exhibited the reverse of this trend —it was less active at temperatures lower than 12ºC and more active at temperatures from 45-65ºC (Supplementary Figure 27). The T_{opt} was ~25ºC, and the enzyme retained >70% activity at 16-55ºC. The enzyme with two reactive sites exhibited a hybrid pattern, retaining >70% rel. act. at temperatures from 4 to 55ºC, still retaining 56% of its activity at 65ºC (Supplementary Figure 27). The two-active site enzyme thus retained the psychrophilic-like phenotype of the native site and the mesophilic-like phenotype introduced by the extra active site.

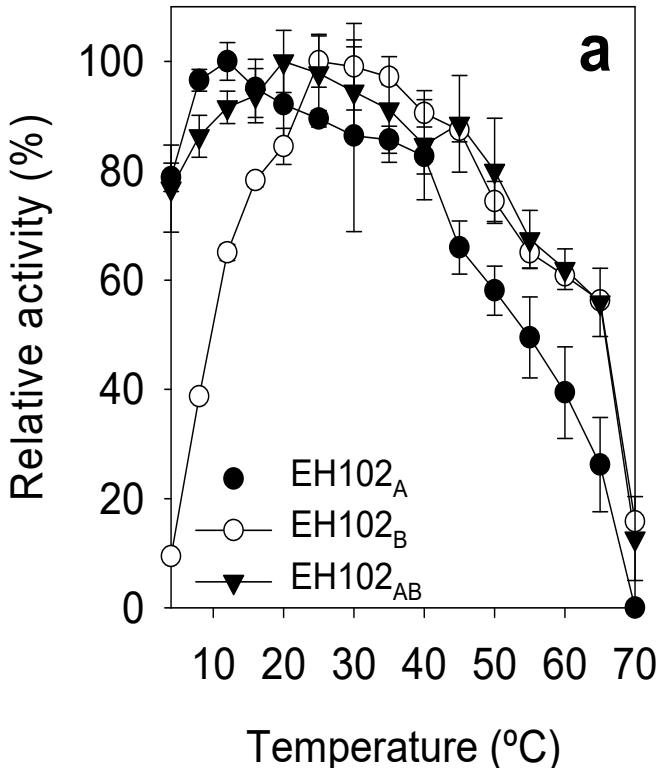

Supplementary Figure 27 Temperature profiles of the purified EH102 sub-enzymes. For T_{opt} determination, calculated on a continuous pH indicator assay[1], conditions are as follows - [protein]: 4.5 μg/ml; [glyceryl tripropionate]: 50 mM; reaction volume: 44 μl; T: 8-65ºC; pH: 8.0. The data, calculated from three independent assays ± SD (calculated using Excel version 2019) and not fitted to any model, represent the relative percentages (%) of specific activity,

expressed as U mg^{-1}, compared with the maximum. Similar results were obtained using α-naphthyl acetate.

Finally, the participation of Ser15 (in EH_{102A} and EH_{102AB}) and Ser30 (in EH_{102B} and EH_{102AB}) as the catalytic nucleophiles was confirmed by using the suicide inhibitors methyl, butyl and octyl 4-nitrophenyl hexylphosphonate. According to our inhibition experiments, treatment with the butyl derivative resulted in total inactivation of $EH102_A$, $EH102_B$ and $EH102_{AB}$ activity when tested with glyceryl tripropionate (Supplementary Figure 28). Methyl and octyl derivatives were also used as substrates and bound irreversibly but at lower rates (not shown). This confirms that Ser15 and Ser30 are the functional nucleophilic groups Supplementary catalysis.

Together, through introducing a second active site (i.e. V_{max} *ca*. 2120.5±9.2 U g^{-1} for glyceryl tripropionate; >99.9% e.e.) to the "mother" EH102 ester-hydrolase already containing a native one (i.e. V_{max} *ca*. 896.2±13.0 U g^{-1}), we intensified the conversion rates (V_{max} to *ca*. 3089.4±59 U g^{-1}), slightly increased the temperature window (by 10ºC considering at least 80% of the activity at the optimal temperature), and converted an initially non-enantiospecific serine ester-hydrolase into a synthetic biocatalyst capable of converting a chiral molecule with stringent stereo-chemistry (>99.9% e.e.). Note that the native site was not capable of converting the chiral esters which were hydrolysed by the artificial site, and this is why the stereo-preference is not compromised. The analysis of EH102 variants also demonstrated that the substrate spectrum can be expanded, because the newly introduced preferences of the artificial site.

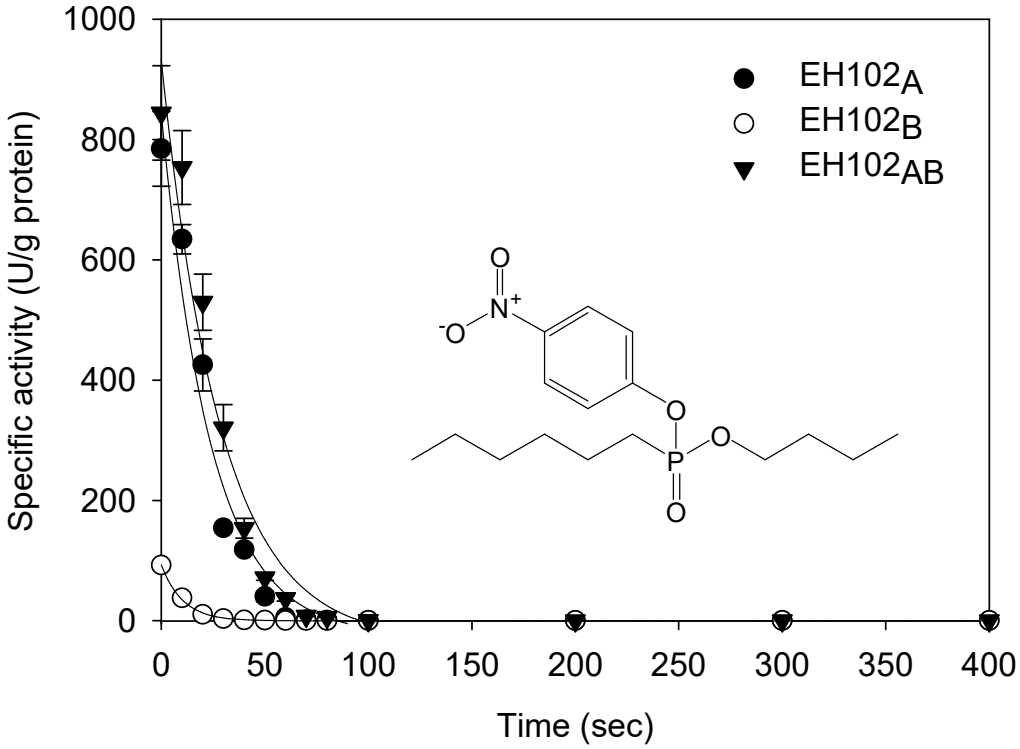

Supplementary Figure 28 Small-scale inhibition of EH102 sub-enzymes by butyl 4-nitrophenyl hexylphosphonate. Experimental conditions as follow. For inhibition experiment - [sub-enzyme]: 7.5 μM; [inhibitor]: 30 μM; volume: 500 μl; T: 25ºC; pH: 7.5; incubation time: 0-400 sec. For activity test - [protein]: 1.7 mM; [glyceryl tripropionate]: 50 mM; reaction volume: 44 μl; T: 30ºC; pH: 8.0. Values are percentages of inhibition of the indicated sub-enzyme in comparison to enzyme activity without inhibitor. Reactions were performed in triplicates with standard deviations, calculated using Excel version 2019, indicated. Fits were

performed using single exponential decay with Sigma Plot 13.0. The structure of the inhibitor is shown.

Remarks on plurizyme reproducibility

Taken together, the results with two random (EH1 and EH102) ester-hydrolases (Supplementary Note 2 and Supplementary Note 8) demonstrated that adding catalytically efficient artificial active sites into ester-hydrolases containing a native one, and thus that two active sites can coexist in the same polypeptide without compromising the original hydrolytic activity, is reproducible. We should emphasize that we obtained two *plurizymes* in the two ester-hydrolases that we attempted. One open question is: How frequently can a catalytic triad and an oxyanion hole be introduced after the docking simulation is done in other ester-hydrolases? As stated, we have proven this by just picking two random ester-hydrolases, one being among those with a broad substrate spectrum, and one with a narrow substrate spectrum, but these calculations may be needed in a broader sense to find whether this is a "general" methodology in other "mother" ester-hydrolases or other enzymes that are not naturally esterase's. Regardless, the results reported here provide evidences demonstrating that incorporation of a second active site with the same chemistry catalyzed as the native one, is reproducible and may significantly improve the catalytic capabilities of "mother" ester hydrolases. We hypothesized it can open new catalytic opportunities, an aspect that should be studied in depth in the future by combining enzymatic active sites with different chemistry, so that to create multi-catalytic enzyme systems in one, or by selectively introducing chemical catalysts to create hybrid chemo-biocatalysts with different chemistry for domino reactions as the ones created with EH1-based *plurizyme*.

We should highlight that adding extra sites with same chemistry catalyzed (ester-hydrolysis in this study) to create *plurizymes* may thus be beneficial to increase conversion rate and temperature range (as shown in the two examples herein reported). However, the *plurizyme* concept cannot be claimed, as other engineering approaches, as a general approach to improve the catalytic performance and thermal behavior of all ester-hydrolases, as the results may vary from enzyme to enzyme and from one active site to other because differences in preference and configurations. This may be particularly noticeable regarding chemo-, regio- and stereoselectivity. Thus, adding extra active sites may be also a disadvantage if one active site has one (chemo-, regio- and stereoselectivity) preference and the artificial site has a different preference. Then, the catalytic outcome may be a mixture of both properties which is not desired for an applied point of view. Imagine that one active site is highly stereo-selective, but the other active site is not; then the optical purity (e.e.) of the product may be logically lowered making its application useless whatever the increase in conversion rate. In this case, the beneficial effects of the extra reactive site can only be evaluated for chiral substrates only or preferentially converted by one of the sites. This is herein exemplified when studying the kinetic resolution of a racemic mixture of a target chiral ester; one of the chiral esters is preferentially or only converted by the newly introduced artificial site compared to the native one, a feature (>99.9% e.e.) that is transferred to the *plurizyme* in which both sites are introduced.

Supplementary Note 9:

***Plurizyme* utility *versus* a traditional multi-catalyst system**

Our study demonstrated that a genetically engineered *plurizyme* allow producing a single catalyst for synergistic chemo- and bio-catalysis. It is unclear what the advantage to having two activities in one single scaffold (one an artificial esterase and the second a labeled chemo-catalyst that substitute the native esterase). This combination could even be done with the native esterase ($EH1_{A1}$) just prepared in two separate ways, one bearing the Cu^{2+}-organic molecule and the other being the native, and then combined. This multi-enzyme system, which will be referred as $EH1_{A1}$ + modified $EH1_{A1}$, was tested for the two model reactions used in this study. Results revealed that using this multi-catalyst system the transformation of 1-naphthyl acetate to 1,4-naphthoquinone (Supplementary Figure 29a) and that of vinyl crotonate/benzene to 3-phenylbutyric acid (Supplementary Figure 29b) reached final conversions slightly lower or in the same range than that using the modified *plurizyme* (see Supplementary Table 4).

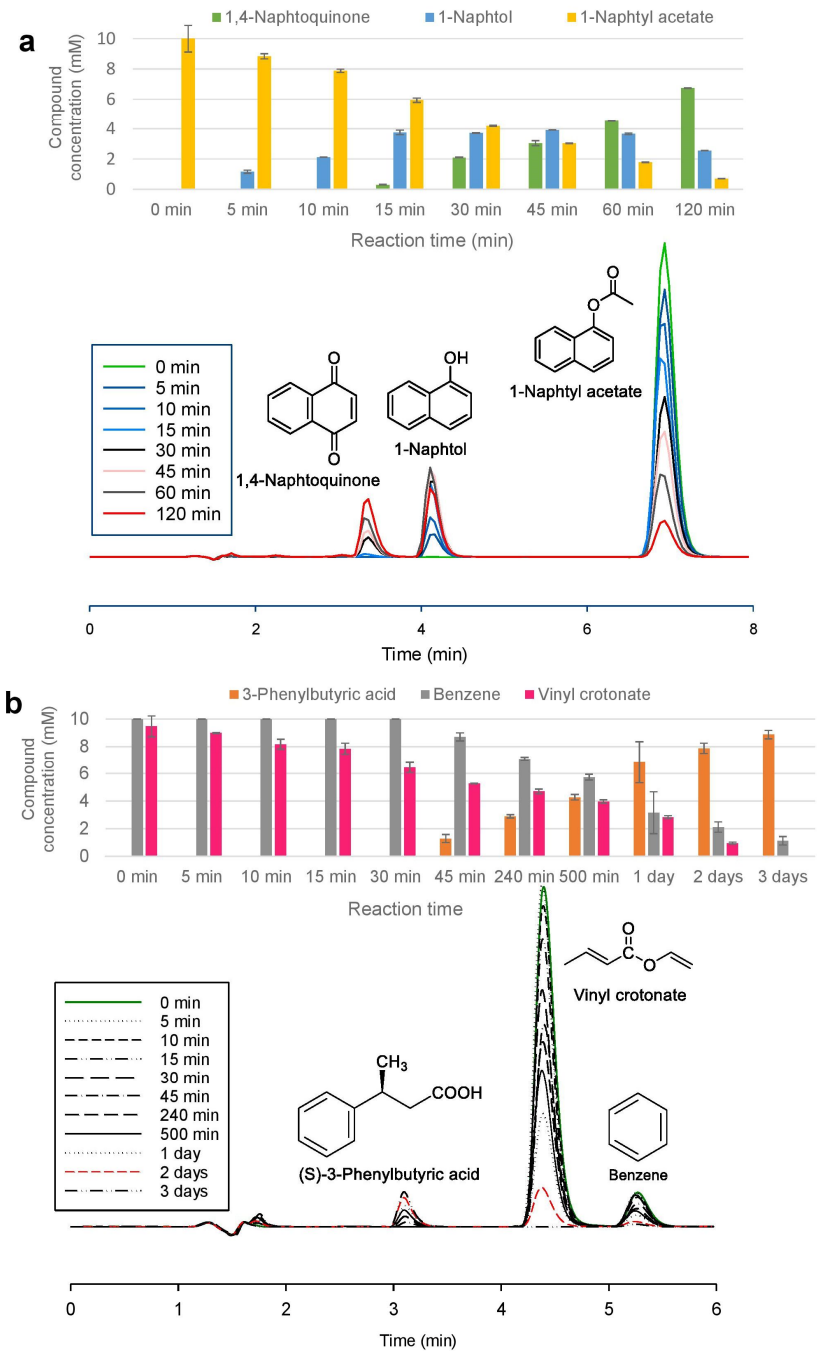

Supplementary Figure 29 Production of 1,4-naphthoquinone from 1-napthyl acetate (a) and 3-phenylbutyric acid from vinyl crotonate and benzene (b) using non-modified and modified EH1$_{A1}$ multi-catalyst system. Reaction conditions as described in Figs. 7 and 8, but in this case EH1$_{A1}$ and modified EH1$_{A1}$ (80 μM each) were used instead of modified *plurizyme*. Note: in this separate multi-catalysts system we used 80 μM of EH1$_{A1}$ and 80 μM of modified EH1$_{A1}$; this guarantee that, albeit the total protein concentration (160 μM) is double than that when using the modified *plurizyme* (80 μM), the concentration of each catalytic entity (the biological and the chemical) is maintained in both tests and the results are comparable. Reactions were performed in triplicates with average value and standard deviations (calculated using Excel version 2019) indicated.

Supplementary Table 4 Catalytic advantage of the *plurizyme* catalyst compared to multi-catalyst systems.

One-pot transformation of 1-naphthyl acetate to 1,4-naphthoquinone				
		1- Naphtyl acetate		1-Naphtoquinone
Catalytic system[1]	Final conversion (%)[2] at 120 min	Conversion rate[3] (μmol/min)	$t_{1/2}$ (min)[4]	$t_{1/2}$ (min)[5]
Modified AB_1	> 99.9	512.4 ± 33	9.3	22.5
Modified A_1+ B_1	72.1	529.5 ± 6	9.4	28.4
A_1 + Modified A_1	67.5	196.9 ± 25	24.0	48.3
One-pot transformation of vinyl crotonate/benzene to 3-phenylbutyric acid				
		Vinyl crotonate		3-Phenylbutyric acid
	Conversion (%)[2] at 3 days	Conversion rate[3] (μmol/min)	$t_{1/2}$ (min)[4]	$t_{1/2}$ (h)[5]
Modified AB_1	87.9	198.5 ± 29	25.5	1.7
Modified A_1+ B_1	77.9	178.2 ± 20	21.3	3.2
A_1 + Modified A_1	88.7	93.2 ± 5	46.4	9.4

[1]Modified AB_1: *plurizyme* containing a Cu^{2+}-organic molecule and an enzymatic hydrolytic site in one; Modified A_1+ B_1: multi-catalyst system combining $EH1_{A1}$ modified with Cu^{2+}-organic molecule and non-modified $EH1_{B1}$; A_1 + Modified A_1: multi-catalyst system combining $EH1_{A1}$ modified with Cu^{2+}-organic molecule and $EH1_{A1}$.

[2]Conversion referred to 1-naphtoquinone or 3-phenylbutyric acid. Data extracted from Fig. 7, Fig. 8, Supplementary Figure 29, Supplementary Figure 31.

[3]Conversion rate for the first step of the domino reaction. The rate was calculated from the decline of initial substrate (1- naphtyl acetate or vinyl crotonate) over time (using the linear range) using Sigma Plot 13.0. Data extracted from Fig. 7, Fig. 8, Supplementary Figure 28, Supplementary Figure 30. The standard deviation of the simple decay fit with Sigma Plot 13.0 is shown.

[4]Time at which half of the initial substrate is hydrolyzed is shown. Data extracted from Fig. 7, Fig. 8, Supplementary Figure 29, Supplementary Figure 31. The standard deviation of the simple decay fit with Sigma Plot 13.0 is shown.

[5]Time at which half of the final substrate is synthesized. Data extracted from Fig. 7, Fig. 8, Supplementary Figure 29, Supplementary Figure 31. The standard deviation of the simple hyperbolic fit with Sigma Plot 13.0 is shown.

However, we observed that the first steps of the domino reactions, namely the conversion of 1-naphthyl acetate to 1-naphthol and the conversion of vinyl crotonate to crotonic acid, are progressing at rates significantly lower compared to the modified *plurizyme* (*ca*. 2.6-fold and 2.1-fold lower, in the same order); as a consequence the time at which half of the initial substrate is hydrolyzed by the multi-catalyst system compared to the *plurizyme* catalyst is extended from *ca*. 9.3 to 24 min (for 1-naphthyl acetate) and from *ca*. 25.5 to 46 min (vinyl crotonate). This in turn has a negative effect in the progress of the second step, namely the conversion of 1-naphtol to 1,4-naphtoquinone, and of crotonic acid/benzene to 3-phenylbutyric acid, which is observed in a delay in the formation of final products (Supplementary Figure 29a,b). Thus the time at which half of the final product, namely 1-naphthoquine or 3-phenylbutyric acid, is synthesized by the multi-catalyst system compared to the *plurizyme* catalyst is extended from *ca*. 9.3 to 24 min and from *ca*. 25.5 to 46 min, in the same order (Supplementary Table 4).

The observed differences in conversion rate and delay in substrate hydrolysis and product formation can be associated to the higher catalytic performance of the artificial site in our modified *plurizyme* at temperatures at which reactions were performed compared to that of the native site (see Supplementary Note 2). This could make the *plurizyme* more competitive at low temperature compared to the native enzyme (see Supplementary Figure 4). Indeed, slight

differences were found at 25ºC, which were accentuated at 4ºC, where the artificial esterase works significantly better than the native esterase. This difference may explain why the *plurizyme* system is more effective for the first step of the domino reaction, which may thus limit the time frame at which further products are formed in the second step. We cannot rule out also the possibility that the differences in conversion rates of the second step may be due to the fact that both sites in our modified *plurizyme* are co-localized in the same catalytic environment (Supplementary Figure 30) compared to the multi-catalysts system formed by $EH1_{A1}$ + modified $EH1_{A1}$; this may benefit the substrate/product transfer from one to other catalytic site and the earlier formation of products.

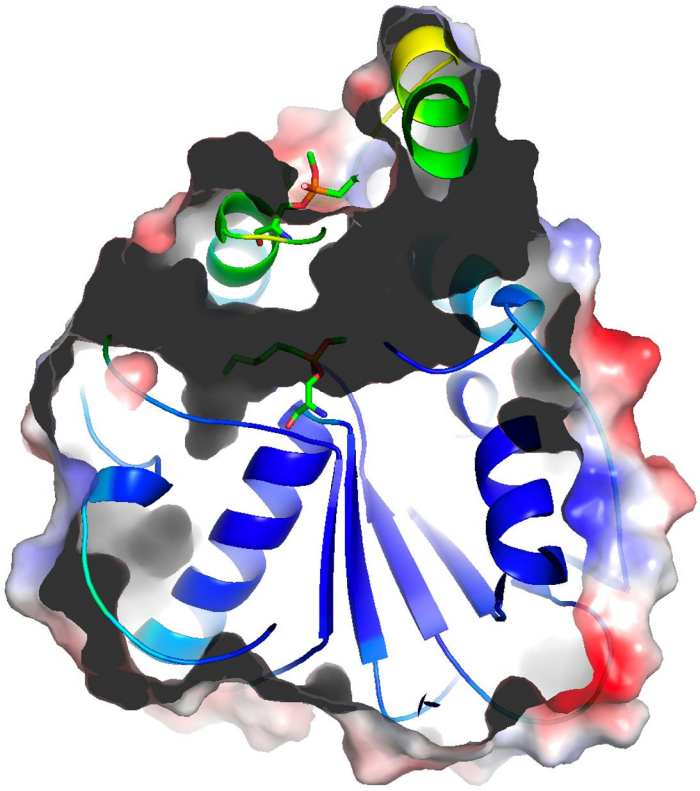

Supplementary Figure 30 A slice of the molecular surface showing the co-localization of Ser161 and Ser211, with bound M4-4NHP inhibitor. In dark grey colour the tunnel through which substrate and products access the Ser161 active site. The Ser211 site is in a pocket accessible from the solvent. The cartoon in shown in rainbow code.

To prove whether the substrate transfer in a traditional multi-catalyst system may have an effect compared to a *plurizyme* system, we performed an additional control experiment in which the reaction was performed using a multi-catalytic system consisting in using together the modified $EH1_{A1}$ (that contributes with metal-complex chemocatalysis) and the non-modified $EH1_{B1}$ (that contributes with biocatalytic hydrolysis). Results were compared to those obtained using the modified *plurizyme* system that combines both chemo- and bio-catalysis in one (see main Fig. 7 and Fig. 8) and with the multi-catalyst systems constituted by the modified $EH1_{A1}$ + $EH1_{A1}$ (Supplementary Figure 29a,b). We found that the multi-system consisting in "modified $EH1_{A1}$ + $EH1_{B1}$" (Supplementary Figure 31a,b) is more efficient for the first step of the domino reaction compared to the multi-catalyst "modified $EH1_{A1}$ + $EH1_{A1}$" system, and almost equally efficient as the modified *plurizyme* (Supplementary Table 4). This is observed when considering the conversion rate of 1-naphthyl acetate to 1-naphthol and of vinyl crotonate to crotonic acid, and the time at which half of the initial substrates are hydrolyzed. However, we observed a slightly higher final product conversion of the *plurizyme* system compared to this multi-catalysis "modified $EH1_{A1}$ + $EH1_{B1}$" system (Supplementary Table 4). Because the first step of

the domino reactions is equally processing we hypothesized that this may be a reflection of the co-localization of both catalytic sites in the *plurizyme* system compared to the different locations in the multi-catalysts system. In agreement with this we observed that the time at which half of the final product, namely 1-naphthoquine or 3-phenylbutyric acid, is synthesized by this multi-catalyst system compared to the *plurizyme* catalyst slightly increased (Supplementary Table 4).

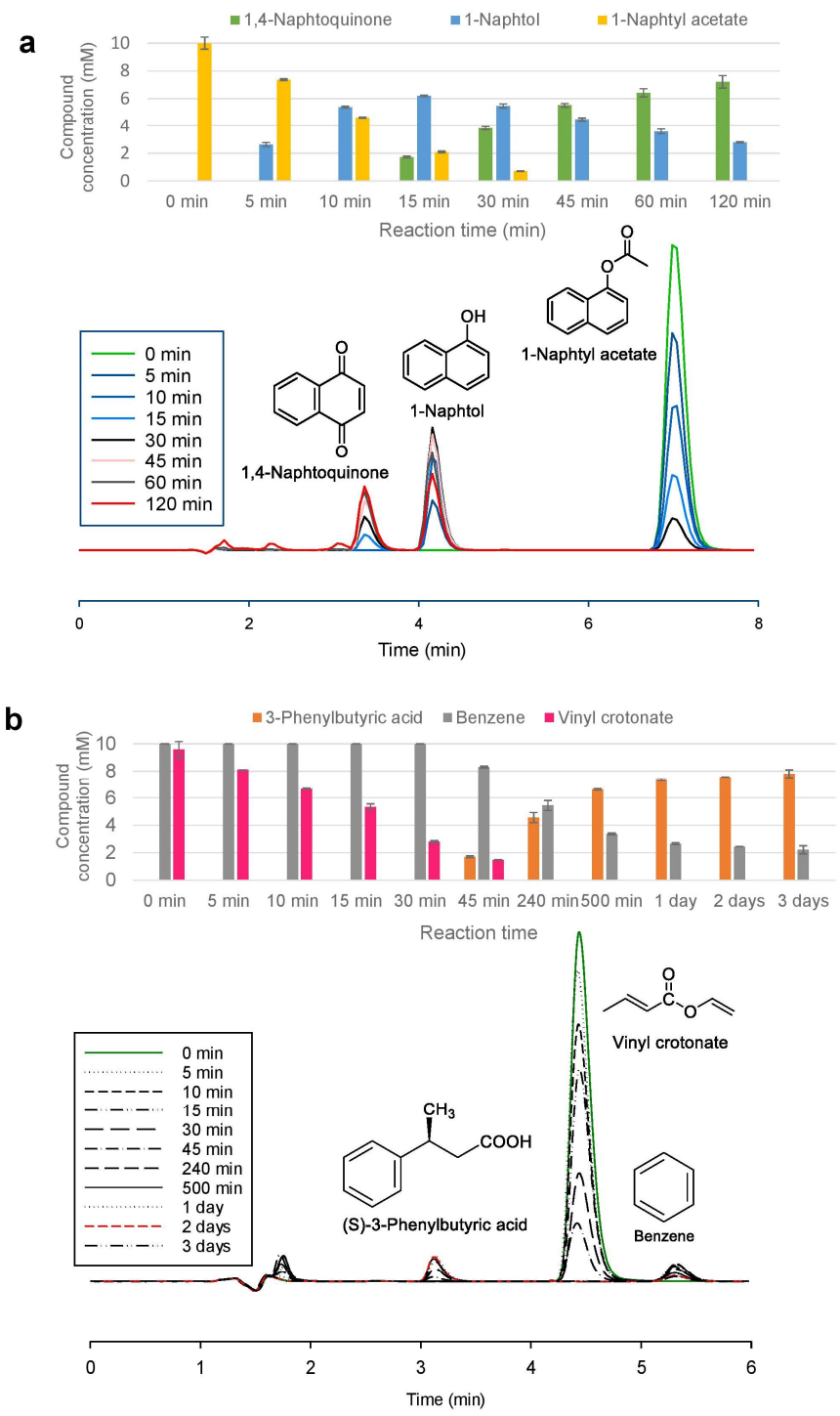

Supplementary Figure 31 Production of 1,4-naphthoquinone from 1-napthyl acetate (a) and 3-phenylbutyric acid from vinyl crotonate and benzene (b) using modified EH1$_{A1}$ and non-modified EH1$_{B1}$ multi-enzyme system. Reaction conditions as described in Figs. 8 and 9,

but in this case modified $EH1_{A1}$ and non-modified $EH1_{B1}$ (80 μM each) were used instead of modified *plurizyme*. Note: in this separate multi-catalysts system we used 80 μM of modified $EH1_{A1}$ and 80 μM of non-modified $EH1_{B1}$; this guarantee that, albeit the total protein concentration (160 μM) is double than that when using the modified *plurizyme* (80 μM), the concentration of each catalytic entity (the biological and the chemical) is maintained in both tests and the results are comparable. Reactions were performed in triplicates with average value and standard deviations (calculated using Excel version 2019) indicated.

Results above suggest that the modified *plurizyme* offers, in domino reactions, advantages compared to multi-catalyst systems. Although this advantage may not be of practical use at industrial level because high substrate concentrations are commonly used, these experiments emphasize that *plurizymes* can favor the conversion rate of one-pot domino reactions because the addition of an extra site, which by local effects may introduce catalytic advantages over the native site (e.g. by introducing a new temperature range for optimal activity) or because the favored substrate transfer by co-localization. Clearly, such advantages may vary from *plurizyme* to *plurizyme*.

Supplementary Note 10:
Protein purity and confirmation of mutations

Purity (>99%) was confirmed by SDS-polyacrylamide gel electrophoresis (Supplementary Figure 32) on 12% gels and Coomassie brilliant blue staining, as determined by densitometry.

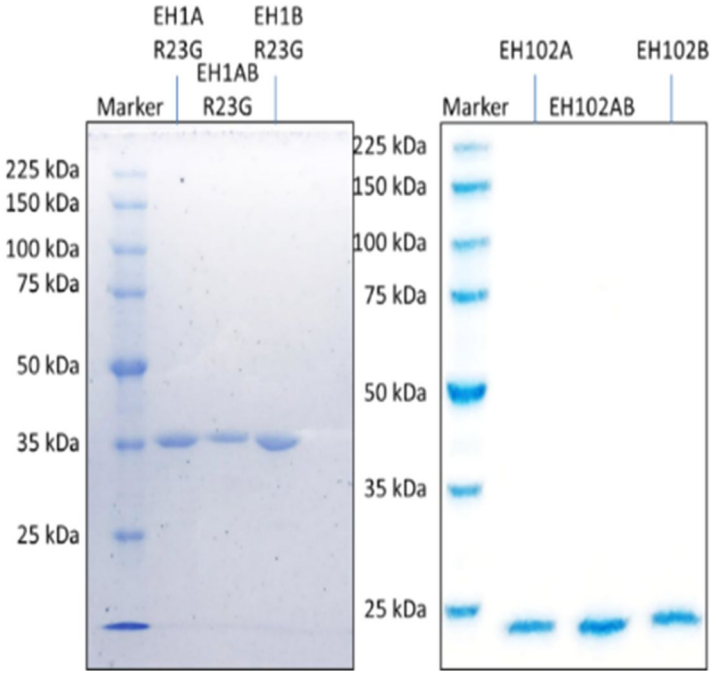

Supplementary Figure 32 Protein purity as determined by SDS-PAGE. A Coomassie brilliant blue (Protoblue Safe, National Diagnostics, GA, USA) stained SDS-PAGE gel in which a total of 20 μg of proteins purified after the His6-tag purification step followed by gel filtration step, are shown for EH1 (left panel) and EH102 (right panel) variants. Purity of the proteins was high (>99% by densitometry), which was further confirmed by mass spectrometry. The theoretical molecular mass of the native $EH1_A$ and $EH102_A$ proteins is 33936.23 and 24328.83 Da, respectively. SDS-PAGE was performed in a Mini PROTEAN electrophoresis system (Bio-Rad).

MALDI mass spectrometry of purified proteins was used to confirm the purity of the purified recombinant protein variants. We found that the molecular mass experimentally

obtained (~35 kDa) in all cases by MALDI agree with the theoretical monoisotopic mass of intact proteins calculated on the basis of sequence information, Supplementary the recombinant proteins do show the expected molecular masses (Supplementary Figure 33). MALDI intact mass analysis can also interpret the full mass spectrum without any deconvolution step and the analysis therefore gives a good indication of purity of protein samples. As shown in Supplementary Figure 33, the chromatographic protein purity was higher than 99%.

MALDI-TOF/TOF is a technique that can be also utilized to analyze the peptides for primary sequence confirmation and presence of mutations. For this reason, to confirm that the proteins contained the introduced mutations, peptide fingerprint by MALDI-TOF/TOF was performed using the purified proteins, and mutations were confirmed in $EH1_{A1}$ (Supplementary Figure 34), $EH1_{B1}$ (Supplementary Figure 35) and $EH1_{AB1}$ (Supplementary Figure 36). We also used DNA sequencing to also ensure that the mutations were correctly introduced.

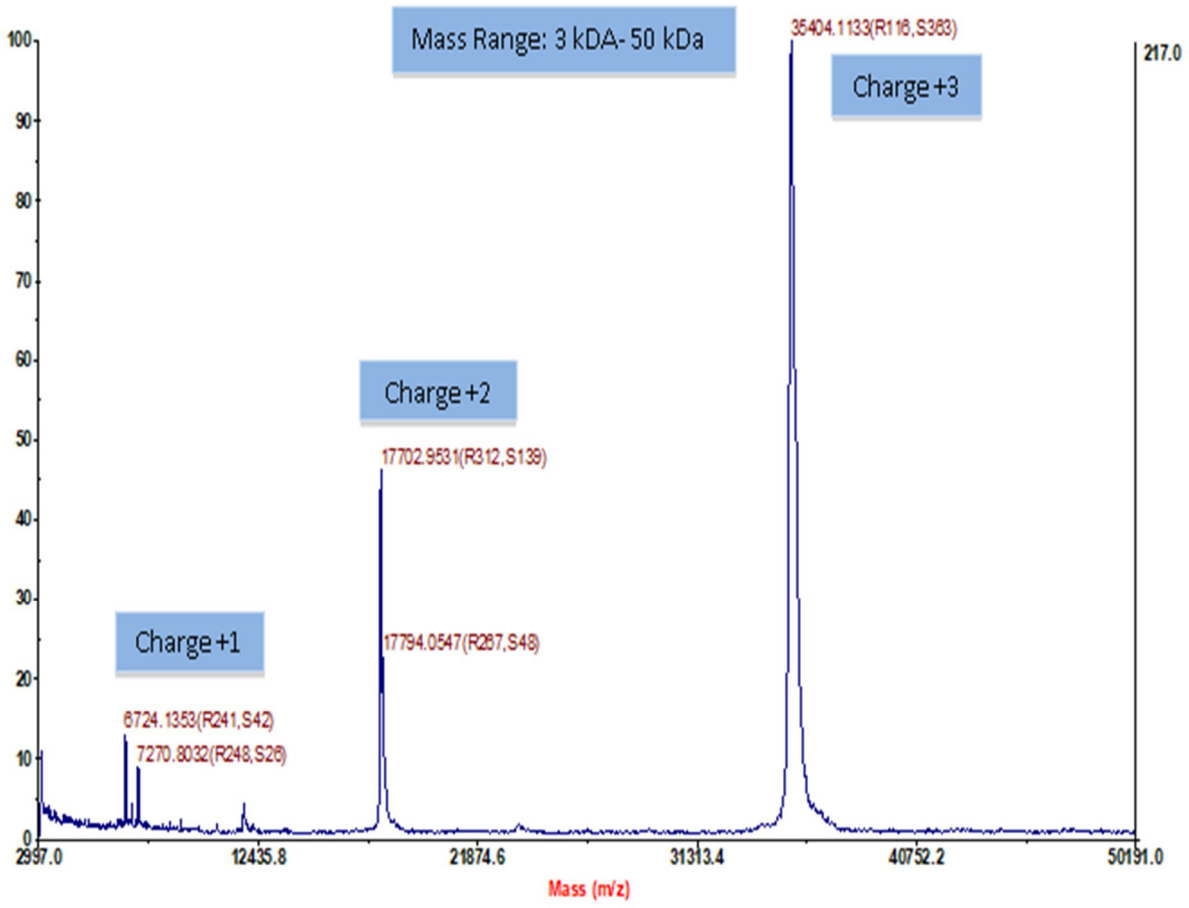

Supplementary Figure 33A. Analysis of $EH1_{A1}$ purified protein solution by MALDI-TOF/TOF. The mass (m)-to-charge (z) ratios (*m/z*) for the mass range from 3 to 50 kDa is shown. The MALDI analysis revealed a protein with estimated molecular mass of ~35 kDa, with no apparent contaminants. In the spectra, the peaks corresponding to the double and triple charge of the precursors are indicated.

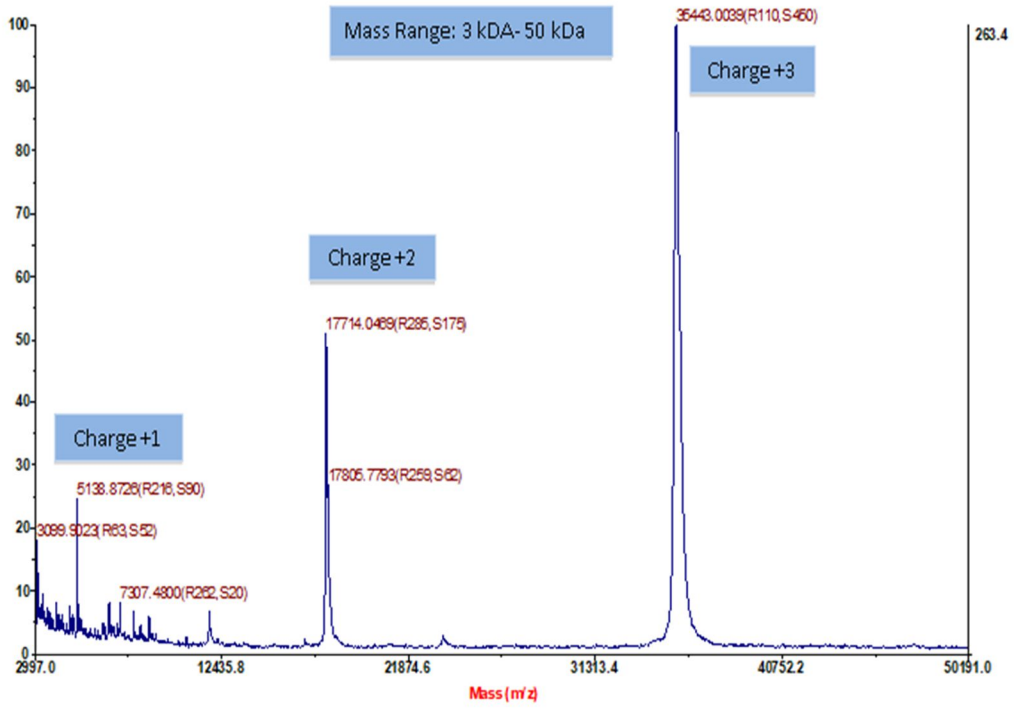

Supplementary Figure 33B. Analysis of EH1$_{B1}$ purified protein solution by MALDI-TOF/TOF. The mass (m)-to-charge (z) ratios (*m/z*) for the mass range from 3 to 50 kDa is shown. The MALDI analysis revealed a protein with estimated molecular mass of ~35 kDa, with no apparent contaminants. In the spectra, the peaks corresponding to the double and triple charge of the precursors are indicated.

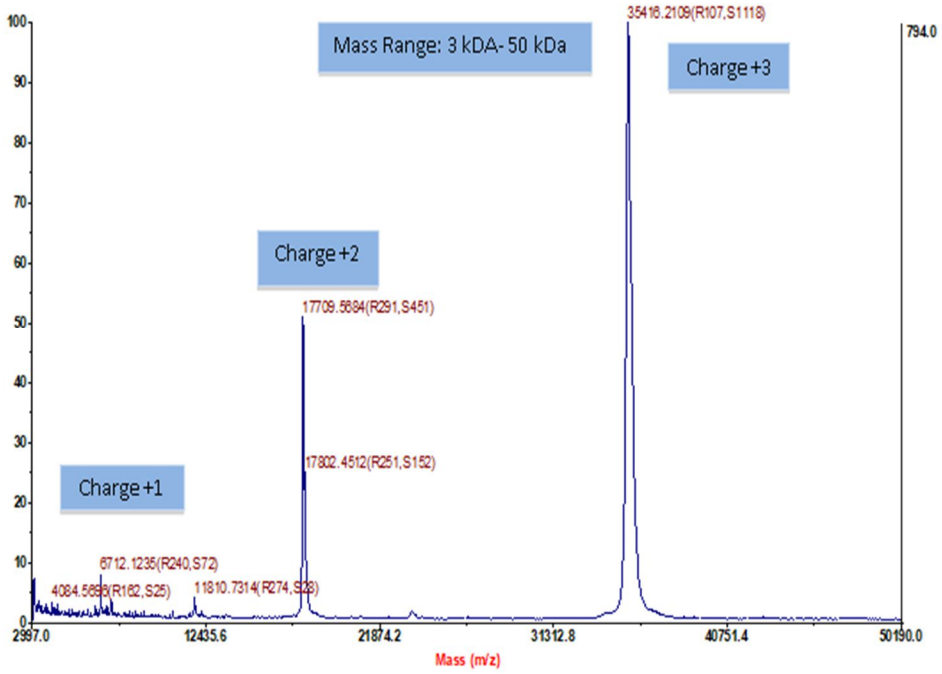

Supplementary Figure 33C. Analysis of EH1$_{AB1}$ purified protein solution by MALDI-TOF/TOF. The mass (m)-to-charge (z) ratios (*m/z*) for the mass range from 3 to 50 kDa is shown. The MALDI analysis revealed a protein with estimated molecular mass of ~35 kDa, with no apparent contaminants. In the spectra, the peaks corresponding to the double and triple charge of the precursors are indicated.

Supplementary Figure 34 MALDI-TOF/TOF analysis of $EH1_{A1}$ protein solution. (A) $EH1_{A1}$ sequence in which the detected peptides are shown in red color. In yellow are the residues conforming the native catalytic triad. In gray color the original residues that were needed to further accommodate the artificial active site, are indicated. In dark green color the residue which has been found key for improving the catalytic performance of the artificial site is indicated; this residue (number 23) was originally an Arg in the native $EH1_A$ protein, but was substituted by Gly in $EH1_{A1}$. (B) MS/MS chromatogram which shows the mass (m)-to-charge (z) ratios (*m*/*z*) of identified peptides, with those being specific for $EH1_{A1}$ being specifically indicated. (C) MASCOT search results of the mass of identified peptides.

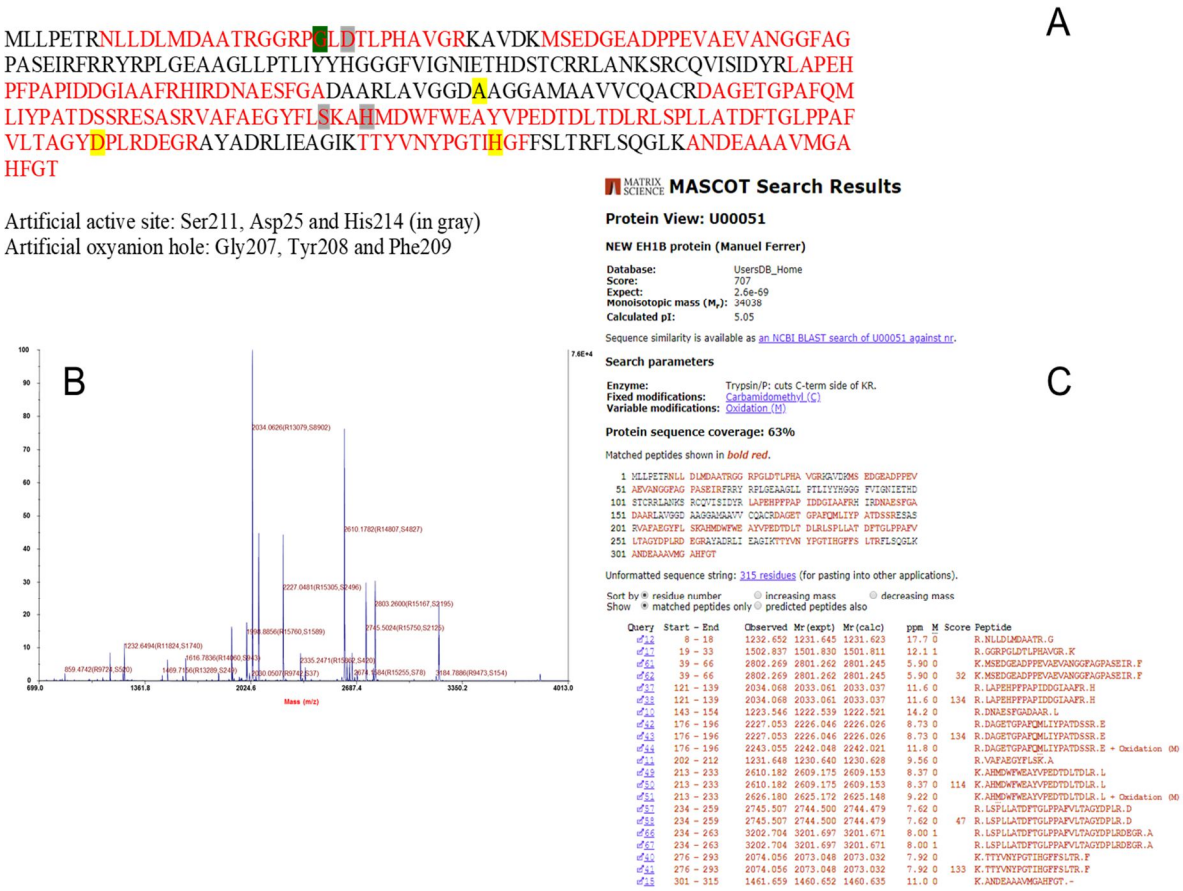

Supplementary Figure 35 MALDI-TOF/TOF analysis of $EH1_{B1}$ protein solution. A) $EH1_{B1}$ sequence in which the detected peptides are shown in red color. In yellow are the residues conforming the native catalytic triad. In gray color the original residues that were needed to further accommodate the artificial active site, are indicated. In dark green color the residue which has been found key for improving the catalytic performance of the artificial site is indicated; this residue (number 23) was originally an Arg in the native $EH1_A$ protein, but was substituted by Gly in $EH1_{A1}$. B) MS/MS chromatogram which shows the mass (m)-to-charge (z) ratios (*m/z*) of identified peptides, with those being specific for $EH1_{B1}$ being specifically indicated. C) MASCOT search results of the mass of identified peptides.

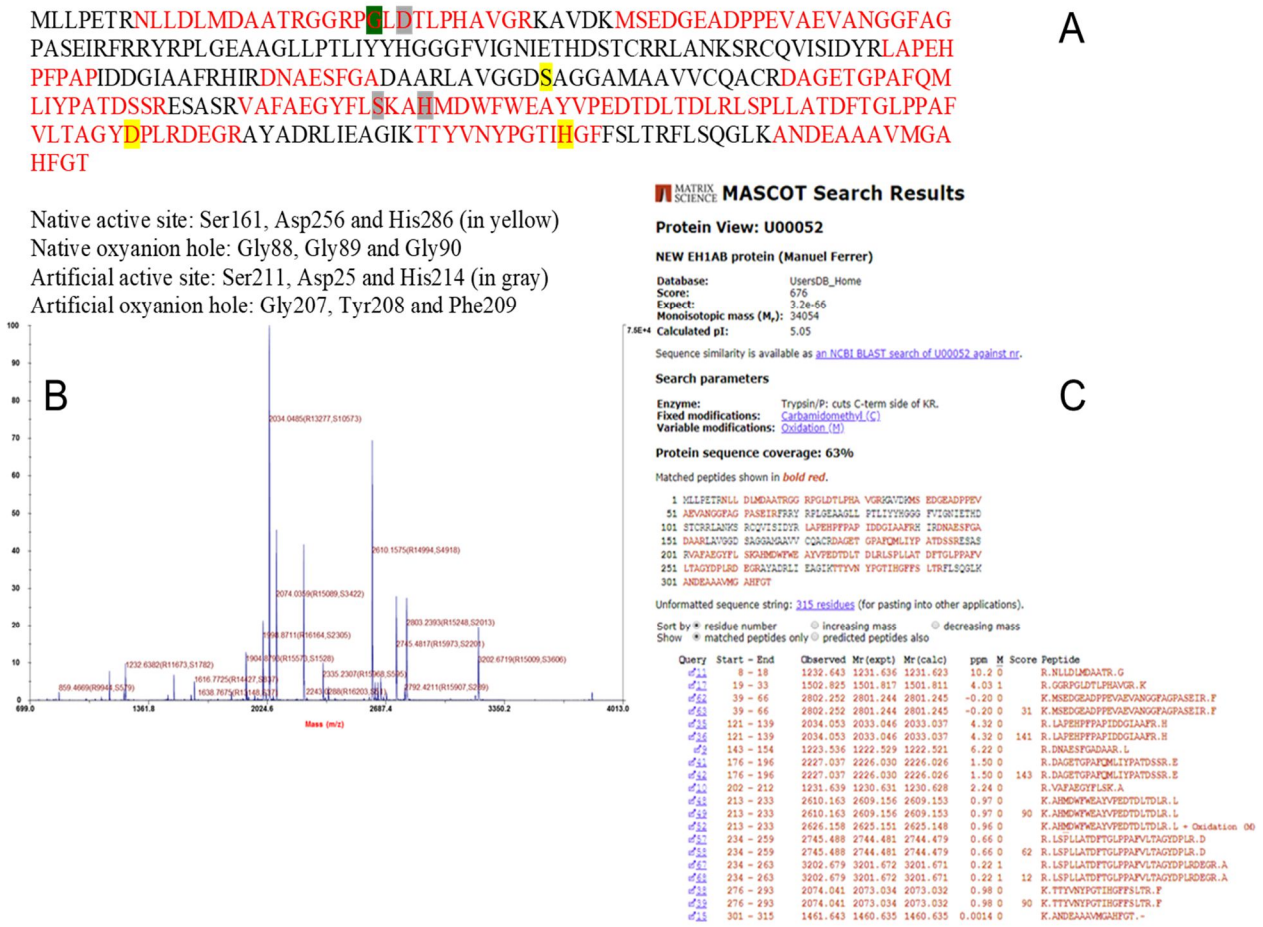

Supplementary Figure 36 MALDI-TOF/TOF analysis of $EH1_{AB1}$ protein solution. A) $EH1_{AB1}$ sequence in which the detected peptides are shown in red color. In yellow are the residues conforming the native catalytic triad. In gray color, the residues constituting the artificial active site are indicated. In dark green, the residue which has been found key for improving the catalytic performance of the artificial site is indicated. B) MS/MS chromatogram which shows the mass (m)-to-charge (z) ratios (*m/z*) of identified peptides, with those being specific for $EH1_{AB1}$ being specifically indicated. C) MASCOT search results of the mass of identified peptides.

Supplementary Methods

Chemicals, oligonucleotides, source of enzyme, strains, and medium. The sources of all chemicals (of the purest grade available), oligonucleotides for DNA amplification and serine ester hydrolases $EH1_A$, $EH1_B$, $EH1_{AB}$, and $EH102_A$ (available in the expression vector pET46 Ek/LIC plasmid in *Escherichia coli* BL21 as a host) used in the present study, were reported[1,5].

Site-directed mutagenesis. Mutagenic PCR was developed using the QuikChange Lightning Multi Site-Directed Mutagenesis kit (Agilent Technologies, Cheadle, UK), as described previously[1]. The forward primers used to generate the $EH1_{A1}$, $EH1_{B1}$ and $EH1_{AB1}$ variants with the R23G mutation are as follows: AGG GGC GGC CGG CCC GGG CTG GAG ACC CTG CCG or AGG GGC GGC CGG CCC GGG CTG GAT ACC CTG CCG. The forward primers used to generate the $EH102_B$ and $EH102_{AB}$ variants are as follows: Leu57Asp, CGA ACG GCG GCT GCG Gga CGT CAA CCA GGG CAA C; Leu30Ser, GAT CGG CGG CGA GGG Gag CTT CAA CGC CCA TGG C; Ser15Ala, CCC GCG TCC GTG ATC GcG TCG CCG ATG ATG ACC. To obtain variants containing Ser161Ala, Asp256Gln, and His286Phe (conforming the native sites) and Ser211Ala, Asp25Gln, His214Phe mutations, individually or in combination, the pET46 Ek/LIC plasmid containing $EH1_{A1}$, $EH1_{B1}$, or $EH1_{AB1}$ DNA inserts the primers Ser211Ala Fwd (GCC GAA GGC TAC TTC CTC GCC AAG GCG CAC ATG GAC TGG), Ser161Ala Fwd (GTG GGC GGC GAT GCG GCG GGC GGC G), Asp25Gln Fwd (CGG CCC GGG CTG GCG ACC CTG CCG CAT GC), Asp256Gln Fwd (ACC GCC GGC TAC CAA CCG CTG CGC GAC G), His214Phe Fwd (TTC CTC AGC AAG GCG TTC ATG GAC TGG TTC TGG G) and His286Phe Fwd (T CCC GGC ACC ATC TTC GGC TTC TTC TCG), were used. Mutagenic PCR conditions were as described[1].

Gene expression and protein purification. Expression (performed in Luria-Bertani medium with shaking at 250 rpm and 16ºC overnight) and purification (at 4ºC by binding to a Ni-NTA His-Bind resin, followed by size-exclusion chromatography) of the EH1 (Supplementary Table 5) and EH102 (Supplementary Table 6) protein variants, His-tagged at the N-terminus, were performed as previously described[1]. Purified proteins were stored at -20ºC. Purity (>99%) was confirmed by SDS-polyacrylamide gel electrophoresis on 12% gels and Coomassie brilliant blue staining, along with matrix-assisted laser desorption/ionization-time-of-flight/time-of-flight analysis which was also used to confirm the mutations introduced, as previously described (see Supplementary Note 10)[1]. The protein concentration was determined spectrophotometrically (at 280 nm) according to the corresponding amino acid sequence (www.expasy.org/tools/protparam.html) using a Take3 plate compatible with a Synergy HT Multi-Mode Microplate Reader.

Supplementary Table 5 Purification summary for $EH1_{A1}$, $EH1_{B1}$ and $EH1_{AB1}$ proteins.

Sample	Variant	Total protein (mg)[c]	Total activity (units)[d]	Specific activity (U/mg)[d]	Purity (%)[e]
Crude lysate[a]	$EH1_{A1}$	1467	1763	1.20	-
Purified protein[b]	$EH1_{A1}$	25	1642	65.68	>99
Crude lysate[a]	$EH1_{B1}$	1143	138	0.12	-
Purified protein[b]	$EH1_{B1}$	11	127	11.55	>99
Crude lysate[a]	$EH1_{AB1}$	1360	2084	1.53	-
Purified protein[b]	$EH1_{AB1}$	24	1875	78.13	>99

[a] From 4 g of wet weight *E. coli* cell pellet (from 2000 ml of bacterial culture).
[b] After Ni-NTA His-Bind resin and gel filtration.
[c] Protein concentration determined by Bradford assay using BSA as a standard protein. Values representing averages of three independent fermentations and purifications.
[d] Activity determined using glyceryl tripropionate as substrate[1,2]. Values representing averages of three independent fermentations and purifications.
[e] Calculated by densitometry in the SDS-PAGE. Values representing averages of three independent fermentations and purifications.

Supplementary Table 6 Purification summary for $EH102_A$, $EH102_B$ and $EH102_{AB}$ proteins.

Sample	Variant	Total protein (mg)[c]	Total activity (units)[d]	Specific activity (U/g)[d]	Purity (%)[e]
Crude lysate[a]	$EH102_A$	322	59330	184.3	-
Purified protein[b]	$EH102_A$	59	52860	895.9	>99
Crude lysate[a]	$EH102_B$	317	760	2.4	-
Purified protein[b]	$EH102_B$	41	490	12.0	>99
Crude lysate[a]	$EH102_{AB}$	454	93300	205.6	-
Purified protein[b]	$EH102_{AB}$	91	88300	970.3	>99

[a] From 4 g of wet weight *E. coli* cell pellet (from 2000 ml of bacterial culture).
[b] After Ni-NTA His-Bind resin and gel filtration.
[c] Protein concentration determined by Bradford assay using BSA as a standard protein. Values representing averages of three independent fermentations and purifications
[d] Activity determined using glyceryl tripropionate as substrate[1,2]. Values representing averages of three independent fermentations and purifications
[e] Calculated by densitometry in the SDS-PAGE. Values representing averages of three independent fermentations and purifications

Enzyme assays. Specific activity (units mg^{-1}), V_{max}, k_{cat} and K_m determinations for ester substrates were assayed at 550 nm using a pH indicator (phenol red; $\varepsilon_{550\,nm}$ = 8450 M^{-1} cm^{-1}) assay at 550 nm in 384-well plates as previously described[1,2]. Conditions used for EH1 sub-enzymes kinetic assays are described in Figure S2 legend; V_{max} determination for EH102 sub-enzymes are described in Figure S22 legend. If otherwise not indicated, reactions were performed, in triplicates and corrected for non-enzymatic transformation, at 30ºC and in 5 mM N-(2-hydroxyethyl)piperazine-N'-(3-propanesulfonic acid (EPPS) buffer pH 8.0. For determination of temperatures under which each sub-enzyme displayed maximal activity (T_{opt}), the following conditions were used - [protein]: 4.5 μg/ml; [α-naphthyl acetate or glyceryl tripropionate]: 50 mM; reaction volume: 44 μl; T: 4-55ºC; pH: 8.0.

The K_M fits for the $EH1_{A1}$, $EH1_{B1}$ and $EH1_{AB1}$ variants are shown in Supplementary Note 11.

PELE simulations. PELE (Protein Energy Landscape Exploration) introduces a Monte Carlo (MC) procedure where an stochastic perturbation is followed by a relaxation step using protein structure prediction algorithms. The code, intended to map the energy landscape of protein-ligand complexes[8-10], was designed to use massive parallel HPC, where a computing core runs an individual trajectory; typically, simulations involve from tens to hundreds of processors for thousand MC steps. The heuristic MC procedure involves the following steps:

1) Ligand Perturbation. The ligand, which is built by a rigid core and a set of rotatable fragments, is initially perturbed by forcing a translation and a rotation. About ~20 random poses are tried and scored. Based on the different goals, translation and rotations take different values.

2) Protein Perturbation. As a second step, the backbone is perturbed following normal modes calculated using the Anisotropic Network Model (ANM) It is possible to use a single mode, or to mix several ones; modes are selected from (typically) the 6 lowest frequency modes, since they are the ones more closely related to conformational movements.

3) Side Chain Sampling. Side chains readjustment is done for all residues local to the substrate.

4) Minimization. The sampling procedure ends by a loose (only 0.1 rmsg convergence criteria) multi-scale Truncated Newton minimization.

The resulting structure is then accepted or rejected based on a Metropolis test. PELE uses the OPLS 2005 energy function along with a Surface Generalized Born (SGB) implicit solvation model.

We modeled the binding mode of glyceryl tripropionate with $EH1_A$ and $EH102_A$ structures (PDB codes: 5JD4 and 5JD3), as described previously[1]. Crystal structures were taken from the PDB codes mentioned, and the protonation of the titratable residues was approximated using

Protein Preparation Wizard (PROPKA) and a visual inspection. At pH 8, the value at which reactions were evaluated in this study, the catalytic triad residues form a serine-histidine and histidine-aspartic hydrogen-bonding inner network. The chosen ligand (glyceryl tripropionate) parameters were extracted from full quantum mechanics optimizations using Jaguar from Schrodinger[11].

PELE's maximum allowed translation for the ligand perturbation was 1.5 Å, and the maximum rotation was 20°. During the protein perturbation, all atoms were displaced by a maximum of 0.5 Å by moving the α-carbons following a random linear combination of the 6 lowest eigenvectors obtained in the ANM model. The relaxation step included the repositioning of all amino acid side chains within 6 Å of the ligand and the 5 side chains with the highest energy increases during the previous ANM step. The substrate binding plots contained all accepted conformations for three 12-h simulations performed using 200 processors.

Molecular dynamics. We performed 250-ns molecular dynamics with GROMACS to ensure enzymatic stability[12,13]. After appropriate system preparation, as was previously described[1], an orthorhombic box (minimum distance of 10 Å) was introduced. Then, equilibration was performed, followed by NPT simulation at 300 K and 1 atm with the OPLS-2005 force field. Temperature regulation was controlled by a Berendsen thermostat.

Crystallization and X-ray structure determination of $EH1_{AB1}$. Initial crystallization conditions were explored by high-throughput techniques with a NanoDrop robot (Innovadyne Tecnhologies Inc.), using different protein concentrations in 40 mM HEPES pH 7, 150 mM NaCl, and commercial screens: Index (Hampton Research), JBScreen PACT++ (Jena Bioscience) and JCSG+ Suite (Qiagen). Further optimizations were carried out and thin bar-shape crystals of $EH1_{AB1}$ were grown after one day using 1 μL of protein (30 mg/mL) and 0.5 μL of precipitant solution (45% PEG P400, 0.1 M BIS-TRIS pH 6.5). The complex with the suicide inhibitor, a derivative of methyl 4-nitrophenyl hexylphosphonate (M-4NHP), was obtained by cocrystallization assays incubating a solution of $EH1_{AB1}$ (13 mg/mL) in 40 mM HEPES pH 7, 150 mM NaCl with 20 mM of the inhibitor during 1.5 h. $EH1_{AB1}$ crystals were grown using 1 μL of the mixture, 0.2 μL of microseeding and 1 μL of precipitant solution (24% PEG 3350, 0.2 M NaF). The complex with CuSI was obtained by cocristallization assays incubating $EH1_{AB1}$ (16 mg/mL) with 1.22 mM of the ligand during 1.3 h. $EH1_{AB1}$ crystals were grown using 250 nL of the mixture and 250 nL of precipitant solution (20% PEG 3350, 0.1 M bis-tris propane pH 7.5 and 0.2 M NaF).

For data collection, crystals were transferred to cryoprotectant solutions consisting of mother liquor plus 20-30 % (v/v) glycerol, before being cooled in liquid nitrogen. Diffraction data were collected using synchrotron radiation on the XALOC beamline at ALBA (Cerdanyola del Vallés, Spain) and the ID30A-1/MASSIf-1 beamline at ESRF (Grenoble, France). Diffraction images were processed with XDS[14] and merged using AIMLESS[15] from the CCP4 package[16]. Crystals of native and complex with M-4NHP were indexed in the $P2_12_12_1$ space group, with two molecules in the asymmetric unit and 52% solvent content within the unit cell. Crystals of the CuSI complex belongs to C2 space-group, with four molecules in the asymmetric unit and 56% solvent content. The data-collection statistics are given in Supplementary Table 6. The structure of $EH1_{AB1}$ was solved by Molecular Replacement with MOLREP[17] using the coordinates of the native protein (PDB code 5JD4), while the structures of the complexes were solved using the $EH1_{AB1}$ coordinates. Crystallographic refinement was performed using the program REFMAC[18] within the CCP4 suite with flat bulk-solvent correction, maximum likelihood target features and local non-crystallographic symmetry (NCS). Two regions, 19-33 and 203-218 building the secondary catalytic site, were excluded from the NCS groups in the ligand-free structure. Free R-factor was calculated using a subset of 5% randomly selected structure-factor amplitudes that were excluded from automated refinement. At the later stages, ligands were manually built into the electron density maps with Coot[19] and water molecules were included in the model, which, combined with more rounds of restrained refinement, reached the R factors listed in Supplementary Table 7. For methyl 4-nitrophenyl hexylphosphonate and CuSI derivatives, not present in the Protein Data Bank, a model was built using MacPyMOLX11Hybrid (The PyMOL Molecular Graphics System, Version 2.0 Schrödinger, LLC). The model was used to automatically generate coordinates and molecular

topologies with eLBOW[20] suitable for REFMAC refinement. The figures were generated with PyMOL. The crystallographic statistics of $EH1_{AB1}$ are listed in Supplementary Table 7.

Supplementary Table 7 Crystallographic statistics of $EH1_{AB1}$.

Values in parentheses are for the high resolution shell			
Crystal data	$EH1_{AB1}$	$EH1_{AB1}$ /M-4NHP	$EH1_{AB1}$ - CuSI
Space group	$P2_12_12_1$	$P2_12_12_1$	$C2$
Unit cell parameters			
a (Å)	82.23	83.08	90.77
b (Å)	86.04	86.09	201.92
c (Å)	98.17	97.61	90.64
Data collection			
Beamline	ESRF-ID30A-1	ALBA-XALOC	ALBA-XALOC
Temperature (K)	100	100	100
Wavelength (Å)	0.966000	0.979240	0.97926
Resolution (Å)	43.02-2.11 (2.17-2.11)	43.04-2.35 (2.43-2.35)	49.08-2.79 (2.91-2.79)
Data processing			
Total reflections	237360 (19288)	162578 (16075)	141280 (17628)
Unique reflections	40731 (3301)	29764 (2895)	37139 (4557)
Multiplicity	5.8 (5.8)	5.5 (5.6)	3.8 (3.9)
Completeness (%)	99.9 (100.0)	99.7 (99.8)	99.1 (99.3)
Mean I/σ (I)	10.6 (3.1)	8.6 (2.9)	2.7 (1.6)
R_{merge}[†] (%)	12.4 (64.1)	14.9 (64.6)	27.7 (57.2)
R_{pim}[††] (%)	5.7 (29.6)	6.9 (29.6)	16.1 (32.7)
Molecules per ASU	2	2	4
Refinement			
R_{work} / R_{free}[†††] (%)	16.0/19.8	17.7/21.3	23.9/27.6
Nº of atoms/average B	5245/30.81	5002/29.67	9764/52.46
Macromolecule	4770/29.71	4810/29.59	9628/52.42
Ligands	144/49.89	30/48.80	64/71.13
Solvent	331/38.26	162/28.58	72/40.76
Ramachandran plot (%)			
Favoured	94.3	96.0	95.1
Outliers	0.5	0.6	0.6
RMS deviations			
Bonds (Å)	0.007	0.006	0.007
Angles (°)	1.192	1.4920	1.4764
PDB accession codes	6I8F	6RB0	6RKY

[†] $R_{merge} = \sum_{hkl} \sum_i | I_i(hkl) - [I(hkl)]| / \sum_{hkl} \sum_i I_i(hkl)$, where $I_i(hkl)$ is the ith measurement of reflection hkl and [I(hkl)] is the weighted mean of all measurements.

[††] $R_{pim} = \sum_{hkl} [1/(N - 1)]^{1/2} \sum_i | I_i(hkl) - [I(hkl)]| / \sum_{hkl} \sum_i I_i(hkl)$, where N is the redundancy for the hkl reflection.

[†††] $R_{work} / R_{free} = \sum_{hkl} | Fo - Fc | / \sum_{hkl} | Fo |$, where Fc is the calculated and Fo is the observed structure factor amplitude of reflection hkl for the working / free (5%) set, respectively.

Suicide inhibition assays. We used the suicide inhibitors methyl, butyl and octyl 4-nitrophenyl hexylphosphonate (Eurocodis Bioscience GmbH, Wien, Austria) to test for the ability to inactivate all EH1 and EH102 sub-enzymes reported in this study. For this experiment, 7.5 μM proteins were incubated with 15 μM (for $EH1_{A1}$, $EH1_{B1}$, $EH102_{A}$, and $EH102_{B}$) or 30 μM (for $EH1_{AB1}$ and $EH102_{AB}$) inhibitors (from a 0.3 M-stock solution in dimethylsulfoxide). Incubation was performed in 40 mM 4-(2-hydroxyethyl)-1-piperazineethanesulfonic acid (HEPES) buffer at pH 7.0, with a total volume of 200 μL. The progress of inhibition at 25ºC was followed by taking aliquots (10 μL) at different time intervals and measuring the remaining enzyme activity, at 30ºC and pH 8.0, using the pH indicator assay[1] and glyceryl tripropionate as substrate - [protein]: 1.7 mM; [glyceryl tripropionate]: 50 mM; reaction volume: 44 μl (in 384-well plates); T: 30ºC; pH: 8.0. The capacity of the proteins to perform hydrolysis of the suicide inhibitor was also followed at 405 nm based on the release of *p*-nitrophenol (ε_{pNP} at 405 nm = 14280 M^{-1} cm^{-1}).

The suicide inhibitor 3'-hydroxy-[2,2'-bipyridin]-3-yl methyl hexylphosphonate (SI) was also tested to inactivate the EH1 sub-enzymes. For this small-scale experiments, 15 μM (per monomer) proteins were incubated with an excess (120 μM) of inhibitor (from a 40 mM-fresh stock solution in dimethylsulfoxide). Incubation was performed in 50 mM K_2HPO_4 buffer pH 6.5, with a total volume of 250 μL. The progress of inhibition at 25ºC was followed by taking aliquots (10 μL) at different time intervals and measuring the remaining enzyme activity, at 30ºC and pH 8.0, using the pH indicator assay[1] and glyceryl tripropionate as substrate - [protein]: 3.4 mM; [glyceryl tripropionate]: 50 mM; reaction volume: 44 μl (in 384-well plates); T: 30ºC; pH: 8.0. In all cases, reactions were performed in triplicate and corrected for non-enzymatic transformation. Copper incorporation to the modified proteins was achieved by adding $Cu(NO_3)_2$ (4.720 mg/mL) to a final concentration of 160 μM. The solution was maintained 24 h, after which the samples were extensively dialyzed as will be described below.

The differential affinity of each EH1 sub-enzyme for the SI inhibitor was evaluated as follows. A protein solution containing 80 μM (per monomer) of each sub-enzyme in 50 mM K_2HPO_4 buffer pH 6.5 was prepared in a final volume of 1000 μL. To this, aliquots of a fresh 40 mM-stock solution (in dimethyl sulfoxide) of SI were added to achieve a final concentration ranging from 0 to 100 μM. After 10 min incubation at 25ºC, 10 μL-aliquots were taken and the loss of hydrolytic activity, compared to a control without inhibitor, was measured at 30ºC and pH 8.0 using the pH indicator assay[1] and glyceryl tripropionate as substrate - [protein]: 18 μM; [glyceryl tripropionate]: 50 mM; reaction volume: 44 μl (in 384-well plates); T: 30ºC; pH: 8.0.

In all cases, inhibition tests and reactions were performed in triplicate and corrected for non-enzymatic transformation.

Scale up coupling of Cu^{2+}-organic complex by dose-dependent inhibition. $EH1_{AB1}$ protein solution (80 μM, per monomer) in 50 mM K_2HPO_4 buffer pH 6.5 was prepared to a final volume of 1000 μL. To this, 0.5 μL of a fresh 40 mM-stock solution (in dimethyl sulfoxide) of SI were added, to achieve a final concentration of 20 μM. After 10 min incubation, an additional amount of 20 μM SI was added, and the process repeated four times more. Finally, $Cu(NO_3)_2$ (4.720 mg/mL) was added to a final concentration of 160 μM. The solution was maintained 24 h, after which the protein samples were extensively dialyzed using Pur-A-LyzerTM Maxi 1200 dialysis kit ((Sigma Chemical Co. (St Louis, MO, USA)), as follows. One ml protein solution was dialyzed against 2 L buffer during 1 hour at room temperature, after which the buffer was changed by other 2 L buffer and maintained 1 hour more. Then, the buffer was changed and the dialysis was kept overnight at 4ºC. The dialyzed protein solution was recovered and concentrated by ultra-filtration through low-adsorption hydrophilic 10000 nominal molecular weight limit cutoff membranes (regenerated cellulose, Amicon) to reach a final protein concentration of 80 μM (per monomer). This scale up process was also repeated with $EH1_{A1}$ and $EH1_{B1}$ proteins. A total amount of *ca*. 3 mg protein variants/catalysts were obtained in all cases. (*CAUTION: the copper-bipyridine chemo-biocatalysts were prepared immediately prior to use*).

UV-Vis spectrophotometric analysis of Cu(II)-bipyridine. The absorption spectra of the resulting catalysts generated in this study were recorded in a Synergy HT Multi-Mode Microplate Reader – BioTek to verify the conjugation of copper-bipyridine. Spectra were

recorded at wavelength from 250 to 500 nm in 96-well plates (200 µL) using, if otherwise not indicated, 15 µM Cu^{2+}-bipyridine conjugated sub-enzymes, 15 µM non-conjugated protein, 15 µM SI or 15 µM SICu. Measurements were performed in 50 mM K_2HPO_4 buffer pH 6.5.

Gas chromatography (GC) analysis for determination of chiral selectivity. Enantio-selectivity was evaluated (at 30ºC) by using kinetic resolution of methyl (2*R*)-2-phenylpropanoate and methyl (2*S*)-2-phenylpropanoate, or (+)-ethyl (*R*)-lactate and (−)-ethyl (*S*)-lactate, or ethyl (*S*)-(−)-4-chloro-3-hydroxybutyrate and ethyl (*R*)-(+)-4-chloro-3-hydroxybutyrate. Briefly, 2 µL of racemic ester (from a stock solution of 200 mg/mL in acetonitrile) were added to 96 µL of 40 mM HEPES buffer, pH 7.0. Then, 2 µL of enzyme solution (from a stock solution of 10.0 mg/ml in 40 mM HEPES buffer, pH 7.0) were added. After 60 min (for $EH1_{B1}$ and $EH1_{AB1}$) or 24 h (for $EH1_{A1}$), reactions with racemic mixtures, were stopped by adding 1800 µL HPLC-grade methanol and the reaction products analysed by GC. For EH102 variants, reaction time was fixed to 60 min.

Sample treatment: 100 µL of sample were vigorously mixed (3 minutes) with 20 µL of internal standard and 100 µL of H_2O (30g/100mL NaCl) and subsequently extracted twice by the addition of 100 µL of ethyl acetate (5 minutes of vigorously mixing at 50 Hz, follow by centrifugation at 16000 g, 3 minutes, 4°C).

Analytical method:

a) Methyl (2R) phenylpropanoate / methyl (2S) phenylpropanoate

GC system (Agilent Technologies 7890A) consisted in an auto sampler (Agilent Technologies 7693) and an inert MSD with Quadrupole (Agilent Technologies 5975). 1 µL of the sample were injected through a GC-Column CP-Chirasil-Dex CB (25 m length, 0.25 µm internal diameter, 0.25 µm film) (Agilent J&W GC Columns). The flow rate of the helium carrier gas (1 mL/min), the split ratio (1:25) and the temperature gradient (80°C-1min, 10°C/min to 150°C, 8 minutes total analysis time) were optimized for the separation of the chiral mix. After each injection the column was cleaned up during 2 minutes at 200°C, 1.5 mL/min flow rate. The elution order was previously validated with a standards mix. The semi-quantification of each analyte was performed using MassHunter Qualitative Analysis software (B.08.00, Agilent), reporting the area for the individual peaks in arbitrary units. In order to monitor the extraction procedure and the analytical variability, an internal standard was added ((-)-ethyl (S)-lactate, 200 mg/L).

b) (+)-Ethyl (R)-lactate / (-)-ethyl (S)-lactate

GC system (Agilent Technologies 7890A) consisted in an auto sampler (Agilent Technologies 7693) and an inert MSD with Quadrupole (Agilent Technologies 5975). 1 µL of the sample were injected through a GC-Column CP-Chirasil-Dex CB (25 m length, 0.25 µm internal diameter, 0.25 µm film) (Agilent J&W GC Columns). The flow rate of the helium carrier gas (1 mL/min), the split ratio (1:25) and the temperature gradient (80°C-1min, 5°C/min to 110°C, 10°C/min to 140°C, 140°C-0.5 min, 10.5 minutes total analysis time) were optimized for the separation of the chiral mix. After each injection the column was cleaned up during 2 minutes at 200°C, 1.5 mL/min flow rate. The elution order was previously validated with a standards mix. The semi-quantification of each analyte was performed using MassHunter Qualitative Analysis software (B.08.00, Agilent), reporting the area for the individual peaks in arbitrary units. In order to monitor the extraction procedure and the analytical variability, an internal standard was added (methyl (2R) phenylpropanoate, 200 mg/L).

c) Ethyl (R)-(+)-4-chloro-3-hydroxybutyrate / ethyl (S)-(-)-4-chloro-3-hydroxybutyrate

GC system (Agilent Technologies 7890A) consisted in an auto sampler (Agilent Technologies 7693) and an inert MSD with Quadrupole (Agilent Technologies 5975). 1 µL of the sample were injected through a GC-Column CP-Chirasil-Dex CB (25 m length, 0.25 µm internal diameter, 0.25 µm film) (Agilent J&W GC Columns). The flow rate of the helium carrier gas (0.65 mL/min), the split ratio (1:25) and the temperature gradient (85°C-76min, 1°C/min to 92°C, 83 minutes total analysis time) were optimized for the separation of the chiral mix. After each injection the column was cleaned up during 2 minutes at 200°C, 1.5 mL/min flow rate. The elution order was previously validated with a standards mix. The semi-quantification of each analyte was performed using MassHunter Qualitative Analysis software (B.08.00, Agilent),

reporting the area for the individual peaks in arbitrary units. In order to monitor the extraction procedure and the analytical variability, an internal standard was added (methyl (2S) phenylpropanoate, 200 mg/L).

GC-MS chromatograms representing the retention time and abundance of substrates and products for determination of chiral selectivity are shown in Supplementary Note 12.

Electrochemical measurements. The electrochemical experiments were run at 22±1 ºC in a 3-electrode electrochemical cell configuration. Gold disc electrodes (Metrohm, 2 mm diameter) were used as working electrodes. The reference electrode selected was BAS Ag/AgCl 3M (+210 mV vs SHE) and the counter electrode was a platinum wire. All redox potentials shown in the work are given vs. Ag/AgCl. The electrochemical voltammetric experiments were recorded with an Autolab PGSTAT30 controlled with GPES 4.9 software (EcoChemie, NL) whereas the Impedance measurements were performed using NOVA2 software (EcoChemie, NL).

For gold surface cleaning and modification, gold electrodes were immersed in "piranha" solution (3 H_2SO_4 98% : 1 H_2O_2 30%) during 15 min. Afterwards the electrodes were rinsed with water and polished against alumina slurry 0.05 μm in diameter during 3 min. (*CAUTION: Piranha solution is especially dangerous, is corrosive, and may explode if contained in a closed vessel; it should be handled with special care.*) After rinsing the electrodes were taken into an EtOH/H_2O 2:1 solution and immersed into an ultrasound bath during 15 min. Later the electrodes were taken into an electrochemical cell containing 0.5 NaOH and 20 electrochemical reductive cyclic voltammograms from 0 to -1.5 V using 200 $mV \cdot s^{-1}$ scan rate were performed to clean the gold surface. Final activation/cleaning step consisted on 25 oxidative cyclic voltammograms from 0 to +1.5 V using 100 $mV \cdot s^{-1}$ scan rate and H_2SO_4 0.1M as electrolyte.

Modification of gold electrodes was performed by immersion of the freshly cleaned electrodes into an ethanol solution containing 1mM thiol. The thiols tested were 3-mercaptopropionic acid (MPA), 6-mercapto-1-hexanol (MH) or thioctic acid (TOA). Solutions were let to react overnight and clean by immersion in ethanol during 15 min. Enzyme variants were immobilized by physical adsorption by incubating the electrode inside a solution containing the corresponding modified or non-modified sub-enzyme (*ca*. 0.43 mM), in phosphate buffer 50 mM pH 6.5, during 1 hour. Afterwards it was taken into the electrochemical cell to determine the electrochemical response. In case of the control samples, Cu^{+2} (1 mM) or SICu (1 mM) in phosphate buffer 50 mM pH 6.5 were added directly to the electrochemical cell.

Chemo-biocatalyst catalysed hydrolytic & oxidation reaction from 1-napthyl acetate. The catalytic solution contained 80 μM of the copper-bipyridine chemo-biocatalyst ($EH1_{AB1CB}$) in HEPES buffer (40 mM HEPES, pH 7.0) to a final volume of 1000 μL. To this 50 μL of a 200 mM-fresh stock solution of substrate **1** (in acetonitrile) was added. The reaction was mixed for up to 240 min at 25^{0}C. At indicated time, 100 μL were taken and reaction stopped by the addition of 900 μL of methanol, and the conversion was determined using HPLC.

A control reaction using modified sub-enzymes (80 μM) without Cu^{2+} was used under the same conditions. To compare the catalytic advantage of a *plurizyme* combining a biocatalytic hydrolytic active site acting in concert with a metal-complex chemocatalytic site over a traditional multi-catalyst system, we performed a second control experiment. In this control tests 80 μM of modified $EH1_{A1}$ (bearing a Cu^{2+}-organic molecule) and 80 μM of non-modified $EH1_{A1}$ were combined for the reaction, which was performed as above.

Chemo-biocatalyst catalysed hydrolytic & Friedel-Crafts reaction. The catalytic solution contained 80 μM of the copper-bipyridine chemo-biocatalyst ($EH1_{AB1CB}$) in HEPES buffer (40 mM HEPES, pH 7.0) to a final volume of 1000 μL. To this 20 μL of a 200 mM-fresh stock solution of substrate **7** (in acetonitrile) and 50 μL of 200 mM-fresh stock solution of substrate **9** (in acetonitrile) were added. The reaction was mixed for up to 3 days by continuous inversion at 4 ^{0}C. At indicated time, 100 μL were taken and reaction stopped by the addition of 900 μL of methanol, and the conversion and enantio-specificity were determined using HPLC and GC.

A control reaction using modified sub-enzymes (80 μM) without Cu^{2+} was used under the same conditions. To compare the catalytic advantage of a *plurizyme* combining a biocatalytic hydrolytic active site acting in concert with a metal-complex chemocatalytic site over a traditional multi-catalyst system, we performed a second control experiment. In this control

tests 80 µM of modified $EH1_{A1}$ (bearing a Cu^{2+}-organic molecule) and 80 µM of non-modified $EH1_{A1}$ were combined for the reaction, which was performed as above.

HPLC analysis method for 1-naphtol, 1-naphtyl acetate and 1,4-naphtoquinone determinations. The progress of the reactions was followed by HPLC. Prior to the analysis, samples were filtered through a 0.45 mm filter and the presence of the substrates and reaction products were quantified by HPLC analysis, performed using a quaternary pump (model 600, Waters) coupled to an autosampler (Varian ProStar, model 420). The injection volume was 10 µL. The temperature of the column was kept constant at 40 °C. The detection of peaks was carried out using a photodiode array detector (ProStar, Varian). Quantification was performed at 270 nm and integration was carried out using the Varian Star LC workstation 6.41. The column was a Zorbax Eclipse Plus C-18 (4.6 x 100 mm, 3.5 µm, Agilent Technologies) and the mobile phase was acetonitrile/H_2O 48:52 (v/v), degassed with helium, in isocratic during 8 minutes. Both solvents contained 0.1% (v/v) of formic acid degassed with helium. The flow rate was 0.8 ml/min. The peak area corresponding to 1-naphthylacetate, 1-naphthol and 1,4-naphtoquinone was extracted from chromatograms and the compound amount at different times was quantified. Note that calibration curves for substrates and products were performed and used to extract exact concentrations in reaction mixtures.

HPLC analysis method for benzene, vinyl crotonate and 3-phenylbutyric acid determinations. The progress of the reactions was followed by HPLC. Prior to the analysis, samples were filtered through a 0.45 mm filter and the presence of the substrates and reaction products were quantified by HPLC analysis, performed using a quaternary pump (model 600, Waters) coupled to an autosampler (Varian ProStar, model 420). The injection volume was 10 µL. The temperature of the column was kept constant at 40 °C. The detection of peaks was carried out using a photodiode array detector (ProStar, Varian). Quantification was performed at 254 nm and integration was carried out using the Varian Star LC workstation 6.41. The column was a Zorbax Eclipse Plus C-18 (4.6 x 100 mm, 3.5 µm, Agilent Technologies) and the mobile phase was acetonitrile/H_2O 48:52 (v/v), degassed with helium, in isocratic during 6 minutes. Both solvents contained 0.1% (v/v) of formic acid degassed with helium. The flow rate was 0.8 ml/min. The peak area corresponding to benzene, vinyl crotonate and 3-phenylbuturic acid was extracted from chromatograms and the conversion compared to a control reaction was quantified.

Enantioselectivity was determined by using a liquid chromatography. Prior to the analysis the samples were diluted (1:10) by mixing with ethyl acetate and subsequently vortex (1 minute). Standards (3(*R*/*S*)-phenylbutyric acid and 3(*S*)-phenylbutyric acid) were prepared in ethyl acetate to a final concentration of 100 mg/L. It was used a liquid chromatography system consisting of a degasser, a binary pump, and an autosampler (1290 infinity II, Agilent). Samples (0.5 µL) were applied to a column (Chiralpack IB-3 150 x 2.1 mm, 3 µm; Daicel Corporation), which was maintained at 40°C during the analysis. The system was operated at a flow rate of 0.2 mL/min with solvent A (H_2O containing 0.1% formic acid (FA)) and solvent B (acetonitrile containing 0.1% FA). The gradient was 0% B (0–0.5 min), 0 to 70% B (0.5–14 min), and 70 to 0% B (14–14.5 min). The system was finally held at 0% B for 4.5 min to re-equilibrate the system (19 min of total analysis time). Data were collected in negative ESI mode using QTOF (Agilent 6545). The analyses were performed in negative ion mode in full-scan from *m/z* 100 to 200. The capillary voltage was 2500 V and the nozzle voltage was 1000 V with a scan rate of 1.0 spectrum per second. The gas temperature was 250°C, the drying gas flow was 12 L/min, the nebulizer was 52 psi, the sheath gas temperature 370°C and the sheath gas flow 11 L/min. The MS-TOF parameters included the following: fragmentor 175 V, skimmer voltage 65 V, and octopole radio frequency voltage 750 V. During the analyses, one reference mass was used: 112.9855 (TFA(NH_4), detected *m/z* $[C_2O_2F_3(NH_4)\text{-}H]^-$). It was continuously infused into the system, enabling constant mass correction. Samples were analyzed in randomized runs, during which they were incubated in an autosampler at 4°C. The analytical run was set up starting with the analysis of five blanks. 3(*R*)-phenylbutyric acid elutes at 11.48 minutes and 3(*S*)-phenylbutyric acid at 11.58 minutes

Experimental conditions for HPLC-HR-MS. ESI was further used to verify the selective conjugation, the coupling efficiency and the purity of the modified proteins. Mass spectra were

performed using an ultra-high-resolution QTOF instrument (MAXIS II, BRUKER, Bremen-Germany). Electrospray ionization source in positive mode was used for all the analyses and the parameters were adjusted as follows: Capillary voltage 3400 V, End plate offset 500 V, in-source Collision Induced Dissociation energy (isCID) 130 eV. Nitrogen was used as nebulizer gas (pressure of 3 Bar) and drying gas (heated to 250°C, flow 4 L/min). The scans of MS spectra were conducted in the *m/z* range of 1000 to 12000. For accurate high resolution mass spectrometry (HRMS) external calibration was performed after each chromatographic run by means of a mixture of phosphazenes. Prior to mass detection samples were separated in a HPLC instrument (HP1100 Series, Agilent Technologies) using a Vydac-C4 Protein column (300 Å, 250 mm, 4.6 mm id, 5 mm particle size), the flow rate was set to 0.5 mL/min, solutions of 0.1% trifluoroacetic acid in water (v/v) and 0.1% trifluoroacetic acid in acetonitrile (v/v) were used as mobile phases A and B respectively. For each sample a 3 mg/mL solution was prepared in H_20 and 100 µL of it were loaded on the column. Separation was achieved by a 25 min linear gradient from 30% to 80% B, afterwards isocratic conditions were kept for a 60 min total run time. Finally, the MaxEnt algorithm was applied to the protein spectrum to deconvolute the multicharged signals in order to obtain the neutral intact mass protein. The analysis was performed at the *Servicio Interdepartamental de Investigación* (SIDI) from the Autonomous University of Madrid.

Mass Spectrometry. Confirmation of product identity was performed by conventional mass spectrometry performed on a hybrid quadrupole time-of-flight (QTOF) analyzer, model QSTAR, Pulsar I, from AB Sciex (Framingham, MA, U.S.A.). Reaction samples were analyzed by direct infusion and ionized by electrospray ionization mass spectrometry (ESI–MS) with methanol as the mobile phase in positive reflector mode. High-resolution mass spectrometry (HR-MS) analysis was carried out by flow injection analysis combined with electrospray ionization mass spectrometry (FIA–ESI–MS) on a QTOF Agilent G6530A accurate mass QTOF liquid chromatography–mass spectrometry (LCMS) system (Agilent Technologies, Santa Clara, CA, U.S.A.). The sample was directly infused and ionized by ESI in negative reflector mode. Ionization was enhanced by JetStream technology, and the mobile phase was 99.9:0.1 (v/v) H_2O/formic acid. Data were processed with Masshunter Data Acquisition B.05.01 and Masshunter Qualitative Analysis B.07.00 software (Agilent Technologies). The analysis was performed at the *Servicio Interdepartamental de Investigación* (SIDI) from the Autonomous University of Madrid.

Synthesis of 3'-hydroxy-[2,2'-bipyridin]-3-yl methyl hexylphosphonate. All reagents were purchased from commercial suppliers and used without further purification unless noted otherwise. Reagents were bought from SigmaAldrich, 2,2‘-bipyridine-3,3‘-diol was purchased from TCI. Solvents were purchased from Carl Roth. HPLC-MS samples were analyzed on a Waters Alliance HPLC equipped with a UV detector and an ESI-MS detector (Acquity QDA). Samples were separated on a C18 column (Phenomenex; 0D-4462-EO, 2.6 µm; 4.6 x 100 mm) at 40 °C, detection was performed at 254 nm. A gradient of water (0.1% FA, solvent A) and acetonitrile (0.1% FA, solvent B) was used, as detailed in Supplementary Table 8.

Supplementary Table 8 Gradient used for HPLC-MS analysis.

Time [min]	Solvent A H_2O (0.1% FA) [%]	Solvent B ACN (0.1% FA) [%]	Flow [ml/min]
0	75	25	0.5
3	75	25	0.5
10	5	95	0.5
11	5	95	0.5
13	0	100	0.5
14	0	100	0.5
19	75	25	0.5
20	75	25	0.5

HR-MS was recorded by VBCF metabolomics facility on a Q Exactive™ Focus Hybrid Quadrupole-Orbitrap™ Mass Spectrometer. The mass spectrometer is on-line coupled to an inert Ultimate 3000 HPLC (Dionex; Thermo Fisher Scientific). ^{1}H, ^{13}C and ^{31}P NMR spectra were recorded from d_4-MeOD solutions on a Bruker Avance III HD 600 (600 MHz) spectrometer by TU Wien. Chemical shifts (δ) are reported in ppm using tetramethylsilane as internal standard coupling constants (J) are in Hertz (Hz). The following abbreviations were used to explain the multiplicities: s = singlet, d = doublet, t = triplet, m = multiplet.

Dry glassware was used and the reaction was performed under Argon atmosphere. In a 4 ml vial 2,2'-bipyridine-3,3'-diol (83 mg, 0.44 mmol, 0.9 equiv.) was suspended in DMF (700 µl) and DIPEA (301 µl, 1.77 mmol, 3.6 equiv.). The reaction was cooled to 0 °C and hexylphosphonic dichloride (100 mg, 0.49 mmol, 1 equiv.) was added. The color changed from turbid yellow to clear red. The reaction was allowed to warm up to room temperature after 30 min. After 120 min additional hexyl phosphonium dichloride (0.1 equiv.) was added and stirring continued for 60 min. HPLC-MS was used for reaction control, samples were diluted (1:40) using methanol.

Methanol (1.79 ml, 90 equiv.) was added after 180 min total stirring time and the solution was stirred at room temperature for 180 min. HPLC-MS was used for reaction control, samples were diluted (1:40) using acetonitrile.

Water was added and the solution was extracted three times with MTBE. The combined organic phases were dried over Na_2SO_4, filtered and the solvent was removed *in vacuo*. Product was stored at -20 °C under argon until purification. The product was purified by silica gel column chromatography (~100x amount of silica, gradient PE:EtOAc = 10:1-0:1)

Supplementary References

1. Santiago, G. et al. Rational engineering of multiple active sites in an ester hydrolase. *Biochemistry* **57**, 2245-2255 (2018).
2. Martínez-Martínez, M. et al. Determinants and prediction of esterase substrate promiscuity patterns. *ACS Chem. Biol*. **13**, 225-234 (2018).
3. Zandonella, G. et al. Interactions of fluorescent triacylglycerol analogs covalently bound to the active site of a lipase from *Rhizopus oryzae*. *Eur. J. Biochem.* **262**, 63-69 (1999).
4. Tokuriki, N. et al. Diminishing returns and tradeoffs constrain the laboratory optimization of an enzyme. *Nat. Commun.* **2012**, *3*, 1257.
5. Leger, C. et al. Effect of a dispersion of interfacial electron transfer rates on steady state catalytic electron transport in [NiFe]-hydrogenase and other enzymes. *J. Phys. Chem. B* **106**, 13058-13063 (2002).
6. Gutiérrez-Sánchez, C. et al. Gold nanoparticles as electronic bridges for laccase-based biocathodes. *J. Am. Chem. Soc*. **134**, 17212-17220 (2012).
7. Martínez-Martínez, M. et al. Biochemical Diversity of carboxyl esterases and lipases from Lake Arreo (Spain): a metagenomic approach. *Appl. Environ. Microbiol.* **79**, 3553-3562 (2013).
8. Lecina, D., Gilabert, J.F. & Guallar, V. Adaptive simulations, towards interactive protein-ligand modeling. *Sci Rep*. **7**, 8466 (2017).
9. Cossins, B.P. et al. Exploration of protein conformational change with PELE and Meta-Dynamics. *J. Chem. Theory Comput.* **8**, 959-965 (2012).
10. Borrelli, K.W. et al. PELE: Protein Energy Landscape Exploration. A novel Monte Carlo based technique. *J. Chem. Theory Comput.* **1**, 1304-1311 (2005).
11. Schrödinger Release 2017-1: Jaguar, Schrödinger, LLC, New York, NY, 2019.
12. Abraham, M. J. et al. GROMACS: High performance molecular simulations through multi-level parallelism from laptops to supercomputers. *SoftwareX* **1-2**, 19-25 (2015).
13. Bekker, H. et al. "Gromacs: A parallel computer for molecular dynamics simulations"; pp. 252–256 in *Physics computing 92*. Edited by R.A. de Groot and J. Nadrchal. World Scientific, Singapore, 1993.
14. Kabsch, W. XDS. *Acta Cryst.* **D66**, 125-132 (2010).
15. Evans, P. R. & Murshudov, G. N. How good are my data and what is the resolution? *Acta Cryst* **D69**, 1204-1214 (2013).

16. Winn, M. D. *et al*. Overview of the CCP4 suite and current developments. *Acta Cryst.* **D67**, 235-242 (2011).
17. Vagin, A. & Teplyakov, A. MOLREP: an automated program for molecular replacement. *J. Appl. Cryst.* **30**, 1022-1025 (1997).
18. Murshudov, G.N., Vagin, A.A. & Dodson, E. J. Refinement of macromolecular structures by the maximum-likelihood method. *Acta Cryst.* **D535***,* 240-255 (1997).
19. Emsley, P. et al. Features and development of Coot. *Acta Cryst.* **D60**, 2126-2132 (2004).
20. Moriarty, N.W., Grosse-Kunstleve, R.W. & Adams, P.D. Electronic Ligand Builder and Optimization Workbench (eLBOW): a tool for ligand coordinate and restraint generation. *Acta Cryst.* **D65**, 1074-1080 (2009).

Supplementary Note 11

The K_M fits for the $EH1_{A1}$, $EH1_{B1}$ and $EH1_{AB1}$ variants are shown below.

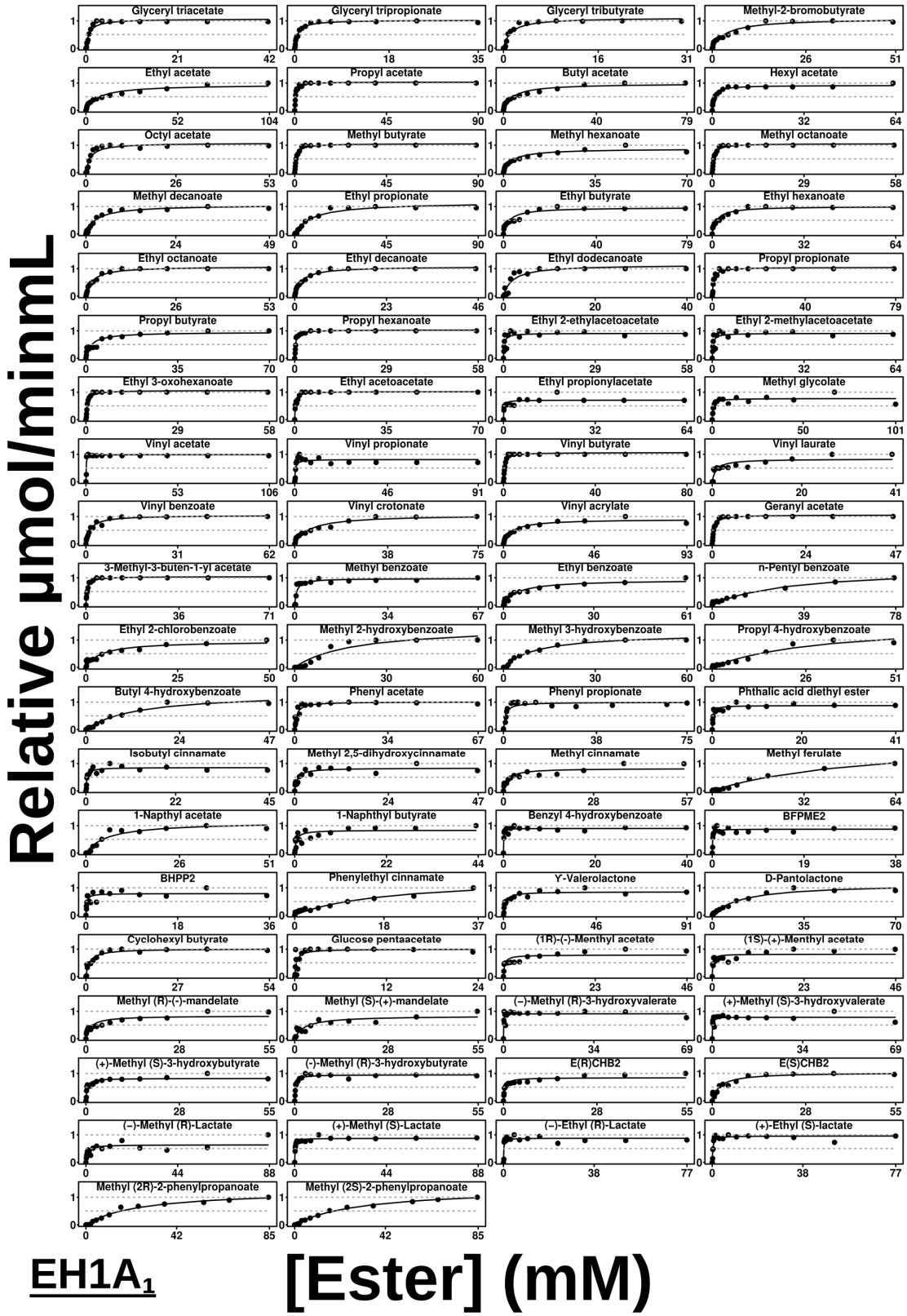

K_M fits for the $EH1_{A1}$ variant for all substrates being converted. For reaction conditions see Supplementary Figure 2 legend.

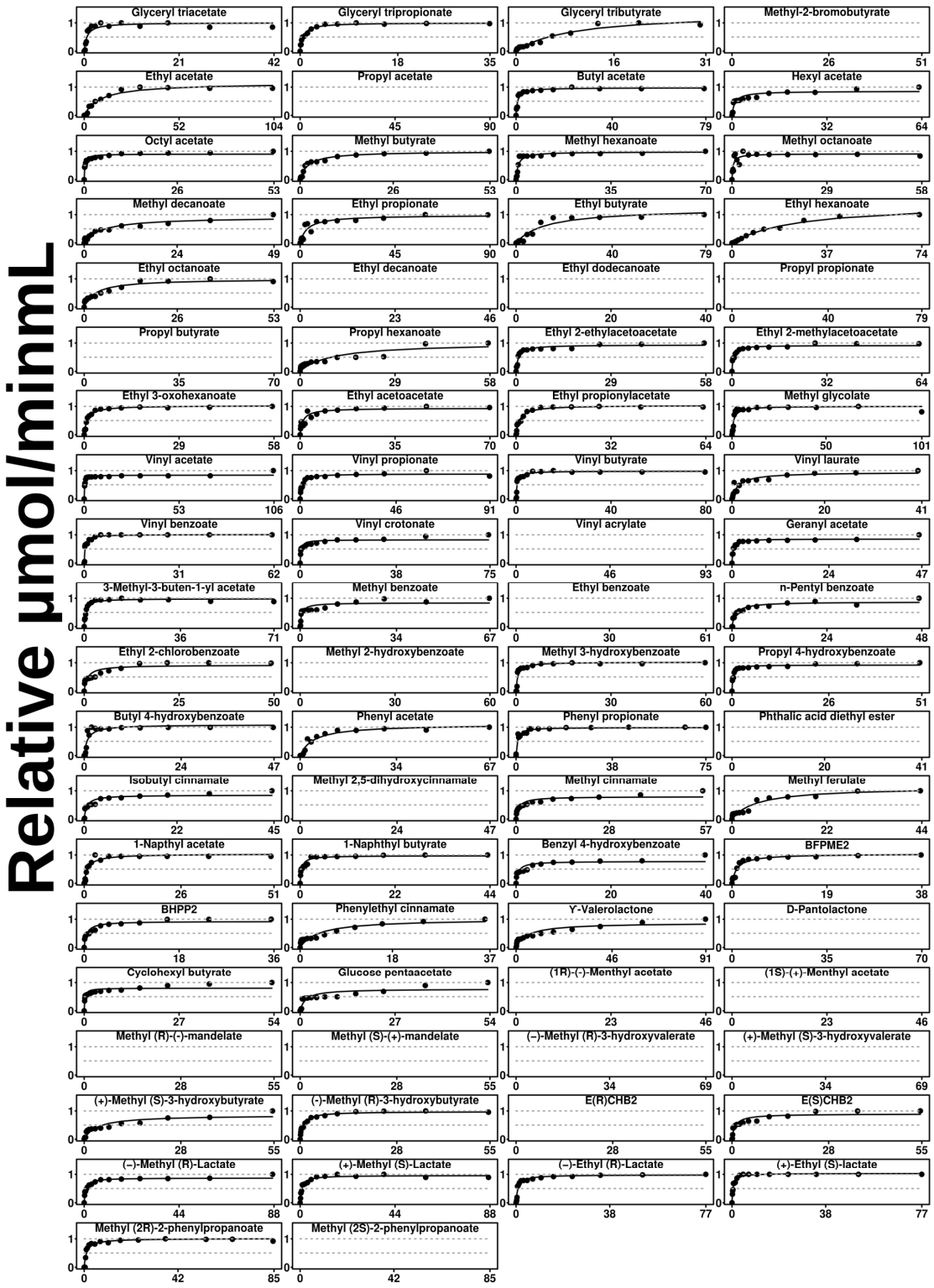

K_M fits for the $EH1_{B1}$ variant for all substrates being converted. For reaction conditions see Supplementary Figure 2 legend.

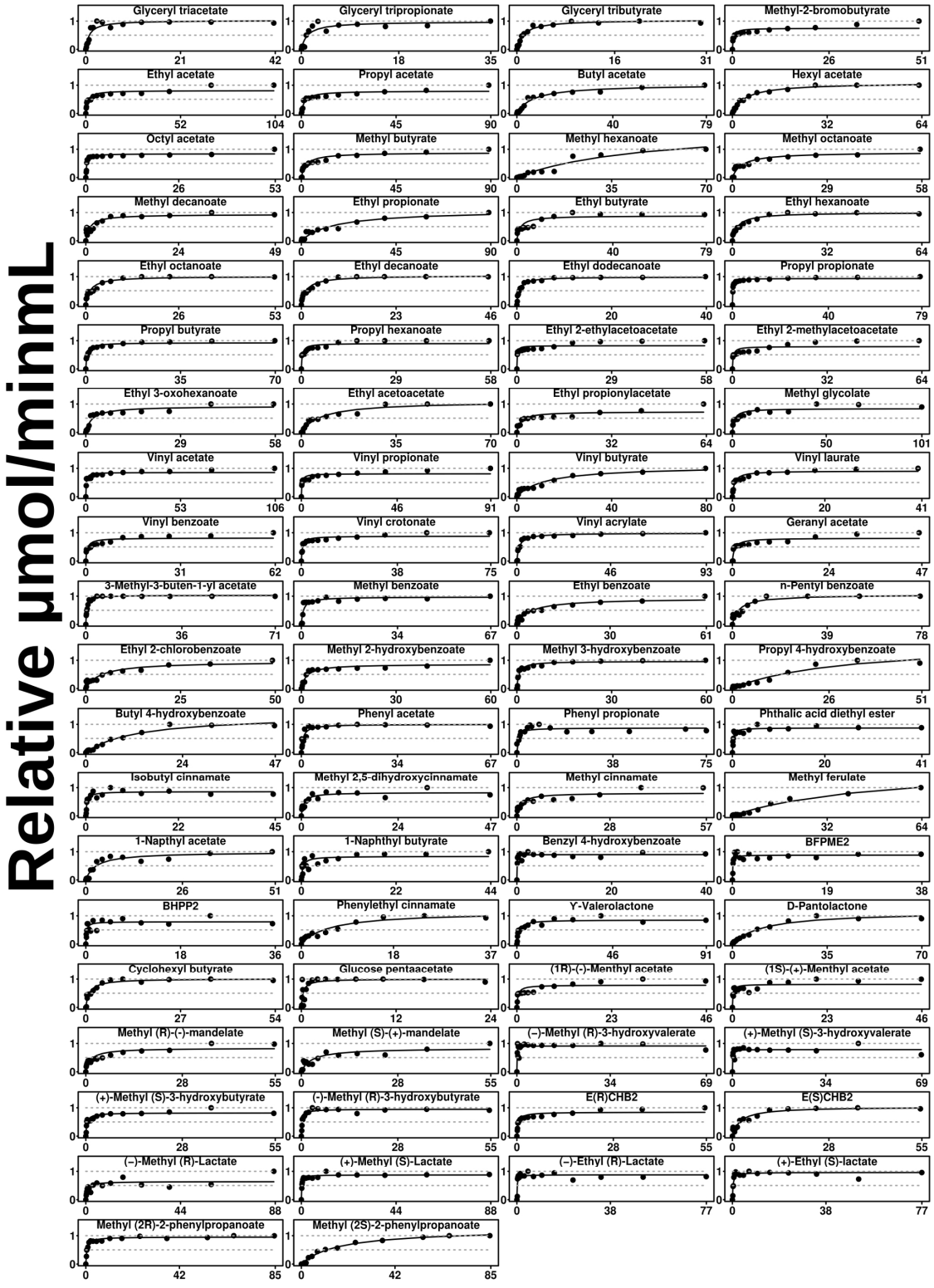

K_M fits for the $EH1_{AB1}$ variant for all substrates being converted. For reaction conditions see Supplementary Figure 2 legend.

Supplementary Note 12

The GC chromatograms for determination of enantioselectivity of $EH1_{A1}$, $EH1_{B1}$ and $EH1_{AB1}$ using racemic mixture of methyl (2*R*) phenylpropanoate / methyl (2*S*) phenylpropanoate, as well as of $EH102_{A}$, $EH102_{B}$ and $EH102_{AB}$ using racemic mixture of (+)-ethyl (*R*)-lactate / (-)-ethyl (*S*)-lactate or ethyl (*R*)-(+)-4-chloro-3-hydroxybutyrate / ethyl (*S*)-(-)-4-chloro-3-hydroxybutyrate, are shown below:

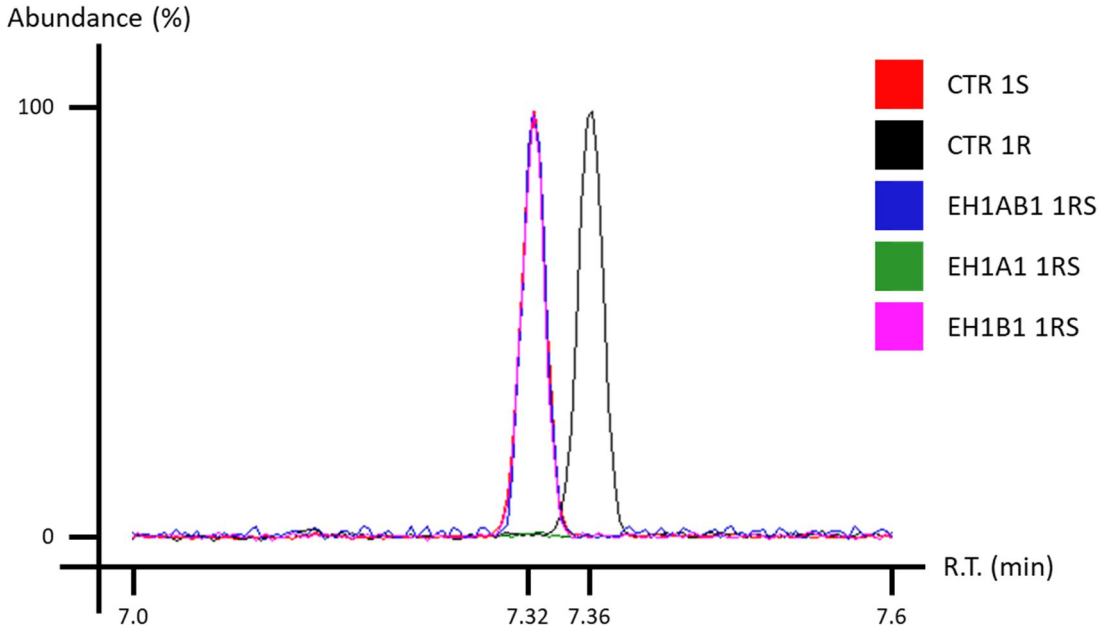

GC-MS chromatograms representing retention time (in minutes) vs abundance (in arbitrary unites) for the chiral mix methyl (2R) phenylpropanoate (abbreviation 1R) / methyl (2S) phenylpropanoate (abbreviation 1S) after hydrolysis in the presence of $EH1_{A1}$, $EH1_{B1}$ and $EH1_{AB1}$. Reactions were performed as detailed in Supplementary Methods, and reaction products analyzed by GC. *(NOTE: samples correspond to 60-min reactions (for $EH1_{B1}$ and $EH1_{AB1}$) or 24-h reactions (for $EH1_{A1}$); in last case both enantiomers are fully degraded).*

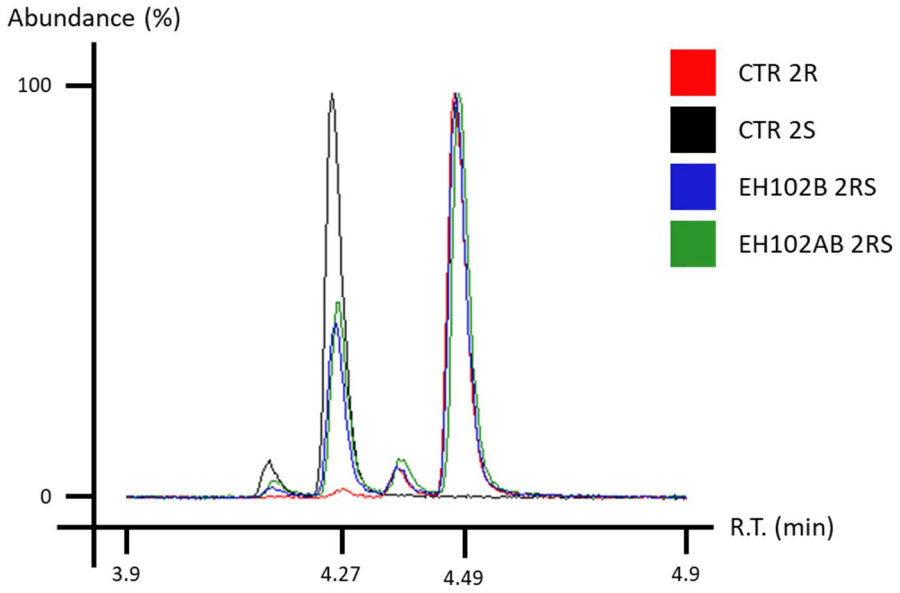

GC-MS chromatograms representing retention time (in minutes) vs abundance (in arbitrary unites) for the chiral mix (+)-ethyl (R)-lactate (abbreviation 2R) / (-)-ethyl (S)-

lactate (abbreviation 2S) after hydrolysis in the presence of $EH102_B$ and $EH102_{AB}$. Reactions were performed as detailed in Supplementary Methods, and reaction products analyzed by GC. *(NOTE: samples correspond to 10-min reactions, which were taken as example; $EH102_A$ was not included as it was not capable of hydrolysing any of the enantiomers).*

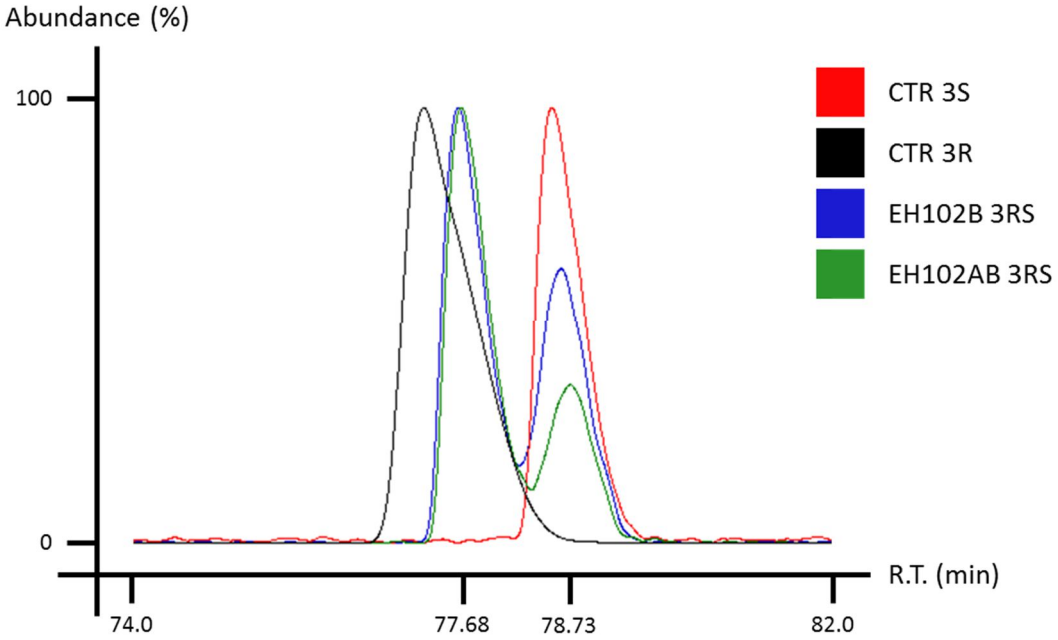

GC-MS chromatograms representing retention time (in minutes) vs abundance (in arbitrary units) for the chiral mix ethyl (R)-(+)-4-chloro-3-hydroxybutyrate (abbreviation 3R) / ethyl (S)-(-)-4-chloro-3-hydroxybutyrate (abbreviation 3S) after hydrolysis in the presence of $EH102_B$ and $EH102_{AB}$. Reactions were performed as detailed in Supplementary Methods, and reaction products analyzed by GC. *(NOTE: samples correspond to 10-min reactions, which were taken as example; $EH102_A$ was not included as it was not capable of hydrolysing any of the enantiomers).*

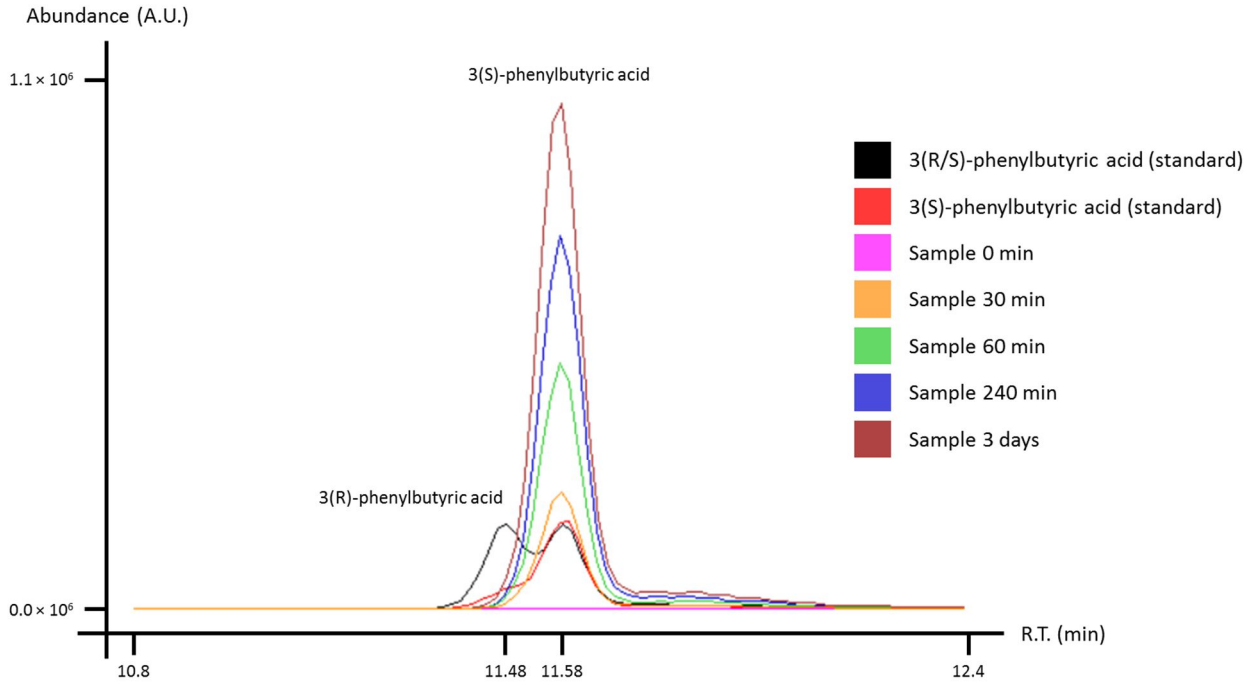

LC-MS chromatogram representing retention time (in minutes) vs abundance (in arbitrary unites) for (S)-3-phenylbutyric acid when vinyl crotonate and benzene react in the presence of $EH1_{AB1C\text{-}B}$ protein containing Cu(II). Reaction was performed as detailed in Supplementary Methods, and reaction product analyzed by LC. *(NOTE: samples correspond to different reaction times; standards are shown).*